Universidad Autónoma de San Luis Potosí
Facultad de Ingeniería
Centro de Investigación y Estudios de Posgrado

Control robusto para vehículos aéreos de tipo cuadricóptero

T E S I S

Que para obtener el grado de:

Maestro en Ingeniería Eléctrica

Presenta:
Ing. David Nieto Hernández

Asesor:

Dr. César Fernando Francisco Méndez Barrios

Co-asesor:

Dr. Diego Langarica Córdoba

San Luis Potosí, S. L. P. Diciembre de 2017

U N I V E R S I D A D
A U T Ó N O M A
D E S A N L U I S
P O T O S Í

>>>

Robust Controller Design for Multirotor Aerial Vehicles

Ing. David Nieto Hernández

In partial fulfillment of the requirements for the degree of

Master in Electrical Engineering

Automatic Control option

Advisor:

Dr. César Fernando Francisco Méndez Barrios

Coadvisor:

Dr. Diego Langarica Córdoba

Centro de Investigación y

Estudios de Posgrado

San Luis Potosí

San Luis Potosí

Tuesday 5th December, 2017

UASLP
Universidad Autónoma
de San Luis Potosí

26 de octubre de 2017

ING. DAVID NIETO HERNÁNDEZ
P R E S E N T E.

En atención a su solicitud de Temario, presentada por los **Dres. César Fernando Francisco Méndez Barrios y Diego Langarica Córdoba**, Asesor y Co-asesor de la Tesis que desarrollará Usted con el objeto de obtener el Grado de **Maestro en Ingeniería Eléctrica**, me es grato comunicarle que en la Sesión del H. Consejo Técnico Consultivo celebrada el día 26 de octubre del presente, fue aprobado el Temario propuesto:

TEMARIO:

"Control Robusto para Vehículos Aéreos de tipo Cuadricóptero"

Introducción.
1. Modelado matemático de vehículos aéreos.
2. Fundamentos de control no lineal para sistemas no lineales.
3. Controladores y observadores no lineales para vehículos aéreos multi-rotor.
4. Resultados numéricos

Conclusiones.
Referencias.

"MODOS ET CUNCTARUM RERUM MENSURAS AUDEBO"

A T E N T A M E N T E

M. I. JORGE ALBERTO PÉREZ GONZÁLEZ
DIRECTOR.

UNIVERSIDAD AUTONOMA DE SAN LUIS POTOSI
FACULTAD DE INGENIERIA
DIRECCION

Copia. Archivo.
*etn.

FACULTAD DE
INGENIERÍA

Av. Manuel Nava 8
Zona Universitaria • CP 78290
San Luis Potosí, S.L.P.
tel. (444) 826 2330 al39
fax (444) 826 2336
www.uaslp.mx

ACKNOWLEDGMENT

Este trabajo está dedicado a mi familia, a mis padres Silvia y Rubén por la paciencia que me han tenido y apoyarme en las decisiones que he tomado. Por ser unos padres ejemplares y haberme educado para llegar hasta este momento. A mis hermanos Abdiel, Aileen y Jesús que han estado siempre conmigo y por los buenos momentos familiares que hemos pasado. A mis abuelas, tíos y primos con los que he pasado excelentes momentos.

A mis amigos y compañeros de primaria, secundaria, preparatoria, licenciatura y posgrado con los que he pasado mis momentos de estudio y han hecho que mi época de estudios sea más amena (no escribo nombres para que no se me olvide ninguno). A todos los compañeros de equipos de futbol en los que he estado, especialmente a la Roma y Suministros que son con los que más tiempo he jugado, gracias por ayudarme a desestresarme practicando lo que más me gusta.

A mis asesores de licenciatura y maestría, el Dr. Homero Miranda Vidales, que gracias a él seguí el camino de la investigación al guiarme durante mi carrera, y al Dr. César Méndez Barrios quien me dió la oportunidad de trabajar con usted. Dr. Diego Langarica Córdoba quien compartió parte de su conocimiento y consejos y la oportunidad de trabajar juntos (el mundo es pequeño). Gracias por todas las lecciones y atención brindada durante la obtención de este trabajo.

A los actuales Doctores que conocí en mi primer estancia en Francia, Belem, Nohemi, Diego, Victor, José Luis, Pablo, Erick, Rafa y Lupe, quienes me apoyaron durante mi estancia y facilitaron las cosas en París. Al Dr. Juan Antonio Escareño quien me permitió trabajar con éĺ en mi segunda estancia y haberme ayudado a redactar mi primer articulo y sobretodo haberme tratado tan bien. A Erick (top trainer) con quien cotorré durante ésta segunda estancia, gracias por los buenos momentos.

A mis becarios Diego y Bryan Josué que me ayudaron con la implementación y me "distrajeron" durante la realización de este documento.

A mis sinodales Dr. Ricardo Álvarez Salas y Dr. Emilio Jorge González Gálvan por tomarse el tiempo de leer este trabajo y hacerme las correcciones pertinentes. Al coordinador del posgrado Dr. Jorge Morales Saldaña por facilitar los trámites para la obtención de este trabajo.

Finalmente al consejo nacional de ciencia y tecnología (CONACYT) por otorgarme la beca para desarrollar mis estudios de posgrado.

Índice

CONTENTS

LIST OF FIGURES

LIST OF TABLES

NOTATION AND SYMBOLS

Variable	Description
b	Torque Constant.
$C(q, \dot{q})$	Coriolis matrix.
d_i	Distance between the rolling axis and the force application point.
e_η	Rotational tracking error.
e_ξ	Translational tracking error.
f_i	Force of each engine.
T	Thrust force.
f_{xy}	Force applied to generate the torque in the plane $x - y$.
g	Gravity.
$G(q)$	Gravity vector.
h_i	Linear functions.
I_n	Inertia matrix of the quadrotor.
I_{xx}	Inertia momement on x axis.
I_{yy}	Inertia momement on y axis.
I_{zz}	Inertia momement on z axis.
$I\&I$	Immersion and Invariance.
$J(\eta)$	Rotational inertia matrix.
k	Control gains.
$\mathcal{K}$	Kinetic energy.
$\mathcal{L}$	Lagrangian.
m	Mass of the rotorcrafts.
MAV	Micro Aerial Vehicles.
$M(q)$	Inertia matrix.
$\mathcal{P}$	Potential energy.
P	Backstepping gain.
q	Generalized coordinates.
R	Rotation matrix.
R_x	Rotation matrix on x axis.
R_y	Rotation matrix on y axis.
R_z	Rotation matrix on z axis.
$SO(3)$	Special orthogonal group.
U_1	Thrust force control input.

Variable	Description
UAV	Unmanned Aerial Vehicle.
$VTOL$	Vertical take-off landing.
Δ	Disturbance.
ξ	Vector of quadrotor's position.
η	Vector of quadrotor's angles.
τ_ϕ	Torque generated on the x axis.
τ_θ	Torque generated on the y axis.
τ_ψ	Torque generated on the z axis.
ϕ	Rotation angle on the x axis.
θ	Rotation angle on the y axis.
ψ	Rotation angle on the z axis.
Ω_i	Angular speed of each rotor.
σ_i	Linear saturation.
$\pi(\cdot)$	Map for immersion condition.
μ	Observed state.
γ	control gain.

INTRODUCTION

It is well accepted that micro aerial vehicles (MAVs) are one of the most popular and challenging technologies that have recently attracted the interest of the scientific community. Furthermore, the MAVs can be included into the Unmanned Air Vehicles (UAVs) category, whose main advantage is that they operate without a human pilot aboard, in order to achieve a desired task or mission. We can say that they are able to take off or land by themselves.

Another advantage is the vertical take off landing (VTOL), which allows to this rotorcrafts to fly into places where others aircrafts can not maneuver as easy as them, for example the airplanes, which need a long track to land or take off.

In addition to the aforementioned advantages, the rotorcrafts have the particularity that they can be suspended during flight and its maneuverability depends on the speed of their motors, which provides an easy displacement in any plane.

Moreover, there are multiple applications for the multirotor aircraft, which can be splitted into civilian or military tasks, as follows:

- Civilian tasks:
  - photography (wildlife monitoring, volcano research, social events);
  - medical assistance (survival kit and blood samples delivering);
  - commercial (package delivering);
  - entertainment (recreational drones, racer drones);
- Military tasks:
  - spying (Suspect research, recognition of places);
  - medical assistance in combat (survival kit and blood samples delivering);
  - search and rescue tasks,

just to mention a few.

Due to its different applications there are multiple configurations for multirotors aircrafts among the more commons we can mention: octocopters, hexacopters and quadcopters. These kind of rotorcrafts are mechanically simple for attitude-stability purposes. Additionally, the class of aerial robots having less than four rotors (tricopters and bicopters), they integrate tilt mission mechanisms to cope with the attitude dynamics.

Interactive MAVs are a recent tendency whose main feature is to overcome the passive profile on traditional/classical unmanned systems (UAS). The latter represents an appealing subject featuring high scientific and technological potential. Interactive capabilities allow that autonomous aerial vehicles enhance the classical mission profile, participating, for instance, in tasks as aerial maintenance, cracks detection, self-recharging, and parcel acquiring.

In this work, we will be focused in the study of multirotor aircrafts with a quadrotor configuration. This rotorcraft is one of the most complex flying machines, due to its versatility and maneuverability to perform multiple tasks.

The quadcopter's displacement and rotations in the $x-y$ plane are generated due to rotors' velocity difference. Consequently, vertical rotation is achieved by creating an angular speed difference between the two pairs of rotors. Increasing or decreasing the speed of the four propellers simultaneously allows climbing and descending. Rotation about the longitudinal and the lateral axis and consequently horizontal motions are achieved by tilting the vehicle. This is possible by conversely changing the propeller speed of one pair of rotors as described in the following figure:

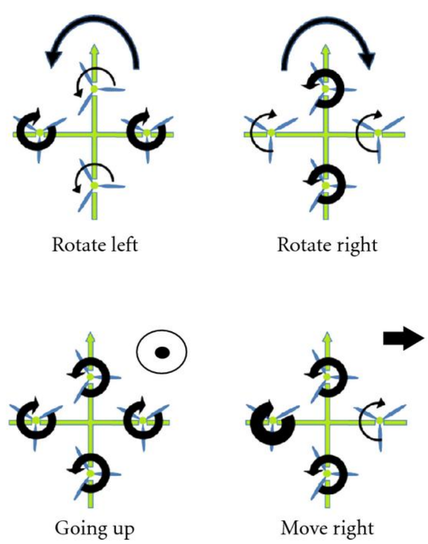

Figure 0.1. Quadcopter's displacement and rotations.

Once the dynamics of quadrotor's flight are found, it is possible to proceed to design the nonlinear controllers for the aircraft. In this work three nonlinear control techniques are applied for a tracking task and two nonlinear observers are designed in order to improve the flight performance or estimate an unknown state of the rotorcraft. These control approaches are developed in the following chapters.

Also, a new interactive rotorcraft configuration is introduced during this work. This new configuration, unlike the regular quadrotor, tilts its rotors for the spacial displacement. Furthermore, it is proposed with a robotic arm of one degree of freedom, where it is pretended to achieve different kinds of tasks.

State of Art

In the literature, there is a large number of works developed during the recent years for the control of quadrotors. The projects' number dealing this problem has considerably increased and it seems that such a tendency will be kept for a while longer. Most of these projects are based on commercially available toys like the Draganfly, the Parrot drones like the AR Drone and the Bebop, modified afterwards to have more sensory and communication capabilities. Also there is a software development in order to deal with the vision problems, an example is the ROS operative system.

In [1] a quadcopter's dynamical model is obtained via the Euler-Lagrange formalism. Subsequently, the nonlinear control techniques, Backstepping and a control based on Lyapunov theory, are designed for altitude. It is worth to mention that, in the thesis of Samir Bouabdallah, the control laws are validated in an experimental platform, which is the commercial drone "Draganfly".

From [2] we can notice that the dynamical model of the Quadrotor can be derived from the Newton-Euler formalism and the Euler-Lagrange approach. Besides, the control laws are derived from an input-output decoupling, Backstepping and its robustification with H_∞. The experimental validation is obtained from the same platform used in the work of Samir Bouabdallah, mentioned before.

In [3], the aircraft's dynamical model is derived from the Euler-Lagrange approach. Also a PD controller is developed for the multirotor aircraft and it is useful for the validation of the nonlinear control approaches. Additionally, they implement in an commercial experimental platform known as "Draganfly III".

On the other hand, in [4], a nonlinear observer is presented. The dynamical model, as in the work from Samir Bouabdallah and the book of Pedro Castillo [3], is obtained from the Euler-Lagrange formalism. The control law obtained for a tracking task is designed from the Backstepping approach, but, the most important is the design of an observer for the velocity state of the system. In such a work they assume that the state can not be measured, therefore they apply a Backstepping approach to design an observer.

In recent works, like [5] the nonlinear control laws derived from Backstepping approach and Nested Saturations are introduced and applied to an hexacopter system. The dynamical model of the hexacopter is obtained by means of the Newton-Euler formalism. It is worth to mention that they set the basis for the experimental platform that we pretend to use. The chosen dron is the "DJI F450" model in a four rotor version.

About the Immersion and Invariance controller, there is not a big amount of information of its application in multirotor aircrafts. In [6], Y. Bouzid and H. Siguerdidjane introduce this nonlinear control approach for an octocopter configuration, in its translational subsystem. Afterwards, they design a nonlinear internal model control for the rotational subsystem.

In the works of [7] and [8], an adaptive Immersion and Invariance control approach is presented for a quadcopter. In those works the the quadrotor's dynamical model has been derived from the Newton-Euler formalism. The experimental platform choose in this work is the commercial quadrotor "X450", and it is used for the control laws validation.

Concerning the interactive part of the work, this is a recent area of research among the multirotor aircrafts studies. In different works, the interactive application, commonly considered as a robotic arm, and in cosequence, the problem is reduced into a simpler system, like a pendulum-like one.

In [9], the dynamical model of a quadrotor with a suspended load is presented. The kinematic equation are derived from the Euler-Lagrange formalism. The suspended load is assumed as a noncontrolled pendulum-like system. In order to accomplish the flight task, the Backstepping control approach is applied, considering the dynamics of the pendulum.

The dynamical model of a rotorcraft with a suspended load is obtained by means of the Euler-Lagrange approach is presented in [10]. The control law proposed in such a work is a PD control, with the proposal of an observer designed by the Linear Kalman Filter (LKF), in order to estimate the disturbances and improve the performance of the aircraft.

Problem Statement

One of the main issues detected for the autonomous flight concerns the parametric uncertainties, which prevent the system to reach the desired reference or even to completely lose it. Based on this observation, the present work presents a first step in designing a robust controller capable to cope with such an issue.

In addition, it is worth to mention that quadrotors are not modeled to perform interactive tasks. Thus, as noticed in some of the works mentioned previously, the interactive tasks for rotorcraft have not been sufficiently analized. In this vein, in this thesis, we are interested in deriving a mathematical model that accurately captures the whole dynamics of a quadrotor that perform such interactive tasks, and at the same time, such a model must be suitable for control purposes.

Therefore we will summarize our main contributions for the problems addressed in this work:

- ***Nonlinear Control Strategy.*** A robust controller is developed in order to provide a different approach for a tracking task. Also, we propose a certain control strategy in order to obtain a non agressive control input.
- ***Disturbances.*** The disturbances can be presented due to random situations, for example the wind or any unpredicted impact. Therefore, we will design a disturbance observer to cope with such disturbances.
- ***Parametric Uncertainties.*** The parametric uncertainties can be seen as disturbances. Due to its differents applications the quadcopter can carry some tools or any unpredicted load, this activity is interpretated as a mass and inertial moment variation. For this reason an estimator for a parametric uncertainty is proposed.
- ***New Quadrotor Configuration.*** We propose a new quadrotor configuration appropiated to perform some interactive tasks.
- ***Interactive Applications.*** A non trivial task for the quadrotor is the interaction with the environment. In order to accomplish a given mission, the drone should carry a load, hang from a wire, etc... This kind of interactivity is not developed enough yet, that is the reason why we propose the mathematical model for a rotorcraft with an interactive robot arm.

Therefore we can establish the following methodology and objectives for this work,

Main Objectives

- To develop robust nonlinear control scheme to be implemented in the prototype.

- To develop a dynamical model for a new Quadrotor configuration.

Particular Objectives

- To obtain for the multirotor air vehicles, the mathematical models suitable for control application.
- To develop position/orientation estimation algorithms for multirotor aerial vehicles.
- To propose some control laws.
- To analyse the stability of the closed/loop system.
- To report of results (article(s), thesis).

Outline

The remaining part of the thesis is organized as follows.

- In chapter 1 we introduced the Euler-Lagrange formalism theory, where we set the minimal requirements, like kinetic and potential energy equations, to derived the kinematics equations of any dynamical system. Then, we set the frames where our dynamical system will be applied, thus, the earth fixed frame and the quadcopter fixed frame are defined. Subsequently, a rotation matrix is introduced in order to link the position between the quadrotor and the inertial frame, hence, the aircraft orientation is defined. Afterwards, we develop the quadcopter's dynamical model derived from the mathematical formulations. Finally, two flight configurations are presented.

  On the other hand, the Interactive Tilt-rotor dynamical model is derived via the Euler-Lagrange formalism. Also, the control input vector for this rotorcraft is defined in order to present the model for the control development.

- In chapter 2 the nonlinear control theory is introduced. First, the basics theory of stability (stability, asymptotic stability, Lyapunov's stability theorem, Barbashin-Krasovskii theorem and LaSalle's theorem) is presented. After that, we introduce the nonlinear controllers theorems to be developed in this work. The first control strategy introduced is the Backstepping approach, the second control strategy is the Nested Saturations approach and finally the Immersion and Invariance approach. These approaches are settled for a tracking task. To conclude this chapter, we submit the nonlinear observers to be designed in this thesis. The chosen observers are the Immersion and Invariance observer, for the mass estimation and the velocity state observation, and the Nonlinear Disturbance Observer for disturbances in the Interactive Tilt-rotor.

- In chapter 3 we proceed to design the nonlinear controllers for the quadrotor's system and the Interactive Tilt-rotor aircraft. This chapter is splitted into two sections, the first section presents the development of the nonlinear controllers and observers for the quadcopter, in the remaining section we design the control laws and the observer for the Interactive rotorcraft. It is worth to mention that we split the Quadrotor system into the translational and rotational subsystems, where the translational subsystem is developed in an scalar form, meanwhile the rotational is in the vector form.

  The control laws developed for the quadcopter are the Backstepping, Nested Saturations and the

Immersion and Invariance approaches, also, we design the Immersion and Invariance nonlinear observer. Whereas, in the Interactive Tilt-rotor we submit the Immersion and Invariance control approach and the Nonlinear Disturbance observer.

- In chapter 4 we submit the simulation results of our nonlinear controllers developed in 3. The first section of this chapter introduces the results of the controllers applied in the quadrotor's system, it is worth to mention that in this part we assume ideal conditions and that all the states are measurable. Afterwards, we consider a mass variation at the quadcopter; therefore we present the results of the Immersion and Invariance parameter estimator with the Backstepping control strategy. Then, we consider that the velocity state can not be measured, hence, we submit the results of the I&I velocity state observer with the Nested Saturations approach. To conclude with the controllers evaluation we assume the worst case scenario. We consider the mass variation and the not measurable state in order to present the results of the Immersion and Invariance control laws with the state and parameter observer.

  In addition, we present the results of the Immersion and Invariance control laws with the Nonlinear Disturbance Observer applied in the Interactive Tilt-rotor in the last part of this section. In this simulation we assume an unknown disturbance and the main objective is to follow a desired trajectory despite the disturbances.

- In the last chapter we present the conclusions derived from this work. We develop a brief analysis of the results obtained and we conclude with future work lines.

Scientific Products

The following products have been derived from this thesis:

- ***Three months internship at Institut Polytechnique des Sciences Avancées (IPSA), Paris.*** During this internship, we proposed a new configuration for a rotorcraft. We derived the dynamical model of an interactive tilt-rotor micro air vehicle via the Euler-Lagrange approach. Also, a non-linear control approach with a disturbance observer were designed for this system. In addition, we had an approach to the experimental platform. Finally, we begun a collaboration with this Institute in order to improve our experimental platform and extend our multirotor aircrafts knowledge.

- ***Submission and acceptance of an article at the 2017 International Workshop on Research, Education and Development on Unmanned Aerial Systems, RED-UAS 2017.*** We submitted an article for an international congress helded in Linköping, Sweden. In this article, we introduced the dynamical model of the Interactive tilt-rotor aircraft. Additionally an Immersion and Invariance control law with nonlinear disturbance observer is designed in order to accomplish a tracking task.

  – D. Nieto-Hernández, J. Escareno, C. F. Méndez-Barrios, I. Boussaada and D. Langarica-Córdoba, "Modeling and control of an interactive tilt-rotor MAV," 2017 Workshop on Research, Education and Development of Unmanned Aerial Systems (RED-UAS), Linköping, Sweden, 2017, pp. 270-275.

CHAPTER 1

AIR VEHICLES DYNAMICAL MODEL

The dynamical modeling for aerial vehicles is an area that has been extensively studied. In fact, quadrotors are one of the most analyzed systems, where its dynamics are completely developed, see, for instance,[3], [11], and references therein. However, there exist some particular configurations of aerial vehicles whose dynamics are still Under study, as well as its control. In particular, Tilt-rotor aircrafts have not been that extensively studied as quadrotors, therefore interactive tilt-rotor aircrafts bibliography is not widespread enough. Additionally, the interactive tasks (transportation, recharging connection, grasping) in the rotorcraft have been rised over the last years. In this subject works like [9] shows the dynamic model of a quadrotor with suspended load. However, it is worth to mention that this work consider the load as an actuated pendulum.

This chapter presents the mathematical model for the aerial vehicles models considered in this thesis. Such a model can be derived from two different approaches: the Newton-Euler formalism and the Euler-Lagrange formalism. The dynamical models are obtained via the Euler-Lagrange formalism since this approach has special characteristics that are exploited later in the control design stage. The remaining part of this chapter is organized as follows. In section 1.1 the Euler-Lagrange approach is presented in order to set the basis for the following sections. The quadrotor's model is derived by the Euler-Lagrange formalism in section 1.2. Finally in section 1.3 the $x - y$ plane model of the interactive tilt-rotor is presented.

1.1 Euler-Lagrange Formalism

The mathematical model for physical systems can be obtained from energy considerations, where the Euler-Lagrange formalism is the most versatile than other approaches. In this approach, it is necessary to know the kinetic ($\mathcal{K}_T$) and the potential ($\mathcal{P}_T$) energy of the system in order to obtain its kinematic equations. The kinetic and potential energy are obtained as

$$\mathcal{K} = \frac{1}{2}mv^2, \tag{1.1}$$

$$\mathcal{P} = mgz, \tag{1.2}$$

where $m \in \mathbb{R}_+$ is the quadrotor's mass, $g \in \mathbb{R}_+$ is the gravity constant, $z \in \mathbb{R}$ is the altitude and $v \in \mathbb{R}$ is the speed.

Also, it is important to define the generalized coordinates ($\boldsymbol{q}$), which are going to be used to describe the instantaneous configuration of the dynamical system relative to an inertial fixed frame. Then, the Lagrangian ($\mathcal{L}$) will be defined by the difference between kinetic and potential energy

$$\mathcal{L} := \mathcal{K} - \mathcal{P}, \tag{1.3}$$

where

$$\mathcal{L} = \mathcal{L}(\boldsymbol{q}, \dot{\boldsymbol{q}}, t). \tag{1.4}$$

Finally, the Euler-Lagrange formulation can be described by the equation

$$\frac{d}{dt}\left(\frac{\partial \mathcal{L}}{\partial \dot{\boldsymbol{q}}}\right) - \frac{\partial \mathcal{L}}{\partial \boldsymbol{q}} = \boldsymbol{U}, \tag{1.5}$$

where $\boldsymbol{U}$ represents the input force of the system.

1.2 Quadrotor Dynamics

In order to obtain the dynamical model, consider the earth fixed frame $\mathbb{A}$ and the quadrotor fixed frame $\mathbb{B}$ as can be seen in figure 1.1.

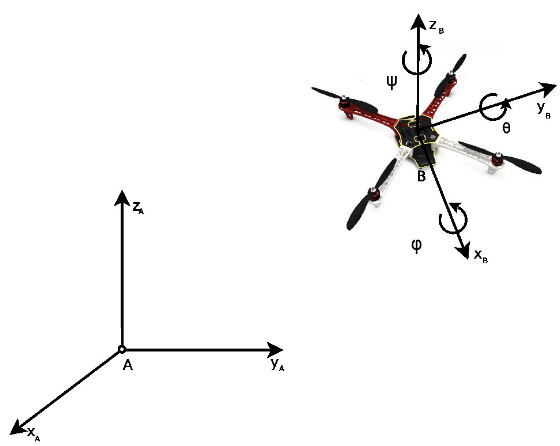

Figure 1.1. Earth fixed frame $\mathbb{A}$ and the quadrotor fixed frame $\mathbb{B}$.

Assume the quadrotor as a rigid body in three dimensions, with a thrust force and three angular torques. Due to the thrust force acts in $z_{\mathbb{B}}$ axis, it allows the rotorcraft to rise above the ground. It is worth to mention that this force does not allow the quadrotor maneuver in the $x_{\mathbb{A}} - y_{\mathbb{A}}$ plane. Then the angular torques let the aircraft rotate and therefore the air vehicle maneuvers along the $x_{\mathbb{A}}$ and $y_{\mathbb{A}}$ axes.

1.2.1 Aircraft Orientation

The generalized coordinates are defined to describe the dynamical model, hence

$$\boldsymbol{q} \colon = \begin{bmatrix} \boldsymbol{\xi} \\ \boldsymbol{\eta} \end{bmatrix} \in \mathbb{R}^6, \tag{1.6}$$

where $\boldsymbol{\xi} = [x_{\mathbb{A}}, y_{\mathbb{A}}, z_{\mathbb{A}}]^T = [x, y, z]^T \in \mathbb{R}^3$ is the quadcopter center of mass position vector referred to the earth fixed frame $\mathbb{A}$, and $\boldsymbol{\eta} = [\phi, \theta, \psi]^T \in \mathbb{R}^3$ is the quadcopter Euler angles vector.

The rotation around the x, y and z axes are named as roll, pitch and yaw, respectively. The three single rotations are written separately as $R(x, \phi)$, $R(y, \theta)$ and $R(z, \psi) \in \mathbb{R}^{3\times 3}$ which are given by

$$R(x,\phi) = \begin{bmatrix} 1 & 0 & 0 \\ 0 & \cos\phi & -\sin\phi \\ 0 & \sin\phi & \cos\phi \end{bmatrix}, R(y,\theta) = \begin{bmatrix} \cos\theta & 0 & \sin\theta \\ 0 & 1 & 0 \\ -\sin\theta & 0 & \cos\theta \end{bmatrix}, R(z,\psi) = \begin{bmatrix} \cos\psi & -\sin\psi & 0 \\ \sin\psi & \cos\psi & 0 \\ 0 & 0 & 1 \end{bmatrix}.$$

As any position in $\mathbb{B}$ experience three successive rotations where each rotation is done around a specific axis, thus any quadrotor's point can be expressed as

$$R_{\mathbb{B}}^{\mathbb{A}} = R(z,\psi)R(y,\theta)R(x,\phi), \tag{1.7}$$

where the rotation matrix (**1.8**) refers any point from $\mathbb{B}$ to $\mathbb{A}$:

$$R_{\mathbb{B}}^{\mathbb{A}} = \begin{bmatrix} \cos\psi\cos\theta & \cos\psi\sin\theta\sin\phi - \sin\psi\cos\phi & \cos\psi\sin\theta\cos\phi + \sin\psi\sin\phi \\ \sin\psi\cos\theta & \sin\psi\sin\theta\sin\phi + \cos\psi\cos\phi & \sin\psi\sin\theta\cos\phi - \cos\psi\sin\phi \\ -\sin\theta & \cos\theta\sin\phi & \cos\theta\cos\phi \end{bmatrix} =: R. \tag{1.8}$$

The special orthogonal group of all 3×3 rotation matrices is denoted by *SO*(3) [12]. Thus, if $R_{\mathbb{B}}^{\mathbb{A}} \in$ *SO*(3), then

$$R^T R = I. \tag{1.9}$$

The time derivative of the last expression is obtained as

$$\dot{R}^T R + R^T \dot{R} = 0, \tag{1.10}$$

where

$$-\dot{R}^T R = R^T \dot{R}, \tag{1.11}$$

and defining the mapping $S \colon \mathbb{R} \to \mathbb{R}^{3\times 3}$:

$$S \colon = R^T \dot{R}, \tag{1.12}$$

then, (**1.12**) allow us to express

$$\dot{R} = RS. \tag{1.13}$$

From (**1.12**), it can be seen that it is possible to solve for S using

$$S = R^T \frac{\partial R}{\partial \phi}\dot{\phi} + R^T \frac{\partial R}{\partial \theta}\dot{\theta} + R^T \frac{\partial R}{\partial \psi}\dot{\psi}, \tag{1.14}$$

where the skew symmetric matrix is obtained and expressed as:

$$S = \begin{bmatrix} 0 & -\cos\phi\cos\theta\dot{\psi} + \sin\phi\dot{\theta} & \cos\phi\dot{\theta} + \cos\theta\sin\phi\dot{\psi} \\ \cos\phi\cos\theta\dot{\psi} - \sin\phi\dot{\theta} & 0 & -\dot{\phi} + \sin\theta\dot{\psi} \\ -\cos\phi\dot{\theta} - \cos\theta\sin\phi\dot{\psi} & \dot{\phi} - \sin\theta\dot{\psi} & 0 \end{bmatrix}. \tag{1.15}$$

Simplifying the notation of S, (**1.15**) can be rewritten as

$$S = \begin{bmatrix} 0 & -c_s & b_s \\ c_s & 0 & -a_s \\ -b_s & a_s & 0 \end{bmatrix}, \tag{1.16}$$

where the mapping $W_n : \dot{\boldsymbol{\eta}} \to \boldsymbol{\omega}$:

$$\boldsymbol{\omega} = W_n(\boldsymbol{\eta}, \dot{\boldsymbol{\eta}})\dot{\boldsymbol{\eta}}, \tag{1.17}$$

gets the relation between the angular speed components and the Tait-Bryan angles time derivatives:

$$\begin{bmatrix} a_s \\ b_s \\ c_s \end{bmatrix} = \begin{bmatrix} 1 & 0 & -\sin\theta \\ 0 & \cos\phi & \sin\phi\cos\theta \\ 0 & -\sin\phi & \cos\phi\cos\theta \end{bmatrix} \begin{bmatrix} \dot{\phi} \\ \dot{\theta} \\ \dot{\psi} \end{bmatrix}. \tag{1.18}$$

1.2.2 Euler-Lagrange Approach

In addition, it is necessary to consider the matrix $D(\boldsymbol{q}, \dot{\boldsymbol{q}})$ defined as:

$$D(\boldsymbol{q}, \dot{\boldsymbol{q}}) := \begin{bmatrix} m \cdot I & 0 \\ 0 & J(\boldsymbol{\eta}) \end{bmatrix}, \tag{1.19}$$

where $I \in \mathbb{R}^{3\times 3}$ is the identity matrix and $J \in \mathbb{R}^{3\times 3}$ is a matrix obtained from

$$J(\boldsymbol{\eta}) = W_n(\boldsymbol{\eta}, \dot{\boldsymbol{\eta}})^T I_n W_n, \tag{1.20}$$

where the inertia matrix I_n takes the cross products terms from the inertia tensor as null, hence I_n is a diagonal matrix defined as

$$I_n := \begin{bmatrix} I_{xx} & 0 & 0 \\ 0 & I_{yy} & 0 \\ 0 & 0 & I_{zz} \end{bmatrix}. \tag{1.21}$$

Under the above considerations, the matrix J is expressed as

$$J(\boldsymbol{\eta}) = \begin{bmatrix} I_{xx} & 0 & -I_{xx}\sin\theta \\ 0 & I_{yy}\cos^2\phi + I_{zz}\sin^2\phi & I_{yy}\cos\theta\cos\phi\sin\phi - I_{zz}\cos\theta\cos\phi\sin\phi \\ -I_{xx}\sin\theta & I_{yy}\cos\theta\cos\phi\sin\phi - I_{zz}\cos\theta\cos\phi\sin\phi & I_{zz}\cos^2\theta\cos^2\phi + I_{xx}\sin^2\theta + I_{yy}\cos^2\theta\sin^2\phi \end{bmatrix}. \tag{1.22}$$

Let us define the translational kinetic energy as

$$\mathcal{K}_{Trasl}(\boldsymbol{q}, \dot{\boldsymbol{q}}) := \frac{1}{2}\dot{\boldsymbol{\xi}}^T m I \dot{\boldsymbol{\xi}}, \tag{1.23}$$

and the rotational kinetic energy as

$$\mathcal{K}_{Rot}(\boldsymbol{q}, \dot{\boldsymbol{q}}) = \frac{1}{2}\dot{\boldsymbol{\eta}}^T J \dot{\boldsymbol{\eta}}. \tag{1.24}$$

The potential energy, can be defined as follows

$$\mathcal{P}(\boldsymbol{q}) = mG\boldsymbol{q}^T, \tag{1.25}$$

where $\boldsymbol{G} \in \mathbb{R}^{1\times 3}$ is the gravity vector

$$\boldsymbol{G} = \begin{bmatrix} 0 & 0 & g & 0 & 0 & 0 \end{bmatrix}^T. \tag{1.26}$$

Now, let us consider the Euler-Lagrange equation

$$\frac{d}{dt}\left(\frac{\partial \mathcal{L}}{\partial \dot{\boldsymbol{q}}_i}\right) - \frac{\partial \mathcal{L}}{\partial \boldsymbol{q}_i} = \begin{bmatrix} \boldsymbol{F}_\xi \\ \boldsymbol{\tau} \end{bmatrix}, \tag{1.27}$$

where the thrust force is only applied in z axis, therefore the input vector $\boldsymbol{F}_\xi$ can be expressed as

$$\boldsymbol{F}_\xi = \begin{bmatrix} 0 \\ 0 \\ u_1 \end{bmatrix}. \tag{1.28}$$

On the other hand, the input vector $\boldsymbol{\tau}$ is made up of the torques generated by the difference between the forces of the quadrotor engines. These torques allow the rotorcraft to tilt in order to position in the $x-y$ frame or rotate in its place

$$\boldsymbol{\tau} = \begin{bmatrix} \tau_\phi \\ \tau_\theta \\ \tau_\psi \end{bmatrix} = \begin{bmatrix} u_2 \\ u_3 \\ u_4 \end{bmatrix}. \tag{1.29}$$

Now, in order to derive the Euler-Lagrange equations (**1.27**), let us compute the following terms:

$$\begin{aligned} \frac{\partial \mathcal{L}}{\partial \dot{\boldsymbol{q}}} &= \frac{1}{2}[D(\boldsymbol{q})\dot{\boldsymbol{q}} + \dot{\boldsymbol{q}}^T D(\boldsymbol{q})], && (1.30) \\ \frac{\partial \mathcal{L}}{\partial \dot{\boldsymbol{q}}} &= D(\boldsymbol{q})\dot{\boldsymbol{q}}. && (1.31) \end{aligned}$$

The time derivative of (**1.31**) is given by

$$\frac{d}{dt}\left(\frac{\partial \mathcal{L}}{\partial \dot{\boldsymbol{q}}}\right) = \dot{D}(\boldsymbol{q})\dot{\boldsymbol{q}} + D(\boldsymbol{q})\ddot{\boldsymbol{q}}, \tag{1.32}$$

finally the partial derivative with respect to the generalized coordinates $\boldsymbol{q}$ is

$$\frac{\partial \mathcal{L}}{\partial \boldsymbol{q}} = \frac{\partial \mathcal{K}(\boldsymbol{q}, \dot{\boldsymbol{q}})}{\partial \boldsymbol{q}} - \frac{\partial \mathcal{P}(\boldsymbol{q})}{\partial \boldsymbol{q}} = \frac{\partial \mathcal{K}(\boldsymbol{q}, \dot{\boldsymbol{q}})}{\partial \boldsymbol{q}} - mG. \tag{1.33}$$

This implies that the Euler-Lagrange equation (**1.27**) can be stated as follows

$$\dot{D}(\boldsymbol{q})\dot{\boldsymbol{q}} + D(\boldsymbol{q})\ddot{\boldsymbol{q}} - \frac{\partial \mathcal{K}}{\partial \boldsymbol{q}} - G = \begin{bmatrix} \boldsymbol{F}_\xi \\ \boldsymbol{\tau} \end{bmatrix}. \tag{1.34}$$

From (**1.34**), the Coriolis matrix is defined as

$$C(\boldsymbol{q}, \dot{\boldsymbol{q}})\dot{\boldsymbol{q}} = \dot{D}(\boldsymbol{q})\dot{\boldsymbol{q}} - \frac{\partial \mathcal{K}}{\partial \boldsymbol{q}}. \tag{1.35}$$

Then solving for (**1.35**) the Coriolis matrix $C(\boldsymbol{q},\dot{\boldsymbol{q}}) \in \mathbb{R}^{3\times 3}$ obtained is

$$C(\boldsymbol{q},\dot{\boldsymbol{q}}) = \begin{bmatrix} C_{11} & C_{12} & C_{13} \\ C_{21} & C_{22} & C_{23} \\ C_{31} & C_{32} & C_{33} \end{bmatrix}, \tag{1.36}$$

where each term is defined as:

$$\begin{aligned}
C_{11} &:= 0, \\
C_{12} &:= -I_{xx}\dot{\psi}\cos\theta + I_{yy}(\dot{\theta}\sin\phi\cos\phi + \dot{\psi}\cos\theta\sin^2\phi - \dot{\psi}\cos\theta\cos^2\phi) \\
&\quad - I_{zz}(\dot{\psi}\cos\theta\sin^2\phi - \dot{\psi}\cos\theta\cos^2\phi + \dot{\theta}\sin\phi\cos\phi), \\
C_{13} &:= -I_{yy}\dot{\psi}\cos^2\theta\sin\phi\cos\phi + I_{zz}\dot{\psi}\cos^2\theta\sin\phi\cos\phi, \\
C_{21} &:= I_{xx}\dot{\psi}\cos\theta + I_{yy}(-\dot{\theta}\sin\phi\cos\phi + \dot{\psi}\cos\theta\cos^2\phi - \dot{\psi}\cos\theta\sin^2\phi) \\
&\quad + I_{zz}(\dot{\psi}\cos\theta\sin^2\phi - \dot{\psi}\cos\theta\cos^2\phi + \dot{\theta}\sin\phi\cos\phi), \\
C_{22} &:= -I_{yy}\dot{\phi}\sin\phi\cos\phi + I_{zz}\dot{\phi}\sin\phi\cos\phi, \\
C_{23} &:= -I_{xx}\dot{\psi}\sin\theta\cos\theta + I_{yy}\dot{\psi}\sin\theta\cos\theta\sin^2\phi + I_{zz}\dot{\psi}\sin\theta\cos\theta\cos^2\phi, \\
C_{31} &:= -I_{xx}\dot{\theta}\cos\theta + I_{yy}\dot{\psi}\cos^2\theta\sin\phi\cos\phi - I_{zz}\dot{\psi}\cos^2\theta\sin\phi\cos\phi, \\
C_{32} &:= I_{xx}\dot{\psi}\sin\theta\cos\theta - I_{yy}(\dot{\theta}\sin\theta\sin\phi\cos\phi + \dot{\phi}\cos\theta\sin^2\phi - \dot{\phi}\cos\theta\cos^2\phi + \dot{\psi}\sin\theta\cos\theta\sin^2\phi) \\
&\quad + I_{zz}(\dot{\phi}\cos\theta\sin^2\phi - \dot{\phi}\cos\theta\cos^2\phi - \dot{\psi}\sin\theta\cos\theta\cos^2\phi + \dot{\theta}\sin\theta\sin\phi\cos\phi), \\
C_{33} &:= I_{xx}\dot{\theta}\sin\theta\cos\theta + I_{yy}(-\dot{\theta}\sin\theta\cos\theta\sin^2\phi + \dot{\phi}\cos^2\theta\sin\phi\cos\phi) \\
&\quad - I_{zz}(\dot{\theta}\sin\theta\cos\theta\cos^2\phi + \dot{\phi}\cos^2\theta\sin\phi\cos\phi).
\end{aligned}$$

Hence, the dynamics of the quadrotor is described by

$$m\ddot{\boldsymbol{\xi}} + mG = R_{\mathbb{B}}^{\mathbb{A}}\boldsymbol{F}_{\xi}, \tag{1.37}$$
$$J(\boldsymbol{\eta})\ddot{\boldsymbol{\eta}} + C(\boldsymbol{\eta},\dot{\boldsymbol{\eta}})\dot{\boldsymbol{\eta}} = \boldsymbol{\tau}. \tag{1.38}$$

As it can be seen, the rotorcraft dynamical equation can be split into two different subsystems, the translational (**1.37**) and rotational (**1.38**) subsystem, where the subsystems are linked by the rotation matrix $R_{\mathbb{B}}^{\mathbb{A}}$. Also, the whole system has six generalized coordinates but only four control inputs, therefore, the quadrotor is considered as an underactuated system.

1.2.3 Flight configuration

From the equations (**1.37**) and (**1.38**) it is noticed that the rotorcraft maneuvers are caused due to the thrust force and the quadrotor tilting. These movements depends on the propulsion characteristics. The main components in the propulsion system are the propellers and the engines, where each component has its own specific feature. In this subsection the propellers attributes will be assumed as ideal, implying that the analysis will be focused on the engines attributes. Hence, the main engine characteristic we look for is the link between the engine force and the angular velocity.

Consider that the thrust force of each engine is given by

$$f_i = b\Omega_i^2, \tag{1.39}$$

where $b \in \mathbb{R}_+$ is the torque constant and $\Omega_i \in \mathbb{R}$ is the angular speed from each motor, with $i \in \{1, \ldots, 4\}$.

The thrust force is the sum of the quadrotor engines, then using (**1.39**) the input $u_1 = T$ can be written as

$$T = \sum_{i=1}^{4} b\Omega_i^2. \tag{1.40}$$

In order to maneuver around the $x_{\mathbb{B}}$ and $y_{\mathbb{B}}$ axes, its rolling moments are described by

$$\tau_i = f_{xy} d_i, \tag{1.41}$$

where $f_{xy} \in \mathbb{R}$ is the force applied to generate the torque in the plane $x - y$ and $d_i \in \mathbb{R}_+$ is the distance between the rolling axis and the force application point.

Once the equations for the propulsion system are derived, the next step is to define the flight configuration for the quadrotor system. It is worth to mention that there exists two flight configurations. The first one is the cross configuration, where two forces are aligned with the axis and this could cause the two remaining forces gets higher when the aircraft is tilting. The second configuration is the X configuration, where the forces are distributed equally because none of the forces are in the axis.

1.2.3.1 Cross configuration

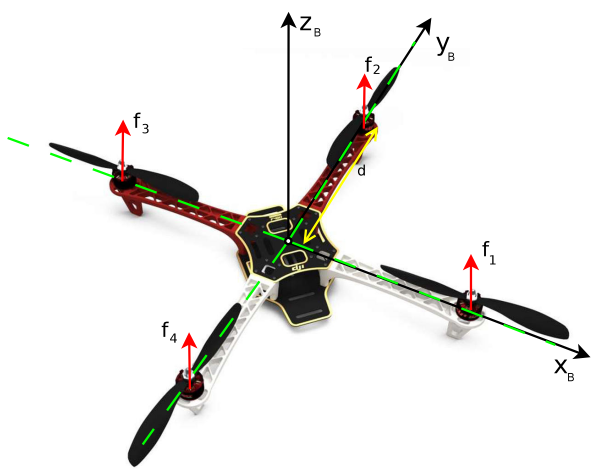

Figure 1.2. Quadrotor's fixed frame in cross configuration.

The force analysis for the cross flight configuration is derived by taking into consideration the figure 1.2. In this diagram it can be seen that the $x_{\mathbb{B}}$ and $y_{\mathbb{B}}$ axes have two forces, respectively. Therefore the forces involved in the rotation against each axis are the two remaining. Thus, the necessary force f_x to rotate in the $x_{\mathbb{B}}$ axis is given by the difference between the forces f_2 and f_4, i.e.,

$$f_x = f_2 - f_4. \tag{1.42}$$

Analogously, the necessary force f_y to rotate in the $y_{\mathbb{B}}$ axis, is the difference between the forces f_1 and f_3, i.e.,

$$f_y = f_1 - f_3. \tag{1.43}$$

The rolling moments are generated due to the force and the distance between the center of mass and the force application point. With the force necessary to rotate and considering the distance where they are applied, the quadrotor rolling moments are given by

$$\begin{aligned} \tau_x &= f_x d = (f_2 - f_4)d, & (1.44)\\ \tau_y &= f_y d = (f_1 - f_3)d. & (1.45) \end{aligned}$$

Besides, there is a torque generated by the $i-th$ motor, which is given by

$$\tau_{\mu i} = k\Omega_i^2, \tag{1.46}$$

with the equation above is possible to get the rolling moment in the z axis defined as

$$\tau_z = \tau_{\mu 1} - \tau_{\mu 2} + \tau_{\mu 3} - \tau_{\mu 4}, \tag{1.47}$$

also substituting (**1.39**) and (**1.46**) into (**1.47**), yields to

$$\tau_z = \frac{k}{b}(f_1 - f_2 + f_3 - f_4). \tag{1.48}$$

It is important to notice that the propulsion system is the input for the quadrotor model, then we can express the system in a matrix form as:

$$\begin{bmatrix} u_1 \\ u_2 \\ u_3 \\ u_4 \end{bmatrix} = \begin{bmatrix} T \\ \tau_x \\ \tau_y \\ \tau_z \end{bmatrix} = \begin{bmatrix} 1 & 1 & 1 & 1 \\ 0 & d & 0 & -d \\ d & 0 & -d & 0 \\ \frac{k}{b} & -\frac{k}{b} & \frac{k}{b} & -\frac{k}{b} \end{bmatrix} \begin{bmatrix} f_1 \\ f_2 \\ f_3 \\ f_4 \end{bmatrix}, \tag{1.49}$$

where the forces can be obtained by

$$\begin{bmatrix} f_1 \\ f_2 \\ f_3 \\ f_4 \end{bmatrix} = \begin{bmatrix} \frac{1}{4} & 0 & \frac{1}{2d} & \frac{b}{4k} \\ \frac{1}{4} & \frac{1}{2d} & 0 & -\frac{b}{4k} \\ \frac{1}{4} & 0 & -\frac{1}{2d} & \frac{b}{4k} \\ \frac{1}{4} & -\frac{1}{2d} & 0 & -\frac{b}{4k} \end{bmatrix} \begin{bmatrix} u_1 \\ u_2 \\ u_3 \\ u_4 \end{bmatrix}. \tag{1.50}$$

Finally, in order to obtain the PWM for implementation, the angular speed can be obtained by substituting (**1.39**) into (**1.50**), the square speed is given by

$$\begin{bmatrix} \Omega_1^2 \\ \Omega_2^2 \\ \Omega_3^2 \\ \Omega_4^2 \end{bmatrix} = \begin{bmatrix} \frac{1}{4b} & 0 & \frac{1}{2bd} & \frac{1}{4k} \\ \frac{1}{4b} & \frac{1}{2bd} & 0 & -\frac{1}{4k} \\ \frac{1}{4b} & 0 & -\frac{1}{2bd} & \frac{1}{4k} \\ \frac{1}{4b} & -\frac{1}{2bd} & 0 & -\frac{1}{4k} \end{bmatrix} \begin{bmatrix} u_1 \\ u_2 \\ u_3 \\ u_4 \end{bmatrix}. \tag{1.51}$$

1.2.3.2 X configuration

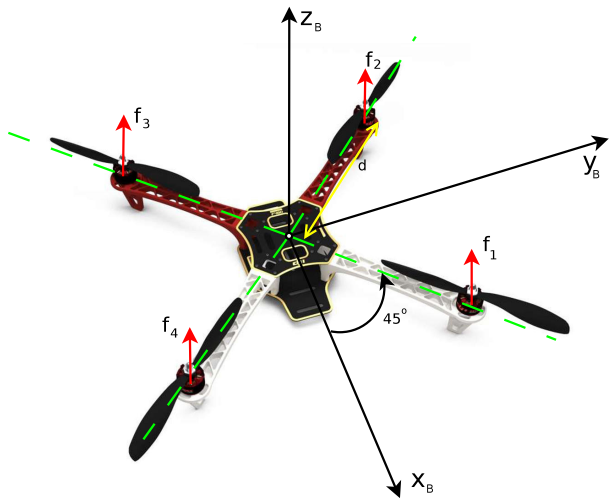

Figure 1.3. Quadrotor's fixed frame in X configuration.

For the X configuration, let us consider figure 1.3. For this case we can observe that the forces are not in the axes, then the quadrotor tilts with the four rotors and not with two as in the cross flight configuration. Hence, the required force to roll in the x axis is given by

$$f_x = f_1 + f_2 - f_3 - f_4. \tag{1.52}$$

Similarly, the necessary force f_y to rotate in the $y_{\mathbb{B}}$ axis is given by the sum of each engine force, i.e.,

$$f_y = f_1 - f_2 - f_3 + f_4. \tag{1.53}$$

Following similar arguments than those presented in the cross configuration, the quadrotor rolling moments are given by

$$\tau_x = f_x \frac{\sqrt{2}}{2} d = (f_1 + f_2 - f_3 - f_4) \frac{\sqrt{2}}{2} d, \tag{1.54}$$

$$\tau_y = f_y \frac{\sqrt{2}}{2} d = (f_1 - f_2 - f_3 + f_4) \frac{\sqrt{2}}{2} d. \tag{1.55}$$

Besides, there is a torque generated by the $i-th$ motor, which is given by the equation (**1.46**), then with this equation is possible to derive the rolling moment in the z axis as

$$\tau_z = \frac{k}{b}(f_1 - f_2 + f_3 - f_4). \tag{1.56}$$

Notice that the propulsion system is the input for the quadrotor model, then we can express the system in a matrix form

$$\begin{bmatrix} u_1 \\ u_2 \\ u_3 \\ u_4 \end{bmatrix} = \begin{bmatrix} T \\ \tau_x \\ \tau_y \\ \tau_z \end{bmatrix} = \begin{bmatrix} 1 & 1 & 1 & 1 \\ \frac{\sqrt{2}}{2}d & \frac{\sqrt{2}}{2}d & -\frac{\sqrt{2}}{2}d & -\frac{\sqrt{2}}{2}d \\ \frac{\sqrt{2}}{2}d & -\frac{\sqrt{2}}{2}d & \frac{\sqrt{2}}{2}d & -\frac{\sqrt{2}}{2}d \\ \frac{k}{b} & -\frac{k}{b} & \frac{k}{b} & -\frac{k}{b} \end{bmatrix} \begin{bmatrix} f_1 \\ f_2 \\ f_3 \\ f_4 \end{bmatrix}, \tag{1.57}$$

where the forces are given by

$$\begin{bmatrix} f_1 \\ f_2 \\ f_3 \\ f_4 \end{bmatrix} = \begin{bmatrix} \frac{1}{4} & \frac{\sqrt{2}}{4d} & \frac{\sqrt{2}}{4d} & \frac{b}{4k} \\ \frac{1}{4} & \frac{\sqrt{2}}{4d} & -\frac{\sqrt{2}}{4d} & -\frac{b}{4k} \\ \frac{1}{4} & -\frac{\sqrt{2}}{4d} & -\frac{\sqrt{2}}{4d} & \frac{b}{4k} \\ \frac{1}{4} & -\frac{\sqrt{2}}{4d} & \frac{\sqrt{2}}{4d} & -\frac{b}{4k} \end{bmatrix} \begin{bmatrix} u_1 \\ u_2 \\ u_3 \\ u_4 \end{bmatrix}. \tag{1.58}$$

Finally, in order to obtain the PWM for implementation, the angular speed must be obtained by substituting (**1.39**) into (**1.58**), where the square speed is given by

$$\begin{bmatrix} \Omega_1^2 \\ \Omega_2^2 \\ \Omega_3^2 \\ \Omega_4^2 \end{bmatrix} = \begin{bmatrix} \frac{1}{4b} & \frac{\sqrt{2}}{4bd} & \frac{\sqrt{2}}{4bd} & \frac{1}{4k} \\ \frac{1}{4b} & \frac{\sqrt{2}}{4bd} & -\frac{\sqrt{2}}{4bd} & -\frac{1}{4k} \\ \frac{1}{4b} & -\frac{\sqrt{2}}{4bd} & -\frac{\sqrt{2}}{4bd} & \frac{1}{4k} \\ \frac{1}{4b} & -\frac{\sqrt{2}}{4bd} & \frac{\sqrt{2}}{4bd} & -\frac{1}{4k} \end{bmatrix} \begin{bmatrix} u_1 \\ u_2 \\ u_3 \\ u_4 \end{bmatrix}. \tag{1.59}$$

1.3 Interactive Tilt-rotor.

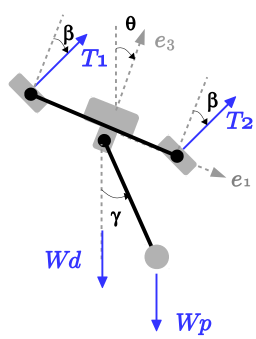

Figure 1.4. Tilt-rotor forces exerted.

The dynamical model is derived by means of the Euler-Lagrange approach. In this formulation, the object is considered as two different systems in two-dimensions. The first one is the rotorcraft system, where it is considered the rotorcraft mass ($m_r \in \mathbb{R}_+$), its angular moment ($\theta \in \mathbb{R}$) and a thrust force ($T = T_1 + T_2$) acting. Then, the pendulumlike system with a pendulumlike payload ($m_p \in \mathbb{R}_+$) and a pendulum angular moment ($\gamma \in \mathbb{R}$). Both systems are illustrated in figure 1.4.

In order to find the equations of motion, we will consider the Euler-Lagrange formalism. To this end, it will be necessary to know the kinetic and potential energies for the rotorcraft and the pendulum-like system.

1.3.1 Kinetic Energy

The kinetic energy $\mathcal{K}_r$ of the rotorcraft is given by:

$$\mathcal{K}_r = \frac{1}{2} I_r \dot{\theta}^2 + \frac{1}{2} I_p \dot{\gamma}^2 + \frac{1}{2} m_r \dot{x}^2 + \frac{1}{2} m_r \dot{z}^2, \tag{1.60}$$

where I_r and $I_p \in \mathbb{R}$ denotes the inertia tensor of the rotor craft and the pendulum-like, respectively. Additionally, $I_p := m_p l_p^2$ and x, $z \in \mathbb{R}$ are the rotorcraft position with respect to the inertial frame of reference. For the kinetic energy of the pendulum-like, we have:

$$\mathcal{K}_p = \frac{1}{2} m_p \dot{x}_p^2 + \frac{1}{2} m_p \dot{z}_p^2, \tag{1.61}$$

where x_p, $z_p \in \mathbb{R}$ are the pendulum-like gravity center position. In fact, these positions can be described as

$$x_p = x - l_p \sin(\gamma + \theta), \tag{1.62}$$
$$z_p = z - l_p \cos(\gamma + \theta). \tag{1.63}$$

Hence, the kinetic energy of the pendulum-like can be rewritten as

$$\begin{aligned}\mathcal{K}_p =& \frac{1}{2} m_p \dot{x}^2 + \frac{1}{2} m_p \dot{z}^2 - \dot{x}(\dot{\gamma} + \dot{\theta}) m_p l_p \cos(\gamma + \theta) + \\ & \dot{z}(\dot{\gamma} + \dot{\theta}) m_p l_p \sin(\gamma + \theta) + \frac{1}{2} m_p l_p^2 (\dot{\gamma} + \dot{\theta})^2.\end{aligned} \tag{1.64}$$

Thus, the total kinetic energy is given by

$$\mathcal{K}_T = \mathcal{K}_r + \mathcal{K}_p. \tag{1.65}$$

1.3.2 Potential Energy

The potential energy of the rotorcraft is given by

$$\mathcal{P}_r = m_r g z, \tag{1.66}$$

while for the pendulum-like is given by

$$\mathcal{P}_p = m_p g \left(z - l_p \cos\left(\gamma + \theta\right)\right). \tag{1.67}$$

Then, the total potential energy can be written as

$$\mathcal{P}_T = \mathcal{P}_r + \mathcal{P}_p. \tag{1.68}$$

1.3.3 Rotorcraft dynamics

Consider the generalized coordinates $\boldsymbol{q} \in \mathbb{R}^4$ and the control inputs vector about the inertial frame $\boldsymbol{U} \in \mathbb{R}^4$ be given by:

$$\boldsymbol{q} := \begin{bmatrix} x & z & \theta & \gamma \end{bmatrix}^T, \quad \boldsymbol{U} := \begin{bmatrix} u_x & u_z & u_\theta & u_\gamma \end{bmatrix}^T.$$

From the Euler-Lagrange formalism we know that the Lagrangian $\mathcal{L} \in \mathbb{R}$ is defined as

$$\mathcal{L} = \mathcal{K}_T - \mathcal{P}_T, \tag{1.69}$$

whereas the Euler-Lagrange equation is derived from (1.5).

The partial derivative of the Lagrangian $\mathcal{L}$ with respect to $\boldsymbol{q}$

$$\begin{aligned}
\frac{\partial \mathcal{L}}{\partial x} &= 0, \\
\frac{\partial \mathcal{L}}{\partial z} &= -m_r g - m_p g, \\
\frac{\partial \mathcal{L}}{\partial \theta} &= \dot{x}(\dot{\gamma}+\dot{\theta})m_p l_p \sin(\gamma+\theta) + \dot{z}(\dot{\gamma}+\dot{\theta})m_p l_p \cos(\gamma+\theta) - m_p g l_p \sin(\gamma+\theta), \\
\frac{\partial \mathcal{L}}{\partial \gamma} &= \dot{x}(\dot{\gamma}+\dot{\theta})m_p l_p \sin(\gamma+\theta) + \dot{z}(\dot{\gamma}+\dot{\theta})m_p l_p \cos(\gamma+\theta) - m_p g l_p \sin(\gamma+\theta),
\end{aligned}$$

afterwards the Lagrangian partial derivative with respect to $\dot{\boldsymbol{q}}$ is

$$\begin{aligned}
\frac{\partial \mathcal{L}}{\partial \dot{x}} &= (m_r+m_p)\dot{x} - (\dot{\gamma}+\dot{\theta})m_p l_p \cos(\gamma+\theta), \\
\frac{\partial \mathcal{L}}{\partial \dot{z}} &= (m_r+m_p)\dot{z} + (\dot{\gamma}+\dot{\theta})m_p l_p \sin(\gamma+\theta), \\
\frac{\partial \mathcal{L}}{\partial \dot{\theta}} &= I_r\dot{\theta} - \dot{x}m_p l_p \cos(\gamma+\theta) + \dot{z}m_p l_p \sin(\gamma+\theta) + m_p l_p^2(\dot{\gamma}+\dot{\theta}), \\
\frac{\partial \mathcal{L}}{\partial \dot{\gamma}} &= -\dot{x}m_p l_p \cos(\gamma+\theta) + \dot{z}m_p l_p \sin(\gamma+\theta) + m_p l_p^2(\dot{\gamma}+\dot{\theta}) + m_p l_p^2\dot{\gamma},
\end{aligned}$$

and finally the time derivative is

$$\begin{aligned}
\frac{d}{dt}\left(\frac{\partial \mathcal{L}}{\partial \dot{x}}\right) &= (m_r+m_p)\ddot{x} - (\ddot{\gamma}+\ddot{\theta})m_p l_p \cos(\gamma+\theta) + (\dot{\gamma}+\dot{\theta})^2 m_p l_p \sin(\gamma+\theta), \\
\frac{d}{dt}\left(\frac{\partial \mathcal{L}}{\partial \dot{z}}\right) &= (m_r+m_p)\ddot{z} + (\ddot{\gamma}+\ddot{\theta})m_p l_p \sin(\gamma+\theta) + (\dot{\gamma}+\dot{\theta})^2 m_p l_p \cos(\gamma+\theta), \\
\frac{d}{dt}\left(\frac{\partial \mathcal{L}}{\partial \dot{\theta}}\right) &= I_r\ddot{\theta} - \ddot{x}m_p l_p \cos(\gamma+\theta) + \dot{x}(\dot{\gamma}+\dot{\theta})m_p l_p \sin(\gamma+\theta) + \ddot{z}m_p l_p \sin(\gamma+\theta) \\
&\quad + \dot{z}(\dot{\gamma}+\dot{\theta})m_p l_p \cos(\gamma+\theta) + m_p l_p^2(\ddot{\gamma}+\ddot{\theta}), \\
\frac{d}{dt}\left(\frac{\partial \mathcal{L}}{\partial \dot{\gamma}}\right) &= -\ddot{x}m_p l_p \cos(\gamma+\theta) + \dot{x}(\dot{\gamma}+\dot{\theta})m_p l_p \sin(\gamma+\theta) + \ddot{z}m_p l_p \sin(\gamma+\theta) \\
&\quad + \dot{z}(\dot{\gamma}+\dot{\theta})m_p l_p \cos(\gamma+\theta) + 2m_p l_p^2\ddot{\gamma} + m_p l_p^2\ddot{\theta}.
\end{aligned}$$

Thus, the dynamics of the aerial robot is described as follows:

$$M(\boldsymbol{q})\ddot{\boldsymbol{q}} + C(\dot{\boldsymbol{q}},\boldsymbol{q})\dot{\boldsymbol{q}} + \boldsymbol{G}(\boldsymbol{q}) = \mathbf{U}, \tag{1.70}$$

with $M(\boldsymbol{q}) \in \mathbb{R}^{4\times4}$ is the inertia matrix, $C(\dot{\boldsymbol{q}},\boldsymbol{q}) \in \mathbb{R}^{4\times4}$ is the Coriolis matrix, and $\boldsymbol{G}(\boldsymbol{q}) \in \mathbb{R}^4$ is the gravity vector. It is worth noting that $M(\boldsymbol{q})$ is a definite positive matrix. These matrices are given as follow

$$M(\boldsymbol{q}) = \begin{bmatrix} m_r + m_p & 0 & a & a \\ 0 & m_r + m_p & b & b \\ a & b & I_r + m_p l_p^2 & m_p l_p^2 \\ a & b & m_p l_p^2 & 2m_p l_p^2 \end{bmatrix},$$

$$C(\dot{\boldsymbol{q}}, \boldsymbol{q}) = \begin{bmatrix} 0 & 0 & c & c \\ 0 & 0 & d & d \\ 0 & 0 & 0 & 0 \\ 0 & 0 & 0 & 0 \end{bmatrix},$$

$$\boldsymbol{G}(\boldsymbol{q}) = \begin{bmatrix} 0 \\ (m_r + m_p)g \\ m_p l_p g \sin(\gamma + \theta) \\ m_p l_p g \sin(\gamma + \theta) \end{bmatrix},$$

where

$$\begin{aligned} a &= -m_p l_p \cos(\gamma + \theta), \\ b &= m_p l_p \sin(\gamma + \theta), \\ c &= \left(\dot{\gamma} + \dot{\theta}\right) m_p l_p \sin(\gamma + \theta), \\ d &= \left(\dot{\gamma} + \dot{\theta}\right) m_p l_p \cos(\gamma + \theta). \end{aligned}$$

Remark 1 *Using Christoffel coefficients, the matrix $C(\boldsymbol{q}, \dot{\boldsymbol{q}})$ and the time derivative of the inertia matrix $\dot{M}(\boldsymbol{q})$ satisfies*

$$\dot{\boldsymbol{q}}^T \left[\frac{1}{2}\dot{M}(\boldsymbol{q}) - C(\boldsymbol{q}, \dot{\boldsymbol{q}})\right] \dot{\boldsymbol{q}} = 0 \quad \forall \quad \boldsymbol{q}, \dot{\boldsymbol{q}} \in \mathbb{R}^n$$

and

$$\dot{M}(\boldsymbol{q}) = C(\boldsymbol{q}, \dot{\boldsymbol{q}}) + C(\boldsymbol{q}, \dot{\boldsymbol{q}})^T \quad \forall \quad \boldsymbol{q}, \dot{\boldsymbol{q}} \in \mathbb{R}^n.$$

Finally, the rotorcraft's control input vector $\boldsymbol{U}$ corresponds to:

$$\boldsymbol{U} = \begin{bmatrix} u_x \\ u_z \\ u_\theta \\ u_\gamma \end{bmatrix} = \begin{bmatrix} (T_1 + T_2)\sin(\theta + \beta) \\ (T_1 + T_2)\cos(\theta + \beta) \\ (T_1 - T_2)\cos\beta \\ \tau_\gamma \end{bmatrix}. \tag{1.71}$$

For control design purposes, the equation (1.71) is rewritten as

$$\boldsymbol{U} = \begin{bmatrix} u_2 \sin(\theta + u_1) \\ u_2 \cos(\theta + u_1) \\ u_3 \cos u_1 \\ u_4 \end{bmatrix}, \tag{1.72}$$

where it is clear that every DOFs can be driven by a corresponding control input u_i with $i \in \{1, \ldots, 4\}$.

CHAPTER 2

NONLINEAR CONTROL APPROACHES FOR NONLINEAR SYSTEMS

The nonlinear systems are the most common physical systems that the postgraduate in control engineering students analyze and design. The dynamics of this systems are described by ordinary differential equations and satisfies some fundamental properties. These properties allows us to set some control approaches like stability, control (backstepping, nested saturations, immersion and invariance) and observer (immersion and invariance and nonlinear disturbance observer) techniques.

In the current chapter, we give a survey of the main theory of the nonlinear control approaches mentioned before. First, an overview of the stability methods is given, afterward, we present an introduction to the concepts of some often used nonlinear control approaches.

2.1 Stability

The stability theory is an important concept for the control engineering subject. There are different kinds of stability problems that arise in the study of dynamical systems. The definitions presented in this section are well known and have been discussed in the nonlinear control literature like [13], [14] and other references.

Consider the following autonomous system

$$\dot{\boldsymbol{x}} = f(\boldsymbol{x}(t)) \tag{2.1}$$

and let $\varphi(t)$ be a particular solution of (**2.1**).

Definition 1 (Stability) *[13] The solution $\varphi(t)$ is "stable" in $[0, +\infty)$, if $\forall \varepsilon > 0$ and $t_0 \geq 0 \; \exists \; \delta(\varepsilon, t_0) =: \delta > 0$ such that $\forall \boldsymbol{x_0} \in B_\delta(\varphi(t_0))$, the solution $\boldsymbol{x}(t; t_0, \boldsymbol{x_0})$ is defined and satisfies*

$$\sup_{t \geq t_0} \parallel \boldsymbol{x}(t; t_0, \boldsymbol{x_0}) - \varphi(t) \parallel < \varepsilon$$

where $\boldsymbol{x}(t; t_0, \boldsymbol{x_0})$ is a solution of (**2.1**) *defined $\forall t \geq t_0$.*

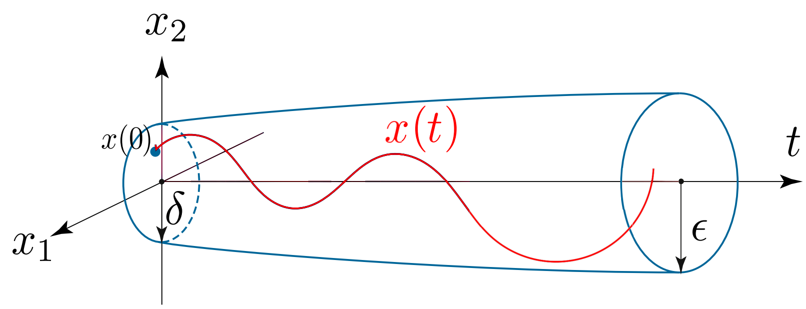

Figure 2.1. Stability.

Definition 2 (Asymptotic Stability) *[13] The solution $\varphi(t)$ is asymptotically stable in $[0, +\infty)$, if it is stable, and besides $\exists\ \gamma(t_0) =: \gamma > 0$ such that $\forall \boldsymbol{x_0} \in B_\delta(\varphi(t_0))$, the solution $\boldsymbol{x}(t; t_0, \boldsymbol{x_0})$ is defined and satisfies*

$$\lim_{t\to\infty} \sup \parallel \boldsymbol{x}(t; t_0, \boldsymbol{x_0}) - \varphi(t) \parallel = \varepsilon$$

where $\boldsymbol{x}(t; t_0, \boldsymbol{x_0})$ is a solution of (**2.1**) *defined $\forall t \geq t_0$.*

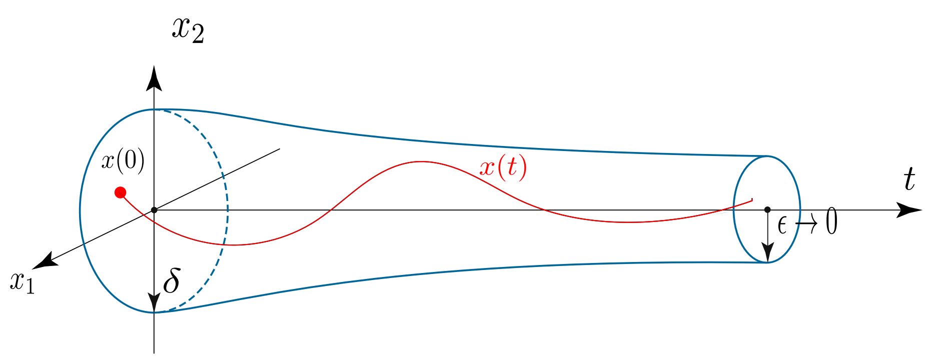

Figure 2.2. Asymptotic stability.

2.2 Lyapunov's Stability Theorem

The most used tool for stability analysis in dynamical systems is the Lyapunov's stability theorem. An equilibrium point is stable if all solutions starting at nearby points stay nearby; otherwise, it is unstable. It is asymptotically stable if all solutions starting at nearby points not only stay nearby, but also tend to the equilibrium point as time approaches infinity [13]. This theorem can be established in

Theorem 1 *[13] Let $\boldsymbol{x} = 0$ be an equilibrium point for* (**2.1**) *and $D \subset \mathbb{R}^n$ be a domain containing the origin. Let $V : \mathbb{R}^n \longrightarrow \mathbb{R}$ be a continuously differentiable (i.e. $V \in \mathscr{C}^1(\mathbb{R}^n, \mathbb{R})$) function such that*

(i) $V(0) = 0$ *and* $V(x) > 0 \qquad \forall x \in D - \{0\}$,

(ii) $\dot{V}(x) \leq 0 \qquad \forall x \in D$.

Then, $x = 0$ is stable. Moreover, if

$$\dot{V}(x) < 0 \quad \in D - \{0\}, \tag{2.2}$$

then $x = 0$ is asymptotically stable.

2.3 Barbashin-Krasovskii Theorem

Theorem 2 *Let $x = 0$ be an equilibrium point for (2.1). Let $V : \mathbb{R}^n \longrightarrow \mathbb{R}$ be a continuously differentiable function such that*

$$V(0) = 0 \qquad and \qquad V(x) > 0, \quad \forall x \neq 0 \tag{2.3}$$
$$\| x \| \longrightarrow \infty \qquad \Rightarrow \qquad V(x) \longrightarrow \infty \tag{2.4}$$
$$\dot{V}(x) < 0 \qquad , \qquad \forall x \neq 0 \tag{2.5}$$

then $x = 0$ is globally asymptotically stable.

2.4 LaSalle's Theorem

A powerful tool to assure asymptotic stability in nonlinear systems is the LaSalle's theorem.

Theorem 3 *[13] Let $\Omega \subset D$ be a compact set that is positively invariant with respect to (2.1). Let $V : D \longrightarrow \mathbb{R}$ be a continuously differentiable function such that*

$$\dot{V}(x) \leq 0 \quad \in \quad \Omega.$$

Let E be the set of all points in Ω where $\dot{V}(x) \leq 0$. Let M be the largest invariant set in E. Then every solution starting in Ω approaches M as $t \longrightarrow \infty$.

Example

Consider

$$\begin{aligned} \dot{x}_1 &= x_2, \\ \dot{x}_2 &= -x_1^3 - x_2. \end{aligned} \tag{2.6}$$

We propose the Lyapunov's function

$$\nu(x) = \frac{1}{2}\left[\frac{x_1^{2p}}{p} + \frac{x_2^{2q}}{q}\right]$$

where its gradient is

$$\nabla \nu = \begin{bmatrix} x_1^{2p-1} \\ x_2^{2q-1} \end{bmatrix}.$$

Therefore the time derivative of the Lyapunov's function is

$$\begin{aligned}\dot{\nu} &= x_1^{2p-1}(x_2) - x_2^{2q-1}(x_1^3 + x_2)\\ &= x_1^{2p-1}x_2 - x_1^3x_2^{2q-1} - x_2^{2q}.\end{aligned}$$

In order to ensure the stability, we solve

$$\begin{aligned}2p-1=3 &\;\;\Rightarrow\;\; p=2,\\ 2q-1=1 &\;\;\Rightarrow\;\; q=1,\end{aligned}$$

where the Lyapunov's function is

$$\nu(x) = \frac{1}{4}x_1^4 + \frac{1}{2}x_2^2$$

then its time derivative is

$$\dot{\nu}(x) = -x_2^2.$$

Thus the equilibrium point is stable.

Applying LaSalle's theorem

$$\mathbb{R} : \{(x,0) \in \mathbb{R}^2 : \dot{\nu} = 0\}.$$

Let $x_2 = 0$, it implies that $\dot{x}_1 = 0 \Rightarrow x_1(t) = k$ with k as a constant. Therefore $\dot{x}_2 = 0$ and from (**2.6**) we have

$$\begin{aligned}0 &= -k^3\\ \Rightarrow x_1 &= 0\end{aligned}$$

as a result $M\{\vec{0}\}$, which implies that the equilibrium point is asymptotically stable.

2.5 Controllers

The nonlinear control is a complex task due to the complexity of the maths. Also, there are different kinds of control problems, like stabilization, tracking, and disturbance rejection or attenuation (and various combinations of them). This wide variety of control problems leads to a large number of controllers for nonlinear or linear physical systems in literature.

This section resumes the nonlinear controllers theory presented in this work. This controllers are presented for stabilization and tracking problems.

2.5.1 Backstepping

Backstepping control is a popular method for controlling nonlinear systems. This control technique was developed in 1990 by Petar V. Kokotvic and nowadays remains as a good introduction into the nonlinear controllers. In the following, a review of this technique is given.

Consider the system

$$\dot{x} = f(x) + g(x)\zeta, \tag{2.7}$$
$$\dot{\zeta} = u, \tag{2.8}$$

where $x \in \mathbb{R}^n$, $\zeta \in \mathbb{R}$ and $f(0) = 0$. Assume that exists a continuous differentiable function $\alpha(x)$ with $\alpha(0)$, such that the origin of the system

$$\dot{x} = f(x) + g(x)\alpha(x) \tag{2.9}$$

is globally asymptotically stable (GAS). Then, it is necessary to find a control law $u(x, \zeta)$ such that the origin $(x, \zeta) = (0, 0)$ is GAS.

Proposition 1 (Backstepping [13]) *Let f and g be smooth vector fields with $f(0) = 0$. Assume that $\exists \alpha(x) \in \mathscr{C}^1$ with $\alpha(0) = 0$ and a positive defined function $\mathcal{V}(x)$ which is radially unbounded such that*

$$\left\langle \frac{\partial \mathcal{V}}{\partial x}, f(x) + g(x)\alpha(x) \right\rangle < 0, \forall x \neq 0. \tag{2.10}$$

Then, the origin $(x, \zeta) = (0, 0)$ of the extended system:

$$\begin{aligned} \dot{x} &= f(x) + g(x)\zeta, \\ \dot{\zeta} &= u, \end{aligned} \tag{2.11}$$

will be GAS, with the control law:

$$u(x, \zeta) = -K(\zeta - \alpha(x)) + \left\langle \frac{\partial \alpha}{\partial x}, \dot{x} \right\rangle - \left\langle \frac{\partial \mathcal{V}}{\partial x}, g(x) \right\rangle, \tag{2.12}$$

and the function:

$$\widetilde{\mathcal{V}}(x, \zeta) := \mathcal{V}(x) + \frac{1}{2}(\zeta - \alpha(x))^2, \tag{2.13}$$

as its Lyapunov's function.

Example

Let

$$\begin{aligned} \dot{x} &= x + x^3 + \xi, \\ \dot{\xi} &= u. \end{aligned} \tag{2.14}$$

Consider the associated system

$$\dot{x} = x + x^3 + \tilde{u}$$

and the Lyapunov's function

$$\nu(x) = \frac{1}{2}x^2.$$

Therefore, the time derivative of the Lyapunov's function is

$$\begin{aligned} \dot{\nu} &= x\dot{x} = x(x + x^3 + \tilde{u}) \\ &= x^2 + x^4 + x\tilde{u}. \end{aligned}$$

Proposing

$$\tilde{u} = -kx$$

the new time derivative of the Lyapunov's function is

$$\begin{aligned} \dot{\nu} &= -(k-1)x^2 + x^4 \\ &= -x^2\left[(k-1) - x^2\right]. \end{aligned}$$

where considering $|x| < \sqrt{k-1}$ with $k > 1$ it is obtained

$$\dot{\nu} < 0,$$

the origin is asymptotically stable.

Assume $\alpha(x) = -2x$, then

$$\begin{aligned} f(x) = x + x^3 \quad &; \quad g(x) = 1; \\ \alpha(x) = -2x \quad &; \quad \nu(x) = \frac{1}{2}x^2; \\ \frac{\partial \nu}{\partial x} = x \quad &; \quad \frac{\partial \alpha}{\partial x} = -2. \end{aligned}$$

Applying the variable change $z := \xi - \alpha(x) = \xi + 2x$ then

$$\begin{aligned} \dot{x} &= x + x^3 + (z - 2x) \\ \dot{z} &= u - \left\langle \frac{\partial \alpha}{\partial x}, \dot{x} \right\rangle = u + 2\left[x + x^3 + (z - 2x)\right] \\ \Rightarrow \dot{x} &= -x + x^3 + z \\ \dot{z} &= u + 2\left[-x + x^3 + z\right]. \end{aligned}$$

Finally

$$\begin{aligned} u(x,\xi) &= -k\left[\xi + 2x\right] + \left\langle \frac{\partial \alpha}{\partial x}, \dot{x} \right\rangle - \left\langle \frac{\partial \nu}{\partial x}, g(x) \right\rangle \\ &= -k\left[\xi + 2x\right] - 2\left[-x + x^3 + (\xi + 2x)\right] - x \\ &= -k\left[\xi + 2x\right] - 2\left[-x + x^3 + z\right] - x \\ &= -k\left[\xi + 2x\right] + x - 2\left[x^3 + z\right]. \end{aligned}$$

2.5.2 Nested Saturation

This nonlinear control approach was presented in 1992 by Andrew Teel in [15], and it proposes the stabilization for a chain of integrators of arbitrary order, via the combination of saturation functions with a linear feedback.

Definition 3 *[15][Lineal Saturation]Given two positive constants $L,\ M$ with $L \leq M$, a function $\sigma : \mathbb{R} \to \mathbb{R}$ is said to be a linear saturation for (L, M) if it is a continuous, nondecreasing function satisfying*

- $s\sigma(s) > 0\ \forall s \neq 0$;
- $\sigma(s) = s$ *when* $|s| \leq L$;
- $|\sigma(s)| \leq M\ \forall s \in \mathbb{R}$

In the subsequent control design, one can choose arbitrarily smooth functions out of this class. Now consider the linear system consisting of multiple integrators

$$\dot{x}_1 = x_2,\ \ldots,\ \dot{x}_n = u. \tag{2.15}$$

We are searching for a bounded control that will globally asymptotically stabilize (**2.15**).The Nested Saturations main result is:

Theorem 4 *There exist linear functions $h_i : \mathbb{R}^n \to \mathbb{R}$ such that, for any set of positive constants $\{(L_i, M_i)\}$ where $L_i \leq M_i$ for $i = 1, 2, \ldots, n$ and $M_i < \frac{1}{2}L_{i+1}$ for $i = 1, 2, \ldots, n-1$, and for any set of functions $\{\sigma_i\}$ that are linear saturations for $\{(L_i, M_i)\}$, the bounded control*

$$u = -\sigma_n(h_n(x) + \sigma_{n-1}(h_{n-1}(x) + \cdots + \sigma_1(h_1(x))\cdots)), \tag{2.16}$$

results in global asymptotic stability for the system (**2.15**).

Corollary 1 *Consider the nonlinear system*

$$\dot{x}_1 = x_2,\ \ldots,\ \dot{x}_n = \sigma_{n+1}(u),\ y = x_1. \tag{2.17}$$

Here σ_{n+1} is a linear saturation for (L_{n+1}, M_{n+1}). The task is to cause y to track a desired reference trajectory y_d given by $y_d, \dot{y}_d, \ddot{y}_d, \ldots, y_d^{(n)}$.

If $|y_d^{(n)}(t) \leq L_{n+1} - \epsilon|$ for all $t \geq t_0$ and for some $\epsilon > 0$ then there exist linear functions $h_i : \mathbb{R}^n \to \mathbb{R}$ such that for any set of positive constants $\{(L_i, M_i)\}$ where $M_n < \epsilon$, $L_i \leq M_i$ for $i = 1, 2, \ldots, n$ and $M_i \leq \frac{1}{2}L_{i+1}$ for $i = 1, 2, \ldots, n-1$, and for any set of functions $\{\sigma_i\}$ that are linear saturations for $\{(L_i, M_i)\}$ the feedback

$$u = y_d^{(n)} - \sigma_n(h_n(\tilde{x}) + \sigma_{n-1}(h_{n-1}(\tilde{x}) + \cdots + \sigma_1(h_1(\tilde{x}))\cdots)), \tag{2.18}$$

where $\tilde{x}$ is defined as $\tilde{x} = x_i - y_d^{(i-1)}$ for $i = 1, 2, \ldots, n$, results in asymptotic tracking for the system (**2.17**).

Example

Consider the pendulum system given by

$$\begin{aligned}\dot{x}_1 &= x_2,\\ \dot{x}_2 &= -\frac{g}{l}\sin(x_1) - \frac{k}{m}x_2 + \frac{1}{ml^2}T\end{aligned}$$

where g, m, l and $k \in \mathbb{R}$ are the gravity, the pendulum mass, the pendulum's arm length and the friction constant respectively and T is the torque input. The states x_1 and x_2 are the angular position and the angular speed.

Defining the control input T as

$$T = (ml^2)\left(\frac{g}{l}\sin(x_1) + \frac{k}{m}x_2 + v\right),$$

the pendulum's system can be rewritten as follows

$$\begin{aligned}\dot{x}_1 &= x_2,\\ \dot{x}_2 &= v.\end{aligned}$$

From nested saturations theorem we know that the control input which stabilizes the system is

$$v = -\sigma_2(h_2(x) + \sigma_1(h_1(x)))$$

where σ_1 and σ_2 are lineal saturation functions, h_1 and h_2 are lineal functions defined by

$$\begin{aligned}h_1(x) &= x_1 + x_2,\\ h_2(x) &= x_2.\end{aligned}$$

Therefore the control input obtained for the pendulum's system is

$$T = (ml^2)\left(\frac{g}{l}\sin(x_1) + \frac{k}{m}x_2 - \sigma_2(h_2(x) + \sigma_1(h_1(x)))\right).$$

2.5.3 Immersion and Invariance (I&I)

The I&I control technique was presented by Alessandro Astolfi and Romeo Ortega in 2003. This method relies upon the notions of system immersion and manifold invariance and, in principle, does not require the knowledge of a (control) Lyapunov function.

Theorem 5 *[16]*

Consider the system

$$\dot{\mathbf{x}} = f(x) + g(x)u \tag{2.19}$$

with state $\mathbf{x} \in \mathbb{R}^n$ and control $\mathbf{u} \in \mathbb{R}^m$ with an equilibrium point $\mathbf{x} \in \mathbb{R}^n$ to be stabilized. Let $p < n$ and assume we can find mappings

$\alpha(\cdot) : \mathbb{R}^p \to \mathbb{R}^p \quad \pi(\cdot) : \mathbb{R}^p \to \mathbb{R}^n \quad c(\cdot) : \mathbb{R}^p \to \mathbb{R}^m \quad \phi(\cdot) : \mathbb{R}^n \to \mathbb{R}^{n-p} \quad \psi(\cdot,\cdot) : \mathbb{R}^{n\times(n-p)} \to \mathbb{R}^m$
such that the following hold

(H1) (Target system) The system

$$\dot{\boldsymbol{\xi}} = \alpha(\xi) \tag{2.20}$$

with state $\boldsymbol{\xi} \in \mathbb{R}^p$, has a globally asymptotically stable equilibrium at $\boldsymbol{\xi} \in \mathbb{R}^p$ and $\mathbf{x} = \pi(\boldsymbol{\xi})$.

(H2) (Immersion condition) For all $\boldsymbol{\xi} \in \mathbb{R}^p$

$$f(\pi(\boldsymbol{\xi})) + g(\pi(\boldsymbol{\xi}))c(\pi(\boldsymbol{\xi})) = \frac{\partial(\pi)}{\partial(\boldsymbol{\xi})}\alpha(\boldsymbol{\xi}) \tag{2.21}$$

(H3) (Implicit manifold) The following set identity holds

$$\{\mathbf{x} \in \mathbb{R}^n \mid \phi(\mathbf{x}) = 0\} = \{\mathbf{x} \in \mathbb{R}^n \mid \mathbf{x} = \pi(\boldsymbol{\xi}), \boldsymbol{\xi} \in \mathbb{R}^p\} \tag{2.22}$$

(H4) (Manifold attractivity and trajectory boundedness) All trajectories of the system

$$\dot{z} = \frac{\partial \phi}{\partial x}[f(x) + g(x)\psi(x, z)] \tag{2.23}$$

$$\dot{\mathbf{x}} = f(\mathbf{x}) + g(\mathbf{x})\psi(\mathbf{x}, z) \tag{2.24}$$

are bounded and satisfy

$$\lim_{t\to\infty} z(t) = 0. \tag{2.25}$$

Then $\mathbf{x}_*$ is a globally asymptotically stable equilibrium of the closed-loop system

$$\dot{\mathbf{x}} = f(\mathbf{x}) + g(\mathbf{x})\psi(\mathbf{x}, \phi(x)). \tag{2.26}$$

Example

Let us consider the system

$$\begin{aligned} \dot{x}_1 &= x_1 x_2^3 \\ \epsilon\dot{x}_2 &= x_2 + u. \end{aligned}$$

Applying the I&I approaches

(H1) The chosen target system is

$$\dot{\boldsymbol{\xi}} = -\boldsymbol{\xi}^5.$$

(H2) For the immersion condition we fix $\boldsymbol{\pi}_1 = \boldsymbol{\xi}$.Thus, we obtain the mapping $\boldsymbol{\pi}$ given by

$$\pi(\boldsymbol{\xi}) = \begin{bmatrix} \pi_1(\boldsymbol{\xi}) \\ \pi_2(\boldsymbol{\xi}) \end{bmatrix} = \begin{bmatrix} \boldsymbol{\xi} \\ -\boldsymbol{\xi}^{\frac{4}{3}} \end{bmatrix}.$$

(H3) According to the Implicit Manifold condition we will fulfilled this condition if the map $\boldsymbol{\phi}$ is defined as

$$\boldsymbol{\phi}(\boldsymbol{x}) = x_2 + x_1^{\frac{4}{3}} = 0. \tag{2.27}$$

(H4) The off-the-manifold dynamics is given as

$$\epsilon \dot{z} = \psi(\boldsymbol{x}, z) + x_2 + \frac{4\epsilon}{3} x_1^{\frac{4}{3}} x_2^3.$$

where we choose $\psi(\boldsymbol{x}, z) = -x_2 - \frac{4\epsilon}{3} x_1^{\frac{4}{3}} x_2^3 - z$ wich yields to

$$\begin{aligned}
\epsilon \dot{z} &= -z \\
\dot{x}_1 &= x_1 x_2^3 \\
\epsilon \dot{x}_2 &= -\frac{4\epsilon}{3} x_1^{\frac{4}{3}} x_2^3 - z
\end{aligned}$$

where all the trajectories are bounded. Therefore the control law is obtained as

$$u = \psi(\boldsymbol{x}, \phi(\boldsymbol{x})) = -2x_2 - x_1^{\frac{4}{3}} \left(1 + \frac{4\epsilon}{3} x_2^3\right).$$

2.6 Observers

While we design nonlinear controllers we assume that all state variables are available for feedback. This assumption may not hold in practice because the state variables are not easy to measure or because sensing devices or transducers are not available or very expensive. For this purpose, we must design a state observer, so we will have an estimation of the state or unknown disturbances of the system.

In this section, we introduce the nonlinear observers theory applied in this work. The first observer presented is an Immersion and Invariance observer and afterward a nonlinear disturbance observer.

2.6.1 Immersion and Invariance Observer

The Immersion and Invariance was presented by Alessandro Astolfi and others in [17] published in 2008. In this book they give the main theorem and some application examples.

We consider nonlinear, time-varying systems described by equations of the form

$$\begin{aligned}
\dot{\eta} &= f_1(\eta, y, t), \\
\dot{y} &= f_2(\eta, y, t),
\end{aligned} \tag{2.28}$$

where $\eta \in \mathbb{R}^n$ is the unmeasured part of the state and $y \in \mathbb{R}^m$ is the measurable part of the state. It is assumed that the vector fields $f_1(\cdot)$ and $f_2(\cdot)$ are forward complete, *i.e.*, trajectories starting at time t_0 are defined for all times $t \geq t_0$.

Definition 4 *The dynamical system*

$$\dot{\xi} = \alpha(\xi, y, t), \tag{2.29}$$

with $\xi \in \mathbb{R}^p$, $p \geq n$, is called an observer for the system (2.28), if there exist mappings $\beta : \mathbb{R}^p \times \mathbb{R}^m \times \mathbb{R} \longrightarrow \mathbb{R}^p$ and $\phi : \mathbb{R}^n \times \mathbb{R}^m \times \mathbb{R} \longrightarrow \mathbb{R}^p$ that are left-invertible (with respect to their first argument) and such that the manifold

$$\mathcal{M} = \{(\eta, y, \xi, t) \in \mathbb{R}^n \times \mathbb{R}^m \times \mathbb{R}^p \times \mathbb{R} : \beta(\xi, y, t) = \phi(\eta, y, t)\} \tag{2.30}$$

has the following properties.

(i) *All trajectories of the extended system (2.28), (2.29) that start on the manifold $\mathcal{M}$ remain there for all future times,i.e., $\mathcal{M}$ is positively invariant.*

(ii) *All trajectories of the extended system (2.28), (2.29) that start in a neighbourhood of $\mathcal{M}$ asymptotically converge to $\mathcal{M}$.*

Theorem 6 *Consider the system (2.28), (2.29) and suppose that there exist $\mathscr{C}^1$ mappings $\beta(\xi, y, t) : \mathbb{R}^p \times \mathbb{R}^m \times \mathbb{R} \to \mathbb{R}^p$ and $\phi(\eta, y, t) : \mathbb{R}^n \times \mathbb{R}^m \times \mathbb{R} \to \mathbb{R}^p$ with a left-inverse $\phi^L : \mathbb{R}^p \times \mathbb{R}^m \times \mathbb{R} \to \mathbb{R}^n$, such that the following hold.*

(A1) *For all y, ξ and t, $\beta(\xi, y, t)$ is left-invertible with respect to ξ and*

$$det\left(\frac{\partial\beta}{\partial\xi}\right) \neq 0.$$

(A2) *The system*

$$\begin{aligned}\dot{z} = &-\frac{\partial\beta}{\partial y}\left(f_2(\hat{\eta}, y, t) - f_2(\eta, y, t)\right) + \frac{\partial\phi}{\partial y}\Big|_{\eta=\hat{\eta}} f_2(\hat{\eta}, y, t)) - \frac{\partial\phi}{\partial y} f_2(\eta, y, t) + \frac{\partial\phi}{\partial\eta}\Big|_{\eta=\hat{\eta}} f_1(\hat{\eta}, y, t)) \\ &- \frac{\partial\phi}{\partial\eta} f_1(\eta, y, t) + \frac{\partial\phi}{\partial t}\Big|_{\eta=\hat{\eta}} - \frac{\partial\phi}{\partial t}\end{aligned}, \tag{2.31}$$

with $\hat{\eta} = \phi^L(\phi(\eta, y, t) + z)$, has a (globally) asymptotically stable equilibrium at $z = 0$, uniformly in η,y and t.

Then the system (2.29) with

$$\alpha(\xi, y, t) = -\left(\frac{\partial\beta}{\partial\xi}\right)^{-1}\left(\frac{\partial\beta}{\partial y} f_2(\hat{\eta}, y, t) + \frac{\partial\beta}{\partial t} - \frac{\partial\phi}{\partial y}\Big|_{\eta=\hat{\eta}} f_2(\hat{\eta}, y, t) - \frac{\partial\phi}{\partial\eta}\Big|_{\eta=\hat{\eta}} f_1(\hat{\eta}, y, t) - \frac{\partial\phi}{\partial t}\Big|_{\eta=\hat{\eta}}\right),$$

where $\hat{\eta} = \phi^L(\beta(\xi, y, t), y, t)$, is a (global) observer for the system (2.28).

Example

Consider the system

$$\begin{aligned}\dot{I}_L &= \frac{1}{L}\left[-(1-u)V_0 + E\right] \\ \dot{V}_0 &= \frac{1}{C}\left[(1-u)I_L - \frac{V_0}{R}\right]\end{aligned}$$

where the unknown parameter is

$$\theta = \frac{1}{R},$$

then rewritting $\dot{V}_0$ is

$$\dot{V}_0 = \frac{1}{C}\left[(1-u)I_L - \theta V_0\right].$$

Defining the error

$$z = \hat{\theta} - \theta \Rightarrow \theta = \hat{\theta} - z.$$

We use the I&I observer main characteristic

$$\hat{\theta} = \xi + \eta(V_0)$$

where substituting in z

$$z = \xi + \eta(V_0) - \theta$$

and its time derivative is

$$\dot{z} = \dot{\xi} + \frac{\partial \eta}{\partial V_0}\dot{V}_0 - \dot{\theta}$$

as θ is a constant, therefore

$$\dot{\theta} = 0.$$

Thus, $\dot{z}$ can be rewritten as

$$\dot{z} = \dot{\xi} + \frac{\partial \eta}{\partial V_0}\frac{1}{C}\left[(1-u)I_L - (\hat{\theta} - z)V_0\right].$$

We propose $\dot{\xi}$ as

$$\dot{\xi} = -\frac{\partial \eta}{\partial V_0}\frac{1}{C}\left[(1-u)I_L - \hat{\theta}V_0\right].$$

where the new system obtained is

$$\dot{z} = \frac{\partial \eta}{\partial V_0}\frac{1}{C}zV_0.$$

Then, in order to ensure asymptotic stability, η is proposed as

$$\eta = -\gamma C V_0 \Rightarrow \frac{\partial \eta}{\partial V_0} = -\gamma C$$

where $\gamma > 0$. Finally

$$\dot{z} = -\gamma z V_0$$

is asymptotically stable.

2.6.2 Nonlinear Disturbance Observer (NDO)

Finally, the nonlinear disturbance observer is presented by Wen-Hua Chen and others in August 2000. In their work, they established the main idea for this observer and they applied it in robotic manipulators.The NDO is used to estimate the friction for a two-link robotic manipulator.

[18] The general Euler-Lagrange model can be represented by

$$J(\theta)\ddot{\theta} + C(\theta, \dot{\theta})\dot{\theta} + G(\theta) = T + d \tag{2.32}$$

where $\theta \in \mathbb{R}^n$, $\dot{\theta} \in \mathbb{R}^n$, $T(t) \in \mathbb{R}^n$ and $d \in \mathbb{R}^n$ are displacement, velocity, control vectors and disturbance torques, respectively.

A basic idea in the design of observers/estimators is to modify the estimation by the difference between the estimated output and the actual output. Since (2.32) can be rewritten as

$$d = J(\theta)\ddot{\theta} + C(\theta, \dot{\theta})\dot{\theta} + G(\theta) - T \tag{2.33}$$

a DO is proposed as

$$\dot{\hat{d}} = -L(\theta, \dot{\theta})\hat{d} + L(\theta, \dot{\theta})\left(J(\theta)\ddot{\theta} + C(\theta, \dot{\theta})\dot{\theta} + G(\theta) - T\right). \tag{2.34}$$

Since, in general, there is no prior information about the derivative of the disturbance , it is reasonable to suppose that

$$\dot{d} = 0 \tag{2.35}$$

which implies that the disturbance varies slowly relative to the observer dynamics. However, it will be illustrated by simulation and experiment that the observer developed in this thesis can also track some fast time-varying disturbances.

Define the observer error

$$e(t) = d - \hat{d}. \tag{2.36}$$

Combining (2.35) with the observer (2.34) yields

$$\dot{e} = \dot{d} - \dot{\hat{d}} = L(\theta, \dot{\theta})\hat{d} - L(\theta, \dot{\theta})d. \tag{2.37}$$

That is, the observer error is governed by

$$\dot{e} + L(\theta, \dot{\theta})e = 0. \tag{2.38}$$

It can be shown that the observer is globally asymptotically stable by choosing

$$L(\theta, \dot{\theta}) = diag\{c, c\} \tag{2.39}$$

where $c > 0$. More specifically, the exponential convergence rate can be specified by choosing c.

2.6.2.1 Modified Observer

Define an auxiliary variable vector

$$z = \hat{d} - p(\theta, \dot{\theta}) \tag{2.40}$$

where $z \in \mathbb{R}^n$. The designed function vector $p(\theta, \dot{\theta})$ is to be determined.

Let the function $L(\theta, \dot{\theta})$ in (2.34) be given by the following nonlinear equation:

$$L(\theta, \dot{\theta})J(\theta)\ddot{\theta} = \begin{bmatrix} \frac{\partial p(\theta,\dot{\theta})}{\partial \theta} & \frac{\partial p(\theta,\dot{\theta})}{\partial \dot{\theta}} \end{bmatrix} \begin{bmatrix} \dot{\theta} \\ \ddot{\theta} \end{bmatrix} \tag{2.41}$$

Invoking (2.40) and (2.41) with (2.34) yields

$$\begin{aligned} \dot{z} &= \dot{\hat{d}} - \frac{dp(\theta, \dot{\theta})}{dt} \\ &= \dot{\hat{d}} \begin{bmatrix} \frac{\partial p(\theta,\dot{\theta})}{\partial \theta} & \frac{\partial p(\theta,\dot{\theta})}{\partial \dot{\theta}} \end{bmatrix} \begin{bmatrix} \dot{\theta} \\ \ddot{\theta} \end{bmatrix} \\ &= -L(\theta, \dot{\theta}) \left(z + p(\theta, \dot{\theta}) \right) + L(\theta, \dot{\theta}) \left(C(\theta, \dot{\theta}) + G(\theta, \dot{\theta}) - T \right). \end{aligned} \tag{2.42}$$

Hence, the NDO is given by

$$\dot{z} = -L(\theta, \dot{\theta})z + L(\theta, \dot{\theta}) \left(C(\theta, \dot{\theta}) + G(\theta, \dot{\theta}) - T - p(\theta, \dot{\theta}) \right) \tag{2.43}$$

and

$$\hat{d} = z + p(\theta, \dot{\theta}) \tag{2.44}$$

where $L(\theta, \dot{\theta})$ is given by (2.41).

CHAPTER 3

NONLINEAR CONTROLLERS AND OBSERVERS FOR MULTI-ROTOR AIR-VEHICLES

In this chapter we will discuss the design of nonlinear controllers and observers for the aircrafts represented by their dynamical models given in chapter 1. We will analyze two differents rotorcrafts, in the first part we develope the nonlinear controllers and observers for a quadrotor, afterwards for an interactive tilt-rotor. It is important to mention that everything developed in this chapter has its theory taken from chapter 2.

3.1 Nonlinear Controllers and Observers for Quadrotor

The Quadrotors analysis has raised over the last years. Works like [2] presents nonlinear control strategies and its application. As it have been said, first we set the controllers and observers for the quadrotor.

3.1.1 Nonlinear Controllers

Our main objective is to ensure the quadrotor follows a desired trajectory with the minimum error possible, therefore, the nonlinear controllers designed in this section are developed for a tracking task.

We design three different control laws, first we introduce the Backstepping, a well known nonlinear control approach, then, Nested Saturations, where we saturate the control inputs and finally the Immersion and Invariance approach, which is a robust controller design.

3.1.1.1 Backstepping

The first control approach developed in this work is the Backstepping control technique for tracking task. The theory behind the Backstepping approach was presented in section 2.5.1.

The first subsystem to be analyzed is the rotational subsystem. For this purpose we consider the tracking error given by

$$e_\eta := \eta_d - \eta, \tag{3.1}$$

where $\eta_d \in \mathbb{R}^3$ is the desired vector for orientation. As a result the states of the rotational subsystem are defined as

$$\begin{aligned} x_{1\eta} &:= e_\eta, && (3.2)\\ x_{2\eta} &:= \dot{e}_\eta, && (3.3) \end{aligned}$$

we obtain the time derivative of each state, so the system of equations is

$$\begin{aligned} \dot{x}_{1\eta} &:= x_{2\eta}, && (3.4)\\ \dot{x}_{2\eta} &:= \ddot{\eta}_d - \ddot{\eta}. && (3.5) \end{aligned}$$

In this stage, we are going to take equation (1.38) and we isolate $\ddot{\eta}$ from it

$$\ddot{\eta} = -J^{-1}C(\eta,\dot{\eta})\dot{\eta} + J^{-1}\tau, \tag{3.6}$$

and substituting (3.6) in (3.5) we get

$$\begin{aligned} \dot{x}_{1\eta} &= x_{2\eta}, && (3.7)\\ \dot{x}_{2\eta} &= \ddot{\eta}_d + J^{-1}C(\eta,\dot{\eta})\dot{\eta} - J^{-1}\tau. && (3.8) \end{aligned}$$

In order to take the rotational subsystem given by (3.4) and (3.5) into the backstepping form, the control input τ is proposed as

$$\tau = J(\ddot{\eta}_d + J^{-1}C(\eta,\dot{\eta})\dot{\eta} - v). \tag{3.9}$$

Therefore the subsystem can be written like

$$\begin{aligned} \dot{x}_{1\eta} &= x_{2\eta},\\ \dot{x}_{2\eta} &= v. \end{aligned} \tag{3.10}$$

Assume the next variables change

$$x_{1\eta} = x, \quad x_{2\eta} = \zeta, \quad v = u,$$

we can rewrite (3.10) into

$$\begin{aligned} \dot{x} &= \zeta,\\ \dot{\zeta} &= u, \end{aligned} \tag{3.11}$$

where the system (3.11) can be viewed as a cascade connection of two components. We assume that ζ is an input of the system, thus, we consider the system $\dot{x} = \tilde{u}$.

We propose the Lyapunov's function

$$\nu(x) = \frac{1}{2}x^T x, \tag{3.12}$$

then, its time derivative is

$$\dot{\nu}(x) = x^T \dot{x}. \tag{3.13}$$

The input $\tilde{u}$ is proposed

$$\tilde{u} = -Gx \tag{3.14}$$

where $G > 0$. Substituting (3.14) in (3.13) we obtain

$$\dot{\nu}(x) = -x^T G x \tag{3.15}$$

as a result, and due to the Lyapunov's theorem, we can ensure that the origin of the system (3.11) is globally asymptotically stable.

Let

$$f(x) = 0; \quad g(x) = I; \quad \alpha(x) = -Gx;$$
$$\nu(x) = \frac{1}{2}x^T x; \quad \tfrac{\partial \nu}{\partial x} = x; \quad \frac{\partial \alpha}{\partial x} = -G;$$

hence, the Backstepping control law (2.12) is given by

$$u(x,\zeta) = -k_\eta[\zeta + Gx] - G\zeta - x, \tag{3.16}$$

which can be rewritten in terms of the states

$$u(x,\zeta) = -([k_\eta + G]\zeta + [k_\eta G + I]x). \tag{3.17}$$

Finally, substituting (3.17) in (3.9) yields to the control input τ for the rotational subsystem

$$\boxed{\tau = J(\ddot{\eta}_d + J^{-1}C(\eta,\dot{\eta})\dot{\eta} + [k_\eta + G]x_{2\eta} + [k_\eta G + I]x_{1\eta}).} \tag{3.18}$$

Meanwhile, for the translational subsystem, we consider it as an scalar problem. Therefore, the Backstepping control input will be designed first for z and afterwards for x and y.

Consider the tracking error given by

$$e_z := z_d - z, \tag{3.19}$$

where $z_d \in \mathbb{R}$ is the desired altitude of the rotorcraft. For this purpose we define the states as

$$\begin{aligned} x_{1z} &:= e_z, \\ x_{2z} &:= \dot{e}_z. \end{aligned} \tag{3.20}$$

Therefore, the time drivative of (3.20) is given by

$$\begin{aligned} \dot{x}_{1z} &:= \dot{x}_{2z}, \\ \dot{x}_{2z} &:= \ddot{z}_d - \ddot{z}. \end{aligned} \tag{3.21}$$

We isolate $\ddot{z}$ from equation (1.37)

$$\ddot{z} = \cos\theta\cos\phi\frac{U_1}{m} - g, \tag{3.22}$$

and we substitute (**3.22**) in (**3.21**) for the translational subsystem in z, which yields to

$$\begin{aligned} \dot{x}_{1z} &= x_{2z}, \\ \dot{x}_{2z} &= \ddot{z}_d - \cos\theta\cos\phi\frac{U_1}{m} + g. \end{aligned} \tag{3.23}$$

The control input U_1 is proposed like

$$U_1 = \frac{m}{\cos\theta\cos\phi}\left(\ddot{z}_d + g - v\right), \tag{3.24}$$

that yields the subsystem (**3.23**) into its backstepping form

$$\dot{x}_{1z} = x_{2z}, \tag{3.25}$$
$$\dot{x}_{2z} = v, \tag{3.26}$$

where, this subsystem, can be viewed as a cascade connection of two components too. The input of the system will be assumed as x_{2z}, hence, we can consider the system $\dot{x}_z = \tilde{u}_z$.

The Lyapunov's function proposed is

$$\nu(x_z) = \frac{1}{2}x_z^2, \tag{3.27}$$

where its time derivative is given by

$$\dot{\nu}(x_z) = x_z\dot{x_z} = x_z\tilde{u}_z. \tag{3.28}$$

In order to ensure stability, we propose the input $\tilde{u}_z$ as

$$\tilde{u}_z = -P_z x \tag{3.29}$$

where $P_z > 0$. Substituting (**3.29**) in (**3.28**) we obtain

$$\dot{\nu}(x) = -P_z x^2. \tag{3.30}$$

Therefore, the origin of the system (**3.25**) is globally asymptotically stable.

Let

$$\begin{aligned} f(x_z) = 0; \quad g(x_z) = 1; \quad \alpha(x_z) = -P_z x_z; \\ \nu(x_z) = \frac{1}{2}x_z^2; \quad \tfrac{\partial\nu}{\partial x_z} = x_z; \quad \frac{\partial\alpha}{\partial x_z} = -P_z; \end{aligned}$$

hence the Backstepping control law (**2.12**) for altitude is given by

$$v(x_{1z}, x_{2z}) = -k_z[x_{2z} + P_z x_{1z}] - P_z(x_{2z} - P_z x_{1z}) - x_{1z}, \tag{3.31}$$

which can be rewritten in terms of the states

$$v(x_{1z}, x_{2z}) = -([k_z + P_z]x_{2z} + [k_z P_z + 1]x_{1z}). \tag{3.32}$$

Finally, substituting (**3.32**) in (**3.24**) yields to the control input U_1 for the altitude in the translational subsystem

$$\boxed{U_1 = \frac{m}{\cos\theta\cos\phi}\left(\ddot{z}_d + g + [k_z + P_z]x_{2z} + [k_z P_z + 1]x_{1z}\right)} \tag{3.33}$$

where

$$\theta \neq \frac{\pi}{2} \quad and \quad \phi \neq \frac{\pi}{2}.$$

In addition the control laws for x and y are designed following a similar procedure. From (**1.37**) we isolate $\ddot{x}$ and $\ddot{y}$

$$\ddot{x} = [\cos\psi\sin\theta\cos\phi + \sin\psi\sin\phi]\frac{m}{U_1}, \tag{3.34}$$

$$\ddot{y} = [\sin\psi\sin\theta\cos\phi - \cos\psi\sin\phi]\frac{m}{U_1}, \tag{3.35}$$

where the control inputs are

$$\boxed{U_x = \frac{m}{U_1}\left(\ddot{x}_d + [k_x + P_x]x_{2x} + [k_x P_x + 1]x_{1x}\right),} \tag{3.36}$$

$$\boxed{U_y = \frac{m}{U_1}\left(\ddot{y}_d + [k_y + P_y]x_{2y} + [k_y P_y + 1]x_{1y}\right),} \tag{3.37}$$

Since the Quadrotor's system is underactuated, it is important to notice that the control laws (**3.36**) and (**3.37**) depends on the control input $U_1 > 0$.

Also, as we have six degrees of freedom, but it is possible to control only four it is necessary to calculate the desired angles required for traslation in x and y. Thus, from the control inputs U_x and U_y given by

$$U_x = \cos\psi\sin\theta\cos\phi + \sin\psi\sin\phi, \tag{3.38}$$

$$U_y = \sin\psi\sin\theta\cos\phi - \cos\psi\sin\phi, \tag{3.39}$$

we can create a system of equations where we can determinate the desired angles for displacement in the $x - y$ plane, which are given by

$$\phi_d = \arcsin(\sin\psi U_x - \cos\psi U_y), \tag{3.40}$$

$$\theta_d = \arcsin\left(\frac{\cos\psi U_x - \sin\psi U_y}{\cos\phi_d}\right), \tag{3.41}$$

where

$$\phi_d \neq \frac{\pi}{2}.$$

3.1.1.2 Nested Saturations

The second controller designed in this work was presented in section 2.5.2. Where the tracking task is introduced in corollary 1. This control approach is designed in order to ensure global asymptotic stability, however the main reason to apply this controller are the saturations implied. The saturations needed in the quadrotor's system are

- to saturate the control efforts,

- to saturate the motor velocities,
- to saturate the ϕ and θ angles.

This bounds are necessary because we need to take into account the physical limits of our electronic devices. The simulation results allow us to have big control efforts, therefore we define these real bounds.

For the rotational subsystem control law, we isolate $\ddot{\eta}$ from equation (**1.38**)

$$\ddot{\eta} = J^{-1}\tau - J^{-1}C(\eta, \dot{\eta})\dot{\eta}, \tag{3.42}$$

where the control input τ is proposed like

$$\tau = J[J^{-1}C(\eta, \dot{\eta})\dot{\eta} + \sigma_3(v)], \tag{3.43}$$

moreover, we define the states $\eta = x_{1\eta}$ and $\dot{\eta} = x_{2\eta}$ we obtain the system of differential equations

$$\begin{aligned} \dot{x}_{1\eta} &= x_{2\eta}, & (3.44)\\ \dot{x}_{2\eta} &= \sigma_3(v), & (3.45) \end{aligned}$$

where $\sigma_3(v)$ is a linear saturation.

From section 2.5.2 we propose the control input

$$v = \ddot{\eta}_d - \sigma_2\left(h_2\left(\tilde{x}_\eta\right) + \sigma_1\left(h_1\left(\tilde{x}_\eta\right)\right)\right), \tag{3.46}$$

where, e_η is the tracking error and the lineal functions $h_1(\tilde{x}_\eta)$ and $h_2(\tilde{x}_\eta)$ are given by

$$\begin{aligned} h_1(\tilde{x}_\eta) &= \tilde{x}_{2\eta} + \tilde{x}_{1\eta} = \dot{e}_\eta + e_\eta, & (3.47)\\ h_2(\tilde{x}_\eta) &= \tilde{x}_{2\eta} = \dot{e}_\eta, & (3.48) \end{aligned}$$

in addition the tracking error is given by

$$\begin{aligned} \tilde{x}_{2\eta} &= \dot{e}_\eta = \dot{\eta} - \dot{\eta}_d, & (3.49)\\ \tilde{x}_{1\eta} &= e_\eta = \eta - \eta_d. & (3.50) \end{aligned}$$

Substituting the tracking error in (**3.46**) the control input can be rewritten

$$v = \ddot{\eta}_d - \sigma_2((\dot{\eta} - \dot{\eta}_d) + \sigma_1(\dot{\eta} - \dot{\eta}_d + \eta - \eta_d)). \tag{3.51}$$

Consequently the control law obtained for the new system of differential equations is

$$\dot{x}_{2\eta} = \sigma_3(\ddot{\eta}_d - \sigma_2((\dot{\eta} - \dot{\eta}_d) + \sigma_1(\dot{\eta} - \dot{\eta}_d + \eta - \eta_d))). \tag{3.52}$$

Finally, the control input τ for the rotational system is expressed by

$$\boxed{\tau = C(\eta, \dot{\eta})\dot{\eta} + J\sigma_3\left(\ddot{\eta}_d - \sigma_2\left((\dot{\eta} - \dot{\eta}_d) + \sigma_1\left(\dot{\eta} - \dot{\eta}_d + \eta - \eta_d\right)\right)\right),} \tag{3.53}$$

where we can observe three linear saturations, which are bounded and satisfy the conditions established in theorem 4.

Meanwhile, in order to obtain the control law via Nested Saturations for the translational subsystem, it is necessary to isolate $\ddot{\xi}$ from (**1.37**)

$$\ddot{\xi} = (R^{\mathbb{A}}_{\mathbb{B}} U - G)\frac{1}{m} \quad \Rightarrow \quad \ddot{z} = \frac{\cos\theta\cos\phi}{m} U_1 - g. \tag{3.54}$$

In order to obtain the nonlinear system (**2.17**) form, we propose the control input U_1 like

$$U_1 = \frac{m}{\cos\theta\cos\phi}\left(g + \sigma_3(w)\right), \tag{3.55}$$

where $\ddot{z}$ is rewritten as linear saturation expressed by

$$\ddot{z} = \sigma_3(w). \tag{3.56}$$

Then we define the states for the altitude in the translational subsystem, $z = x_1$ and $\dot{z} = x_2$, where we obtain the new system given by

$$\begin{aligned} \dot{x}_1 &= x_2, \\ \dot{x}_2 &= \sigma_3(w). \end{aligned} \tag{3.57}$$

and then we apply the nested saturation theorem

$$w = \ddot{z}_d - \sigma_2(h_2(\tilde{x}_z) + \sigma_1(h_1(\tilde{x}_z))) \tag{3.58}$$

where w results in asymptotic tracking for the system (**3.57**). Furthermore, the tracking error will be e_z and the lineal functions $h_1(\tilde{x}_z)$ and $h_2(\tilde{x}_z)$ are given by

$$h_1(\tilde{x}_z) = \tilde{x}_{2z} + \tilde{x}_{1z} = \dot{e}_z + e_z, \tag{3.59}$$

$$h_2(\tilde{x}_z) = \tilde{x}_{2z} = \dot{e}_z, \tag{3.60}$$

also, the tracking error is given by

$$\tilde{x}_{2z} = \dot{e}_z = \dot{z} - \dot{z}_d, \tag{3.61}$$

$$\tilde{x}_{1z} = e_z = z - z_d. \tag{3.62}$$

Subsequently w is rewritten in therms of the tracking error

$$w = \ddot{z}_d - \sigma_2((\dot{z} - \dot{z}_d) + \sigma_1(\dot{z} - \dot{z}_d + z - z_d)), \tag{3.63}$$

hence the dynamic of the state x_2 is

$$\dot{x}_2 = \sigma_3(\ddot{z}_d - \sigma_2((\dot{z} - \dot{z}_d) + \sigma_1(\dot{z} - \dot{z}_d + z - z_d))), \tag{3.64}$$

thus, the control law U_1 for the translational system is given by

$$\boxed{U_1 = \frac{m}{\cos\theta\cos\phi}\left[g + \sigma_3(\ddot{z}_d - \sigma_2((\dot{z} - \dot{z}_d) + \sigma_1(\dot{z} - \dot{z}_d + z - z_d)))\right].} \tag{3.65}$$

Following a similar procedure the underactuated control laws for displacement in the $x - y$ plane are expressed by

$$\boxed{U_x = \frac{m}{U_1}\left[\sigma_3(\ddot{x}_d - \sigma_2((\dot{x} - \dot{x}_d) + \sigma_1(\dot{x} - \dot{x}_d + x - x_d)))\right],} \tag{3.66}$$

$$\boxed{U_y = \frac{m}{U_1}\left[\sigma_3(\ddot{y}_d - \sigma_2((\dot{y} - \dot{y}_d) + \sigma_1(\dot{y} - \dot{y}_d + y - y_d)))\right].} \tag{3.67}$$

3.1.1.3 Immersion and Invariance

The last control developed in this work is the Immersion and Invariance approach, which was introduced in section 2.5.3. The main objective of this nonlinear control approach is to follow a desired trajectory, therefore, let us apply it for a tracking task.

First, we begin with the quadrotor's rotational subsystem (**1.38**), which must be written in an appropriate form, so isolating $\ddot{\eta}$ we get

$$\ddot{\eta} = J^{-1}(\tau - C(\eta, \dot{\eta})\dot{\eta}). \tag{3.68}$$

Defining the tracking error like

$$e := \eta_d - \eta, \tag{3.69}$$

we assume the states in terms of the tracking error

$$x_1 = \eta_d - \eta, \tag{3.70}$$
$$x_2 = \dot{\eta}_d - \dot{\eta}. \tag{3.71}$$

As a result, our rotational subsystem is written in the state space equation

$$\begin{aligned} \dot{x}_1 &= x_2 \\ \dot{x}_2 &= \ddot{\eta}_d + J^{-1}(C(\eta, \dot{\eta})\dot{\eta} - \tau). \end{aligned} \tag{3.72}$$

We propose the virtual control input τ, in order to simplify the problem

$$\tau = J(\ddot{\eta}_d + J^{-1}C(\eta, \dot{\eta})\dot{\eta} - v), \tag{3.73}$$

hence, the new system obtained is

$$\begin{aligned} \dot{x}_1 &= x_2, \\ \dot{x}_2 &= v, \end{aligned} \tag{3.74}$$

which is in its nonlinear form $\dot{x} = f(x) + g\nu$. Where

$$f(x) = \begin{bmatrix} 0 & x_2 \\ 0 & 0 \end{bmatrix}; \quad g = \begin{bmatrix} 0 & 0 \\ 0 & 1 \end{bmatrix}; \quad \nu = \begin{bmatrix} 0 \\ v \end{bmatrix}.$$

Using the theorem introduced in section 2.5.3, we apply the Immersion and Invariance control strategy.

H1) We consider the target system as

$$\dot{\xi} = -k_\eta \xi; \quad with \quad k_\eta > 0, \tag{3.75}$$

where $k_\eta \in \mathbb{R}^{3\times 3}$, $\xi \in \mathbb{R}^3$, we ensure that the dynamics is globally asymptotically stable with unique equilibrium point.

H2) For the immersion condition it is neccesary to satisfy (2.21). We choose a mapping between the dynamical system (3.74) and the target system (3.75), given by

$$x = \pi(\xi) = \begin{bmatrix} \pi_1(\xi) \\ \pi_2(\xi) \end{bmatrix} \tag{3.76}$$

where we can fix

$$\pi_1(\xi) = \xi, \tag{3.77}$$

since we propose that the error's dynamic acts like the target system (3.75). Fixing $\pi_1(\xi)$ we can obtain the mapping $\pi_2(\xi)$, which is given by

$$\pi_2(\xi) = -k_\eta \xi, \tag{3.78}$$

H3) In order to ensure the implicit manifold the identity set must hold

$$\{x \in \mathbb{R}^2 \mid \phi(x) = 0\} = \{x \in \mathbb{R}^2 \mid x_1 = \xi, x_2 = -k_\eta \xi\}, \tag{3.79}$$

where the function $\phi(x)$ that satisfies (3.79) is

$$\phi(x) = x_2 + k_\eta x_1. \tag{3.80}$$

H4) In order to satisfy the manifold attractivity and trajectory boundedness, the trajectories (2.23) and (2.24) of the system

$$\dot{x}_1 = x_2, \tag{3.81}$$
$$\dot{x}_2 = v, \tag{3.82}$$
$$\dot{z} = k_\eta x_2 + v \tag{3.83}$$

must be bounded and satisfy (2.25). Assume v as

$$v = -k_\eta x_2 - k_{\eta 2} z, \tag{3.84}$$

the dynamical system becomes bounded in $\dot{x}$ and with an equilibrium point globally asymptotically stable in $z = 0$

$$\dot{x}_1 = x_2, \tag{3.85}$$
$$\dot{x}_2 = -k_\eta x_2 - k_{\eta 2} z, \tag{3.86}$$
$$\dot{z} = -k_{\eta 2} z. \tag{3.87}$$

After we obtained the virtual control v via the Immersion and Invariance approach, we substitute

(**3.84**) in (**3.73**), where control law for the rotational subsystem τ is given by

$$\boxed{\tau = J(\ddot{\eta}_d + J^{-1}C(\dot{\eta},\eta)\dot{\eta} + k_\eta(\dot{\eta}_d - \dot{\eta}) + k_{\eta 2}((\dot{\eta}_d - \dot{\eta}) + k_\eta(\eta_d - \eta))).} \tag{3.88}$$

On the other hand, for the translational subsystem we apply the I&I approach too. It is worth to mention that the control law design is assumed as a scalar problem. Hence, consider the translational subsystem introduced in equation (**1.37**), the altitude acceleration will be given by

$$\ddot{z} = \frac{1}{m}cos\theta cos\phi U_1 - g \tag{3.89}$$

where U_1 will be the thrust force and our control input.

Consider the next variable change for the tracking error

$$e := z_d - z \tag{3.90}$$

where z_d is the desired trajectory in z. Since we have defined the tracking error in (**3.90**), let the states of the system

$$\begin{aligned} x_1 &= z_d - z, \\ x_2 &= \dot{z}_d - \dot{z}. \end{aligned} \tag{3.91}$$

where the main goal of the control law is to lead to zero the error between the desired trajectory and the measured one.

From the states introduced in (**3.91**), the system for the control altitude in terms of the error is given by

$$\begin{aligned} \dot{x}_1 &= x_2, \\ \dot{x}_2 &= \ddot{z}_d + g - \frac{1}{m}cos\theta cos\phi U_1. \end{aligned} \tag{3.92}$$

Consider the virtual control law

$$U_1 = \frac{m}{cos\theta cos\phi}(\ddot{z}_d + g - v), \tag{3.93}$$

we obtain an appropriate system nonlinear form $\dot{x} = f(x) + g\nu$ for the I&I approach given by

$$\begin{aligned} \dot{x}_1 &= x_2 \\ \dot{x}_2 &= v \end{aligned} \tag{3.94}$$

where

$$f(x) = \begin{bmatrix} 0 & x_2 \\ 0 & 0 \end{bmatrix}; \quad g = \begin{bmatrix} 0 & 0 \\ 0 & 1 \end{bmatrix}; \quad \nu = \begin{bmatrix} 0 \\ v \end{bmatrix}.$$

Applying the Immersion and Invariance approach from section 2.5.3, we proceed to design the control law for z.

H1) The I&I requires the selection of a target system. In general, the classical target dynamics are linear therefore our target system is given by

$$\dot{\xi} = -k_1\xi; \quad with \quad k_1 > 0, \tag{3.95}$$

where we ensure a globally asymptotically stable equilibrium point.

H2) Subsequently, it is neccesary to choose the mapping π, to satisfy the immersion condition (**2.21**). The proposed mapping is given by

$$x = \pi(\xi) = \begin{bmatrix} \pi_1(\xi) \\ \pi_2(\xi) \end{bmatrix} \tag{3.96}$$

where we fix

$$\pi_1(\xi) = \xi. \tag{3.97}$$

In fact, the π_1 selection was done because we want that the trajectory of the error behaves like the dynamic of the target system (**3.95**). Having settled up $\pi_1(\xi)$, we obtain the mapping $\pi_2(\xi)$ given by

$$\pi_2(\xi) = -k_1\xi. \tag{3.98}$$

H3) According to the implicit manifold condition (**2.22**), the identity set must hold.

$$\{x \in \mathbb{R}^2 \mid \phi(x) = 0\} = \{x \in \mathbb{R}^2 \mid x_1 = \xi, x_2 = -k_1\xi\}, \tag{3.99}$$

so the function $\phi(x)$ that clearly fulfill (**3.99**) is

$$\phi(x) = x_2 + k_1x_1. \tag{3.100}$$

H4) For the manifold attractivity and trajectory boundedness, the trajectories (**2.23**) and (**2.24**) of the system

$$\dot{x}_1 = x_2, \tag{3.101}$$
$$\dot{x}_2 = v, \tag{3.102}$$
$$\dot{z} = k_1x_2 + v \tag{3.103}$$

must be bounded and satisfy (**2.25**). Thus, in order to achieve such requirement, v is proposed as

$$v = -k_1x_2 - k_2z. \tag{3.104}$$

Indeed, substituting (**3.104**) the bounded and with an unique equilibrium point globally asymptotically stable in $z = 0$ closed-loop system is given by

$$\dot{x}_1 = x_2, \tag{3.105}$$
$$\dot{x}_2 = -k_1x_2 - k_2z, \tag{3.106}$$
$$\dot{z} = -k_2z. \tag{3.107}$$

Finally, with the virtual control v via the Immersion and Invariance approach, we substitute (**3.104**) in (**3.93**), where control law for the altitude in the translational subsystem U_1 is given by

$$\boxed{U_1 = \frac{m}{cos\theta cos\phi}(\ddot{z}_d + g + k_1(\dot{z}_d - \dot{z}) + k_2((\dot{z}_d - \dot{z}) + k_1(z_d - z))).} \quad (3.108)$$

To conclude, following a similar procedure, the underactuated control laws U_x and U_y for displacement in the $x-y$ plane are expressed by

$$\begin{aligned} U_x &= \frac{m}{U_1}(\ddot{x}_d + k_3(\dot{x}_d - \dot{x}) + k_4((\dot{x}_d - \dot{x}) + k_3(x_d - x))), && (3.109) \\ U_y &= \frac{m}{U_1}(\ddot{y}_d + k_5(\dot{y}_d - \dot{y}) + k_6((\dot{y}_d - \dot{y}) + k_5(y_d - y))). && (3.110) \end{aligned}$$

3.1.2 Nonlinear Observers

After the nonlinear controllers design, we proceed to develope a parameter estimator and a state observer. Both are designed with the Immersion and Invariance Observer approach.

First we present an estimator for the mass of the quadrotor, due to the mass is an easy change parameter. This is because there are some external forces that represent a non direct mass' variation. Subsequently, we develope an observer for the quadrotor's velocities. The reason why we design this observer is because the inertial measurement unit (IMU), does not measure the translational velocity, neither other sensors.

3.1.2.1 Estimator for Quadrotor's mass

Consider the quadrotor's translational subsystem introduced in (**1.37**) with z acceleration given by

$$\ddot{z} = \cos\theta\cos\phi U_1 \frac{1}{m} - g. \quad (3.111)$$

Let $x_1 = z$ and $x_2 = \dot{z}$ be the states of the new system proposed, described by the equations

$$\begin{aligned} \dot{x}_1 &= x_2, && (3.112) \\ \dot{x}_2 &= \cos\theta\cos\phi U_1 \frac{1}{m} - g, && (3.113) \end{aligned}$$

for the procedure of the I&I estimator.

We proceed to the design of an estimator for the unknown mass parameter using the theorem introduced in section 2.6.1. Let

$$\mu := \frac{1}{m} \quad (3.114)$$

and defining the error model of μ as

$$e_{om} = \hat{\mu} - \mu, \quad (3.115)$$

where $\hat{\mu}$ has its integral α and proportional $\beta(x_2)$ part, this is

$$\hat{\mu} = \alpha + \beta(x_2). \quad (3.116)$$

Therefore, we substitute (**3.116**) in the error (**3.115**) we obtain the equation described by

$$e_{om} = \alpha + \beta(x_2) - \mu, \tag{3.117}$$

where, the mass of the quadrotor is assumed as a constant, this yields to $\dot{\mu} = 0$. Hence, the time derivative of the error (**3.117**) is given by

$$\begin{aligned} \dot{e}_{om} &= \dot{\alpha} + \frac{\partial\beta(x_2)}{\partial x_2}\dot{x}_2 - \dot{\mu}, \\ &= \dot{\alpha} + \frac{\partial\beta(x_2)}{\partial x_2}\dot{x}_2. \end{aligned} \tag{3.118}$$

Substituting (**3.113**) in (**3.118**) the error dynamics is described by

$$\dot{e}_{om} = \dot{\alpha} + \frac{\partial\beta(x_2)}{\partial x_2}\left(\cos\theta\cos\phi U_1\mu - g\right) \tag{3.119}$$

From (**3.115**), we know that $\mu = \hat{\mu} - e_{om}$, therefore (**3.119**) results in

$$\dot{e}_{om} = \dot{\alpha} + \frac{\partial\beta(x_2)}{\partial x_2}\left(\cos\theta\cos\phi U_1(\hat{\mu} - e_{om}) - g\right). \tag{3.120}$$

We split (**3.120**) with respect the error variable e_{om}, and $\dot{\alpha}$ is assumed as

$$\dot{\alpha} = -\frac{\partial\beta}{\partial x_2}\left(\cos\theta\cos\phi U_1\hat{\mu} - g\right) \tag{3.121}$$

such that the error's dynamic is transformed into

$$\dot{e}_{om} = -\frac{\partial\beta}{\partial x_2}\left(\cos\theta\cos\phi U_1 e_{om}\right). \tag{3.122}$$

Our main objective is to lead the estimation error to 0, hence, we propose $beta$ to turn (**3.122**) in the well known differential equation $\dot{e} = -Ae$, this is

$$\beta = \frac{\gamma x_2}{\cos\theta\cos\phi} \Rightarrow \frac{\partial\beta}{\partial x_2} = \frac{\gamma}{\cos\theta\cos\phi}, \tag{3.123}$$

which yields (**3.122**) into

$$\dot{e}_{om} = -\gamma U_1 e_{om}, \tag{3.124}$$

where $\gamma \in \mathbb{R}$ is a proportional gain. In conclusion the error $e_{om} \to 0$ when $t \to 0$.

3.1.2.2 Observer for Quadrotor's translational subsystem velocity

We now proceed to design the observer for unmeasured state $\dot{\xi}$ using the teorem from section 2.6.1. Consider the quadrotor's translational subsystem introduced in (**1.37**) with $\ddot{\xi}$ given by

$$\ddot{\xi} = \frac{1}{m}R_{\mathbb{B}}^{\mathbb{A}}U - G, \tag{3.125}$$

where we know that $\xi = \begin{bmatrix} x & y & z \end{bmatrix}^T$ is the position vector. Furthermore, let $x_1 = z$ and $x_2 = \dot{z}$ be the states of the system proposed, described by the equations

$$\begin{aligned} \dot{x}_1 &= x_2, \\ \dot{x}_2 &= \frac{1}{m}\cos\theta\cos\phi U_1 - g. \end{aligned} \tag{3.126}$$

We can rewrite (3.126) into a matrix form expressed by

$$\begin{aligned} \begin{bmatrix} \dot{x}_1 \\ \dot{x}_2 \end{bmatrix} &= \begin{bmatrix} 0 & 1 \\ 0 & 0 \end{bmatrix} x_o + \begin{bmatrix} 0 \\ \frac{1}{m}\cos\theta\cos\phi \end{bmatrix} U_1 - \begin{bmatrix} 0 \\ g \end{bmatrix}, \\ y_o &= \begin{bmatrix} 1 & 0 \end{bmatrix} x_o \end{aligned} \tag{3.127}$$

where we define the virtual control v_z given by

$$v_z := \frac{U_1}{m}(\cos\theta\cos\phi) - g, \tag{3.128}$$

as a result, the equation (3.127) is rewritten like

$$\begin{bmatrix} \dot{x}_1 \\ \dot{x}_2 \end{bmatrix} = \begin{bmatrix} 0 & 1 \\ 0 & 0 \end{bmatrix} x_o + \begin{bmatrix} 0 \\ 1 \end{bmatrix} v_z, \tag{3.129}$$

$$y_o = \begin{bmatrix} 1 & 0 \end{bmatrix} x_o. \tag{3.130}$$

After we have written the system in the correct form to apply the theorem, we proceed to design the observer for the translational velocity. Let

$$\sigma(x_2) := \begin{bmatrix} 0 & x_2 \end{bmatrix}^T \tag{3.131}$$

be the vector of the states to estimate, and we define the error variable

$$e := \beta(\mu_{ov}, x_1) - \sigma(x_2) \Rightarrow \begin{bmatrix} e_1 \\ e_2 \end{bmatrix} = \begin{bmatrix} \beta_1 \\ \beta_2 \end{bmatrix} - \begin{bmatrix} 0 \\ x_2 \end{bmatrix} \tag{3.132}$$

where $\mu_{ov} \in \mathbb{R}^2$ is the observer state and $\beta(\mu_{ov}, x_1)$ is a mapping to be defined. We obtain the time derivative of e, so the error dynamics are given by

$$\dot{e} = \frac{\partial\beta}{\partial\mu_{ov}}\dot{\mu}_{ov} + \frac{\partial\beta}{\partial x_1}x_2 - \frac{\partial\sigma}{\partial x_2}v_z \tag{3.133}$$

where $\frac{\partial\beta}{\partial\mu_{ov}} \in \mathbb{R}^{2\times 2}$ and $\dot{\mu}_{ov}, \frac{\partial\beta}{\partial x_1}, \frac{\partial\sigma}{\partial x_2} \in \mathbb{R}^2$.

From (3.132) we know that $x_2 = \beta_2 - e_2$, hence, we can rewrite (3.133) into

$$\dot{e} = \frac{\partial\beta}{\partial\mu_{ov}}\dot{\mu}_{ov} + \frac{\partial\beta}{\partial x_1}(\beta_2 - e_2) - \frac{\partial\sigma}{\partial x_2}v_z, \tag{3.134}$$

thus allowing to split the dynamics of the error into the error terms e and the state of the observer β, such that

$$\dot{e} = \frac{\partial \beta}{\partial \mu_{ov}}\dot{\mu}_{ov} + \frac{\partial \beta}{\partial x_1}\beta_2 - \frac{\partial \beta}{\partial x_1}e_2 - \frac{\partial \sigma}{\partial x_2}v_z. \tag{3.135}$$

We can select $\frac{\partial \beta}{\partial \mu_{ov}}\dot{\mu}_{ov}$ to transform equation (**3.135**) into the error terms

$$\frac{\partial \beta}{\partial \mu_{ov}}\dot{\mu}_{ov} = \frac{\partial \sigma}{\partial x_2}v_z - \frac{\partial \beta}{\partial x_1}\beta_2, \tag{3.136}$$

yielding the error dynamics

$$\dot{e} = -\frac{\partial \beta}{\partial x_1}e_2. \tag{3.137}$$

The states of the observer β are selected as

$$\beta = \begin{bmatrix} \mu_{ov1} \\ \gamma x_1 + \mu_{ov2} \end{bmatrix} \Rightarrow \frac{\partial \beta}{\partial x_1} = \begin{bmatrix} 0 \\ \gamma \end{bmatrix}, \tag{3.138}$$

where $\gamma > 0$, so we ensure that the jacobian $\frac{\partial \beta}{\partial \mu_{ov}}$ is invertible. Moreover, the error dynamics are given by

$$\dot{e} = -\begin{bmatrix} 0 \\ \gamma \end{bmatrix} e_2. \tag{3.139}$$

As a result the equilibrium $e = 0$ is globally asymptotically stable.

Therefore, we analyze the stability of the error applying the Lyapunov's theorem introduced in 2.2. Let

$$\nu(e) = \frac{1}{2}e_1^2 + \frac{1}{2}e_2^2 \tag{3.140}$$

where the time derivative of (**3.140**) is given by

$$\dot{\nu}(e) = e_1\dot{e}_1 + e_2\dot{e}_2. \tag{3.141}$$

From (**3.139**) we know that $\dot{e}_1 = 0$, hence (**3.141**) is rewritten as

$$\dot{\nu}(e) = e_2\dot{e}_2 = e_2(-\gamma e_2) = -\gamma e_2^2. \tag{3.142}$$

In conclusion the equilibrium $e = 0$ is asymptotically stable.

Finally, we obtain the states of the observer from (**3.136**) we know that

$$\dot{\mu}_{ov} = \frac{\partial \beta}{\partial \mu_{ov}}^{-1}\left[\frac{\partial \sigma}{\partial x_2}v_z - \frac{\partial \beta}{\partial x_1}\beta_2\right], \tag{3.143}$$

where substituting and solving the the partial derivatives we obtain

$$\dot{\mu}_{ov} = \begin{bmatrix} 1 & 0 \\ 0 & 1 \end{bmatrix}^{-1}\left(\begin{bmatrix} 0 \\ v_z \end{bmatrix} - \begin{bmatrix} 0 \\ \gamma^2 x_1 + \gamma\mu_{ov2} \end{bmatrix}\right), \tag{3.144}$$

which yields to the dynamics of the states vector $\dot{\mu}_{ov}$, given by

$$\dot{\mu}_{ov} = \begin{bmatrix} 0 \\ -\gamma^2 x_1 - \gamma\mu_{ov2} + v_z. \end{bmatrix}. \tag{3.145}$$

Hence, the observed state is given by

$$\hat{x}_2 = \dot{z} = \gamma z + \mu_{ov2}. \tag{3.146}$$

As a result, following a similar procedure for the velocities $\dot{x}$ and $\dot{y}$ we obtain the observed states estimated as

$$\boxed{\hat{\dot{x}} = \gamma x + \mu_{ov2x},} \tag{3.147}$$

$$\boxed{\hat{\dot{y}} = \gamma y + \mu_{ov2y},} \tag{3.148}$$

$$\boxed{\hat{\dot{z}} = \gamma z + \mu_{ov2z}.} \tag{3.149}$$

3.2 Nonlinear Controllers and Observers for Interactive Tilt-rotor Air-vehicle

On the other hand, in this section we develope the Immersion and Invariance control approach introduced in 2.5.3 and the Nonlinear Disturbance Observer for the Interactive Tilt-rotor.

It is worth to mention, that the nonlinear controller designed in this section, is for a tracking task. This means that all the control inputs of the system follow desired references. Also, the Nonlinear Disturbance Observer is applied to reject all the unknown disturbances that the tilt-rotor aircraft experiences.

3.2.1 Immersion and Invariance Control Approach

In order to solve the tracking problem, let us consider the following change of variables:

$$\boldsymbol{x}_1 := \boldsymbol{q} - \boldsymbol{q}_d, \quad \boldsymbol{x}_2 := \dot{\boldsymbol{x}}_1.$$

Additionally, let us consider the control law $\boldsymbol{U}$ as

$$\boldsymbol{U}(\dot{\boldsymbol{q}}, \boldsymbol{q}) = M(\boldsymbol{q})[\ddot{\boldsymbol{q}}_d + M(\boldsymbol{q})^{-1}[C(\dot{\boldsymbol{q}}, \boldsymbol{q}) + \boldsymbol{G}(\boldsymbol{q})] + \boldsymbol{v}]. \tag{3.150}$$

Hence, under the above considerations, the system can be rewritten as

$$\dot{\boldsymbol{x}} = \boldsymbol{f}(\boldsymbol{x}) + \boldsymbol{g}(\boldsymbol{x})\boldsymbol{v}$$

where

$$\boldsymbol{f}(\boldsymbol{x}) = \begin{bmatrix} 0 & \boldsymbol{x}_2 \\ 0 & 0 \end{bmatrix}; \quad \boldsymbol{g}(\boldsymbol{x}) = \begin{bmatrix} 0 & 0 \\ 0 & \boldsymbol{I} \end{bmatrix}; \quad \boldsymbol{\nu}(\boldsymbol{x}) = \begin{bmatrix} 0 \\ \boldsymbol{v}(\boldsymbol{x}) \end{bmatrix}.$$

Now, in order to apply Theorem 2.5.3 let us consider the following:

H1) *Target system*. Consider the target system as

$$\dot{\boldsymbol{\xi}} = -K\boldsymbol{\xi}. \tag{3.151}$$

Then, choosing $K > 0$ ensures that this dynamics is globally asymptotically stable with unique equilibrium point at $\boldsymbol{\xi}^* = 0$.

H2) *Immersion condition*. According to (3.95) we have that $\alpha(\boldsymbol{\xi}) = -K\boldsymbol{\xi}$. Then, by fixing $\boldsymbol{\pi}_1(\boldsymbol{\xi}) = \boldsymbol{\xi}$, we solve (2.21) to obtain the map $\boldsymbol{\pi}$ given by

$$\pi(\boldsymbol{\xi}) = \begin{bmatrix} \pi_1(\boldsymbol{\xi}) \\ \pi_2(\boldsymbol{\xi}) \end{bmatrix} = \begin{bmatrix} \boldsymbol{\xi} \\ -K\boldsymbol{\xi} \end{bmatrix}.$$

H3) *Implicit manifold*. According to the Implicit Manifold condition (2.22) we have that:

$$\begin{aligned} &\{\boldsymbol{x} \in \mathbb{R}^8 \mid \boldsymbol{\phi}(\boldsymbol{x}) = 0\} \\ &\quad = \{\boldsymbol{x} \in \mathbb{R}^8 \mid \boldsymbol{x}_1 = \boldsymbol{\xi}, \boldsymbol{x}_2 = -K\boldsymbol{\xi}\}. \end{aligned} \tag{3.152}$$

Clearly this condition will be fulfilled if the map $\boldsymbol{\phi}$ is defined as

$$\boldsymbol{\phi}(\boldsymbol{x}) = \boldsymbol{x}_2 + K\boldsymbol{x}_1. \tag{3.153}$$

H4) *Manifold attractivity and trajectory boundedness*. By taking into account the maps found in (H1)-(H3), (2.23) and (2.24) can be written as:

$$\dot{\boldsymbol{x}}_1 = \boldsymbol{z} - K\boldsymbol{x}_1, \tag{3.154}$$
$$\dot{\boldsymbol{x}}_1 = \boldsymbol{v}(\boldsymbol{x}), \tag{3.155}$$
$$\dot{\boldsymbol{z}} = \boldsymbol{v}(\boldsymbol{x}) + K\boldsymbol{x}_2, \tag{3.156}$$

which must be bounded and satisfy (2.25). Thus, in order to achieve such requirement, $\boldsymbol{v}$ is proposed as

$$\boldsymbol{v} = -K\boldsymbol{x}_2 - K_\zeta \boldsymbol{z}. \tag{3.157}$$

In fact, substituting (3.157) the closed-loop system is given by

$$\dot{\boldsymbol{x}}_1 = \boldsymbol{x}_2, \tag{3.158}$$
$$\dot{\boldsymbol{x}}_2 = -(K_\zeta + K)\boldsymbol{x}_2 - K\boldsymbol{x}_1, \tag{3.159}$$
$$\dot{\boldsymbol{z}} = -K_2\boldsymbol{z} = -K_\zeta(\boldsymbol{x}_2 + K\boldsymbol{x}_1), \tag{3.160}$$

where clearly the system is bounded and with unique equilibrium point globally asymptotically stable at $\boldsymbol{z} = 0$.

3.2.2 Nonlinear Disturbance Observer

The actual work considers that the aerial robot is manipulating (robotic arm motion) while carrying (transportation phase) a payload. Thus, one can notice that the pendulum-like payload experiences rotational and translational fluctuations produced by parametric inaccuracies and external disturbances.

The mathematical model, presented in section 1.2, is extended to include both uncertainties into a lumped disturbance. Thus, regarding the estimation of such lumped disturbance a non-linear observer is implemented.

The equation of motion (**1.70**) is split in its nominal part M_N, $C_N \in \mathbb{R}^{4\times4}$, $G_N \in \mathbb{R}^4$; and its disturbance part M_Δ, $C_\Delta \in \mathbb{R}^{4\times4}$, $G_\Delta \in \mathbb{R}^4$.

$$\begin{aligned} M_N(\mathbf{q})\ddot{\mathbf{q}} + &M_\Delta(\mathbf{q})\ddot{\mathbf{q}} + C_N(\dot{\mathbf{q}},\mathbf{q})\dot{\mathbf{q}} + \\ &C_\Delta(\dot{\mathbf{q}},\mathbf{q})\dot{\mathbf{q}} + \mathbf{G}_N(\mathbf{q}) + \mathbf{G}_\Delta(\mathbf{q}) = \mathbf{U} \end{aligned} \tag{3.161}$$

Taking all the disturbed motion equation as a disturbance

$$\Delta = -(M_\Delta(\mathbf{q})\ddot{\mathbf{q}} + C_\Delta(\dot{\mathbf{q}},\mathbf{q})\dot{\mathbf{q}} + \mathbf{G}_\Delta(\mathbf{q})), \tag{3.162}$$

then, the disturbed kinematic rotorcraft system will be described by

$$M_N(\mathbf{q})\ddot{\mathbf{q}} + C_N(\dot{\mathbf{q}},\mathbf{q})\dot{\mathbf{q}} + \mathbf{G}_N(\mathbf{q}) = \mathbf{U} + \Delta. \tag{3.163}$$

Define the observer error

$$\mathbf{e}_o := \hat{\Delta} - \Delta \tag{3.164}$$

and suppose the disturbance as a constant, then

$$\begin{aligned} \dot{\Delta} &\approx 0 \\ \dot{\mathbf{e}}_o &= \dot{\hat{\Delta}}. \end{aligned} \tag{3.165}$$

The main goal for the observer is to lead the observation error to 0. The observer error dynamic will be defined as:

$$\dot{\mathbf{e}}_o := -K_\Delta L(\mathbf{q},\dot{\mathbf{q}})\mathbf{e}_o \tag{3.166}$$

with $L(\mathbf{q},\dot{\mathbf{q}}) > 0$ and a diagonal matrix $K_\Delta \in \mathbb{R}^{4\times4}$.

Then substituting (**3.164**), (**3.165**) and taking Δ from (**3.163**) in (**3.166**). The observed disturbance dynamic is obtained as

$$\begin{aligned} \dot{\hat{\Delta}} = -K_\Delta L(\mathbf{q},\dot{\mathbf{q}})\hat{\Delta} + &K_\Delta L(\mathbf{q},\dot{\mathbf{q}}) \\ &[M_N(\mathbf{q})\ddot{\mathbf{q}} + C_N(\dot{\mathbf{q}},\mathbf{q})\dot{\mathbf{q}} + \mathbf{G}_N(\mathbf{q}) - \mathbf{U}]. \end{aligned} \tag{3.167}$$

Defining an auxiliary vector $\mathbf{z} \in \mathbb{R}^4$

$$\mathbf{z}_o := \hat{\Delta} - \mathbf{p}(\mathbf{q},\dot{\mathbf{q}}) \tag{3.168}$$

where $\mathbf{p}(\mathbf{q},\dot{\mathbf{q}})$ is going to be defined in the next step.

It is necessary to get rid off the state $\ddot{\mathbf{q}}$, because $\ddot{\theta}$ and $\ddot{\gamma}$ are not easy to measure while the aircraft is on the air. It is proposed the function

$$L(\mathbf{q},\dot{\mathbf{q}})M_N\ddot{\mathbf{q}} = \dot{\mathbf{p}}(\mathbf{q},\dot{\mathbf{q}}). \tag{3.169}$$

In the other hand, the observer dynamics is described by

$$\dot{\mathbf{z}}_o = \dot{\hat{\Delta}} - \dot{\mathbf{p}}(\mathbf{q},\dot{\mathbf{q}}) \tag{3.170}$$

from (**3.167**) and (**3.169**) in (**3.170**) the state observed dynamics yields to

$$\begin{aligned}\dot{\mathbf{z}}_o = &-K_\Delta L(\mathbf{q},\dot{\mathbf{q}})(\mathbf{z}+\mathbf{p}(\mathbf{q},\dot{\mathbf{q}})) + (K_\Delta - I)L(\mathbf{q},\dot{\mathbf{q}})\Delta \\ &+ L(\mathbf{q},\dot{\mathbf{q}})[C_N(\mathbf{q},\dot{\mathbf{q}})\dot{\mathbf{q}} + G_N(\mathbf{q}) - \mathbf{U}].\end{aligned} \tag{3.171}$$

In order to define $L(\mathbf{q},\dot{\mathbf{q}})$, $\mathbf{p}(\mathbf{q},\dot{\mathbf{q}})$ must be proposed in (**3.169**). It is important to remember that $L(\mathbf{q},\dot{\mathbf{q}})$ has to be positive define. So, consider

$$\mathbf{p}(\mathbf{q},\dot{\mathbf{q}}) = \begin{bmatrix}\dot{x}\\ \dot{z}\\ \dot{\theta}\\ \dot{\gamma}\end{bmatrix} \Rightarrow \frac{d\mathbf{p}(\mathbf{q},\dot{\mathbf{q}})}{dt} = \begin{bmatrix}\ddot{x}\\ \ddot{z}\\ \ddot{\theta}\\ \ddot{\gamma}\end{bmatrix} \tag{3.172}$$

and solving for (**3.169**) the function $L(\mathbf{q},\dot{\mathbf{q}})$ is obtained as:

$$L(\mathbf{q},\dot{\mathbf{q}}) = \begin{bmatrix} a_L & b_L & c_L & d_L \\ b_L & e_L & f_L & g_L \\ c_L & f_L & h_L & i_L \\ d_L & g_L & i_L & j_L \end{bmatrix}, \tag{3.173}$$

where

$$\begin{aligned}
a_L &= \frac{m_p\left(m_p\cos^2(\gamma+\theta)+m_r\right)l_p^2 + I_r\left(2m_r - \left(\sin^2(\gamma+\theta)-2\right)m_p\right)}{(m_p+m_r)\,m_p m_r l_p^2 + I_r\,(m_p+2m_r)},\\
b_L &= -\frac{\sin^2(\gamma+\theta)m_p\left(m_p l_p^2 + I_r\right)}{\tan(\gamma+\theta)\,(m_p+m_r)\,m_p m_r l_p^2 + I_r\,(m_p+2m_r)},\\
c_L &= \frac{\cos(\gamma+\theta)l_p m_p}{m_p m_r l_p^2 + I_r\,(m_p+2m_r)},\\
d_L &= \frac{\cos(\gamma+\theta)I_r}{l_p m_p m_r l_p^2 + I_r\,(m_p+2m_r)},\\
e_L &= \frac{m_p\left(m_p\sin^2(\gamma+\theta)+m_r\right)l_p^2 + I_r\left(2m_r - \left(\cos^2(\gamma+\theta)-2\right)m_p\right)}{(m_p+m_r)\,m_p m_r l_p^2 + I_r\,(m_p+2m_r)},\\
f_L &= -\frac{\sin(\gamma+\theta)l_p m_p}{m_p m_r l_p^2 + I_r\,(m_p+2m_r)},\\
g_L &= -\frac{\sin(\gamma+\theta)I_r}{l_p m_p m_r l_p^2 + I_r\,(m_p+2m_r)},\\
h_L &= \frac{m_p+2m_r}{m_p m_r l_p^2 + I_r\,(m_p+2m_r)},\\
i_L &= -\frac{m_r}{m_p m_r l_p^2 + I_r\,(m_p+2m_r)},\\
j_L &= \frac{m_p m_r l_p^2 + I_r\,(m_p+m_r)}{l_p^2 m_p m_p m_r l_p^2 + I_r\,(m_p+2m_r)},
\end{aligned} \tag{3.174}$$

Then, applying the Sylvester Criterion, we have that

$$\begin{aligned}
|\triangle_4| &= \frac{1}{l_p^2 m_p \left(m_p+m_r\right) m_p m_r l_p^2 + I_r \left(m_p+2m_r\right)}, \\
|\triangle_3| &= \frac{2}{\left(m_p+m_r\right) m_p m_r l_p^2 + I_r \left(m_p+2m_r\right)}, \\
|\triangle_2| &= \frac{2I_r + l_p^2 m_p}{\left(m_p+m_r\right) m_p m_r l_p^2 + I_r \left(m_p+2m_r\right)}, \\
|\triangle_1| &= \frac{m_p m_r l_p^2 + I_r \left(m_p+m_r\right)}{l_p^2 m_p^2 m_r l_p^2 + I_r \left(m_p+2m_r\right)},
\end{aligned}$$

since $|\triangle_4|,|\triangle_3|,|\triangle_2|,|\triangle_1| > 0 \Rightarrow L(\boldsymbol{q},\dot{\boldsymbol{q}}) > 0,\ \forall \boldsymbol{q},\dot{\boldsymbol{q}} \in \mathbb{R}^4$.

CHAPTER 4

NUMERICAL EXAMPLES

In the current chapter we introduce the simulation results of the control strategies developed in section 3. It is worth to mention that we worked with the MATLAB's simulation package SIMULINK.

In the first section of this chapter the nonlinear controllers and observers for a Quadrotor simulations are shown, after that, we present the simulation results of the Immersion and Invariance control approach for an Interactive Tilt-Rotor and a nonlinear disturbance observer in order to improve the performance against unknown disturbances.

4.1 Nonlinear Controllers and Observers for Quadrotor

In this section we present the simulation's results of the tracking task using nonlinear control strategies, as well as, the simulations of the nonlinear observers for the rotorcraft's mass estimation and the translational velocity unknown state.

The parameters of the Quadrotor used for the simulation are presented in the following table 4.1.

Parameters	Value	Parameters	Value
m	$1.72kg$	g	$9.81\frac{m}{s^2}$
I_{xx}	$0.0148kg \cdot m^2$	I_{yy}	$0.0148kg \cdot m^2$
I_{zz}	$0.0295kg \cdot m^2$		

Table 4.1. Quadrotor nominal parameters.

4.1.1 Nonlinear Controllers

In this work we applied three different nonlinear controllers for the Quadrotor's system. This control approaches were developed in 3.1.1, therefore, its numerical results are presented in the current section.

It is worth to mention that this nonlinear controllers are simulated with ideal conditions, we assume that we can measure all the states and there are not disturbances.

The main objective of these nonlinear controllers is to follow the desired trajectory proposed as a vertical helix described by the equations

$$x = \sin(t/2); \quad y = \cos(t/2); \quad z = 1 + (t/20); \quad \psi = \frac{\pi}{6},$$

it means that the vertical helix's radius is 1 meter and it begins 1 meter above the ground.

The block diagram applied for all the controllers' simulation is introduced in the following figure 4.1.

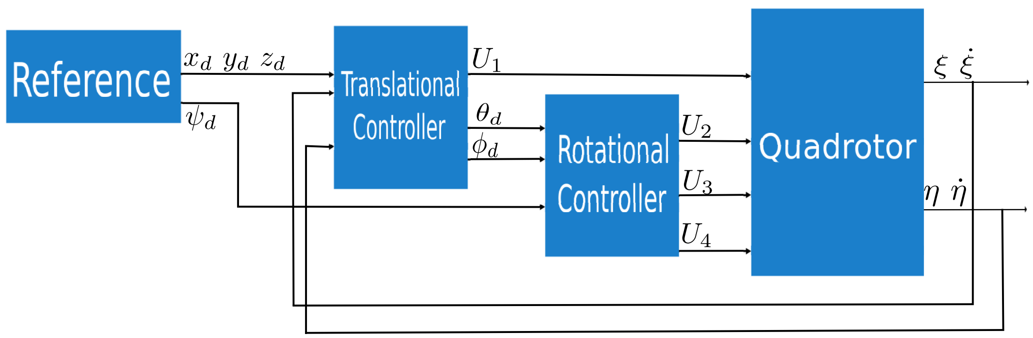

Figure 4.1. Block diagram for nonlinear controllers.

4.1.1.1 Backstepping

The first control approach to be evaluated was the well known Backstepping control law, which was developed in section 3.1.1.1. The main goal of this simulation is to follow the desired trajectory.

The control gains for the Backstepping approach are given by the following table 4.2.

Gain	Value	Gain	Value	Gain	Value
k_z	10	k_x	10	k_y	10
P_z	2	P_x	2	P_y	2
k_ϕ	40	k_θ	40	k_ψ	40
P_ϕ	20	P_θ	20	P_ψ	20

Table 4.2. Backstepping control gains.

With these Backstepping control gains we ensure a globally asymptotically stable tracking task.

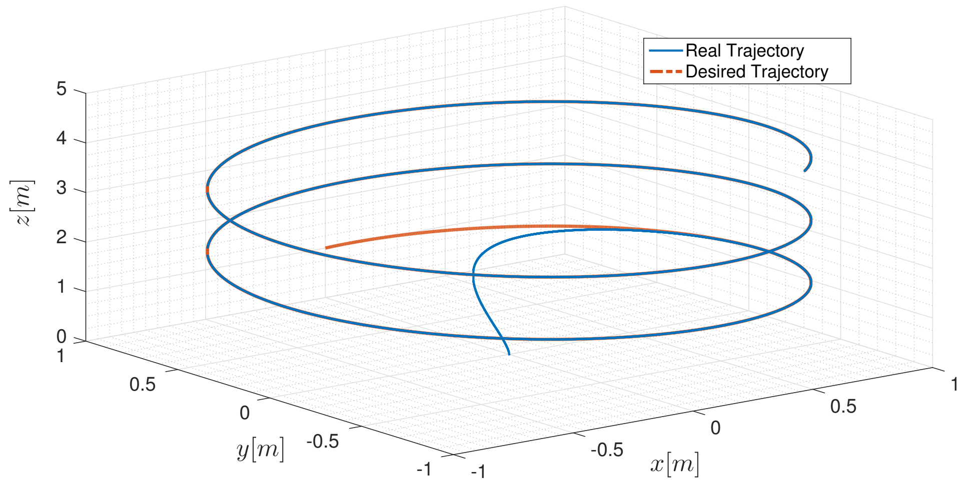

Figure 4.2. Helix trajectory for Backstepping Approach.

In figure 4.2 we notice that the tracking task is accomplished, hence, we proceed to analyze the translational and the rotational states presented in figures 4.3 and 4.4.

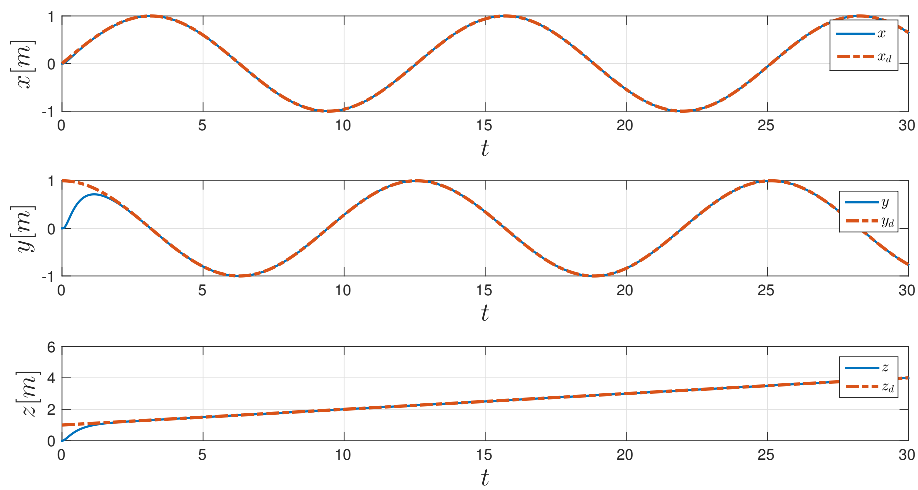

Figure 4.3. Translational states for Backstepping Approach.

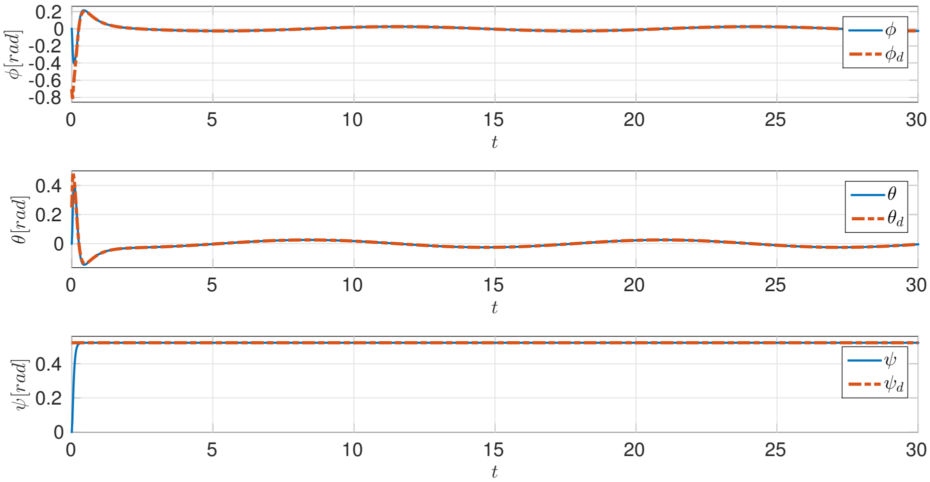

Figure 4.4. Rotational states for Backstepping Approach.

From the states figures we almost can ensure a perfect tracking, but it is not enough, therefore we must evaluate the error of each state, which are presented in the coming figures.

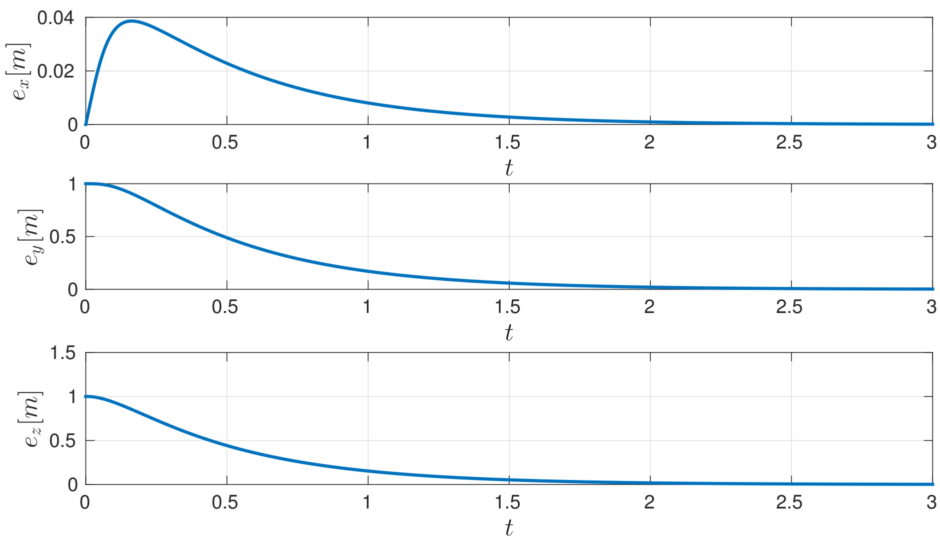

Figure 4.5. Translational error for Backstepping Approach.

In figure 4.5 we can see that the error for x leads to 0 in 2.5 seconds approximately, meanwhile the error in y and z leads to 0 in 2 seconds. This is consider as a good performance for the translational subsystem.

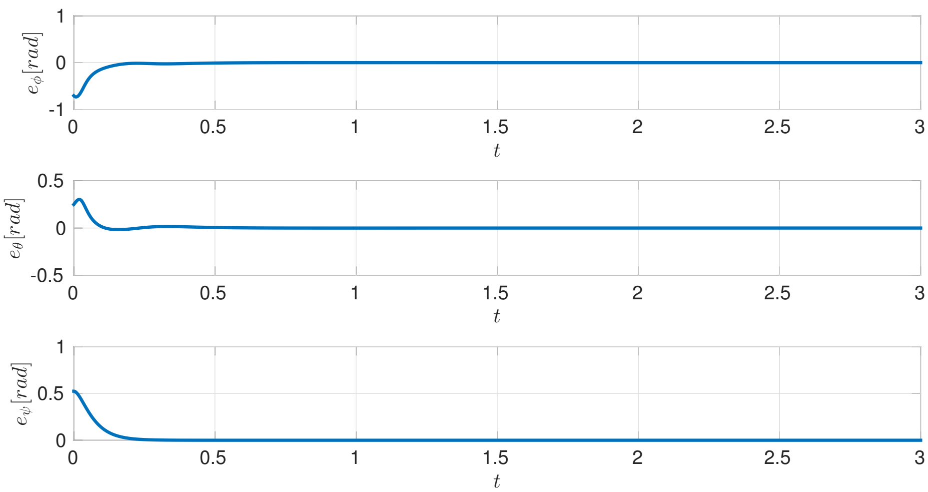

Figure 4.6. Rotational error for Backstepping Approach.

Simultaneously, in figure 4.6 we notice that the rotational subsystem lead to 0 faster than the translational subsystem. The error becomes 0 in less than 0.5 seconds.

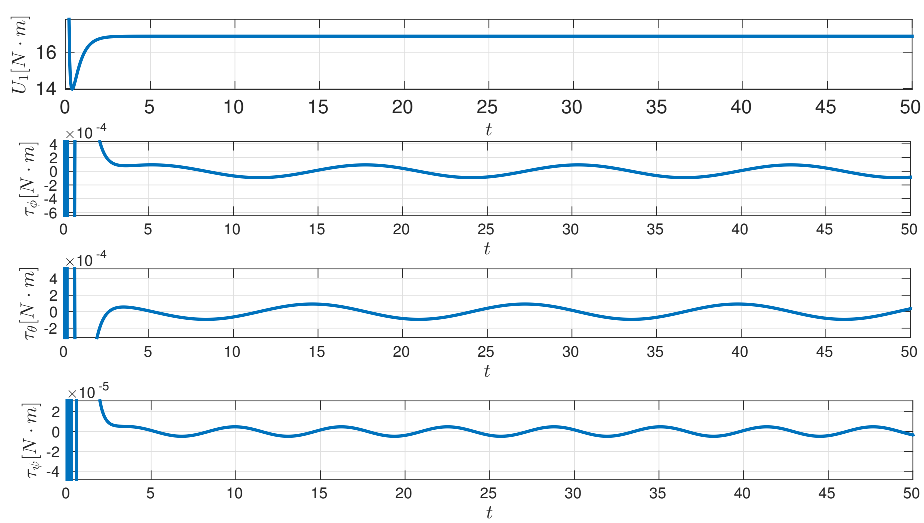

Figure 4.7. Control inputs for Backstepping Approach.

Finally, but not less important, we have the control inputs presented in figure 4.7. We can notice that the control input U_1 begins above the $20N \cdot m$, which is physically unfeasible for the Quadrotor's motors, but it stabilize under $17N \cdot m$, that is feasible for the motors. The control inputs for the rotational subsystem have a similar behavior, begin in a feasible point but stabilize in a possible one.

4.1.1.2 Nested Saturations

The second control approach simulated was the Nested Saturations control law, developed in section 3.1.1.2. The main goal of this simulation is to follow the desired trajectory too, but this approach saturates the control inputs as a bonus.

The Nested Saturations works on saturations, thus, the control saturations are given by the following table 4.3.

Saturation	Value	Saturation	Value	Saturation	Value
σ_{1z}	1.5	σ_{1x}	1.2	σ_{1y}	6
σ_{2z}	3.4	σ_{2x}	3	σ_{2y}	12.4
σ_{3z}	5.8	σ_{3x}	8	σ_{3y}	16.8
$\sigma_{1\phi}$	1	$\sigma_{1\theta}$	0.5	$\sigma_{1\psi}$	1.5
$\sigma_{2\phi}$	3	$\sigma_{2\theta}$	2.5	$\sigma_{2\psi}$	3.5
$\sigma_{3\phi}$	5.5	$\sigma_{3\theta}$	4.7	$\sigma_{3\psi}$	6

Table 4.3. Saturations for Nested Saturations.

With these saturations we ensure a globally asymptotically stable tracking task.

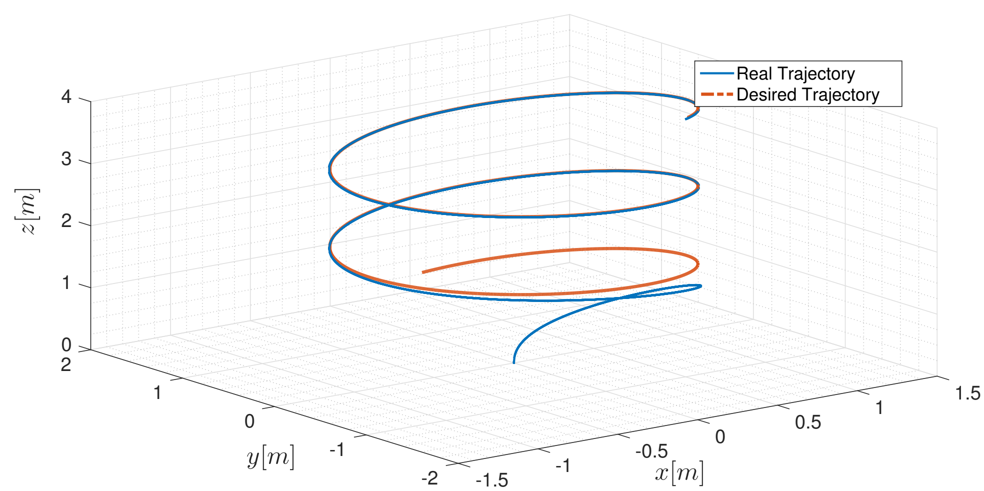

Figure 4.8. Helix trajectory for Nested Saturations Approach.

From figure 4.8 we can see that the tracking task is accomplished, hence, we proceed to analyze the translational and the rotational states presented in figures 4.9 and 4.10.

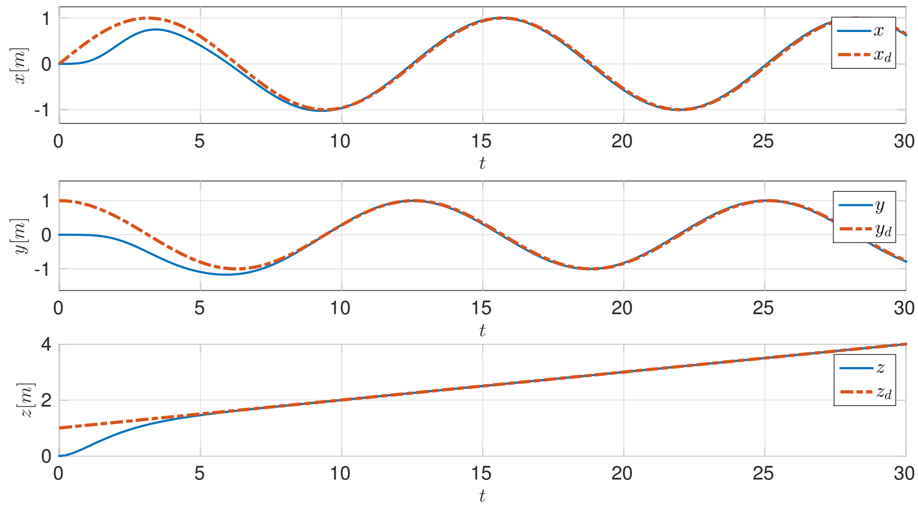

Figure 4.9. Translational states for Nested Saturations Approach.

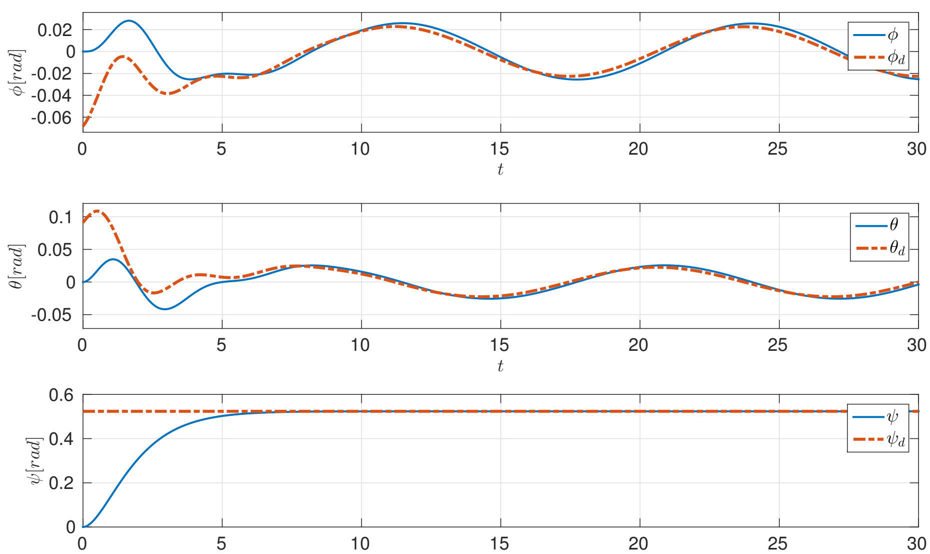

Figure 4.10. Rotational states for Nested Saturations Approach.

In the states figures we notice an almost perfect tracking, therefore we must evaluate the error of each state in order to ensure it. We present the states' error in the coming figures.

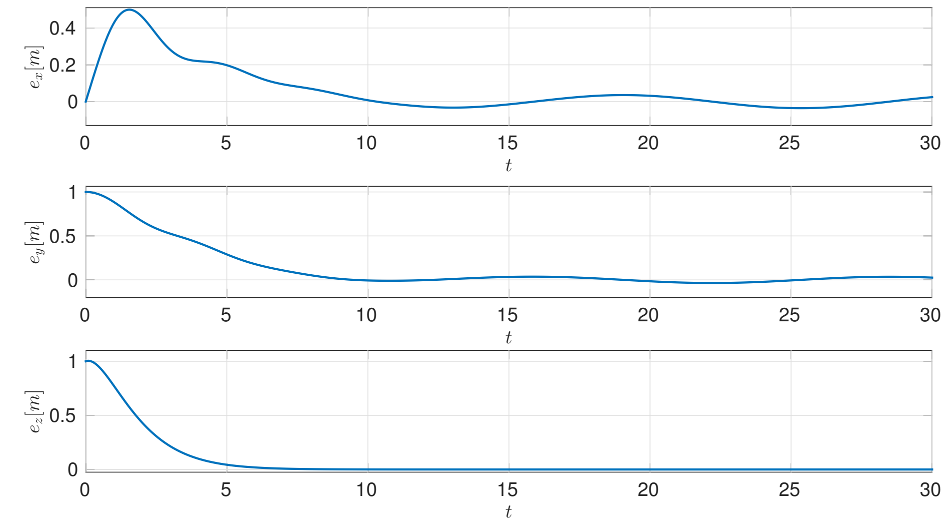

Figure 4.11. Translational error for Nested Saturations Approach.

In figure 4.11 we can see that the error for x does not leads to 0, this error is not constant, this means that we have a variable error around the $3\ cm$, meanwhile the error in y has a similar behavior, this error is variable too and it is around the $5\ cm$. Finally, the error in z leads to 0 in 7 seconds. This is considered as a good performance for the translational subsystem but it does not ensure an asymptotic stable tracking task.

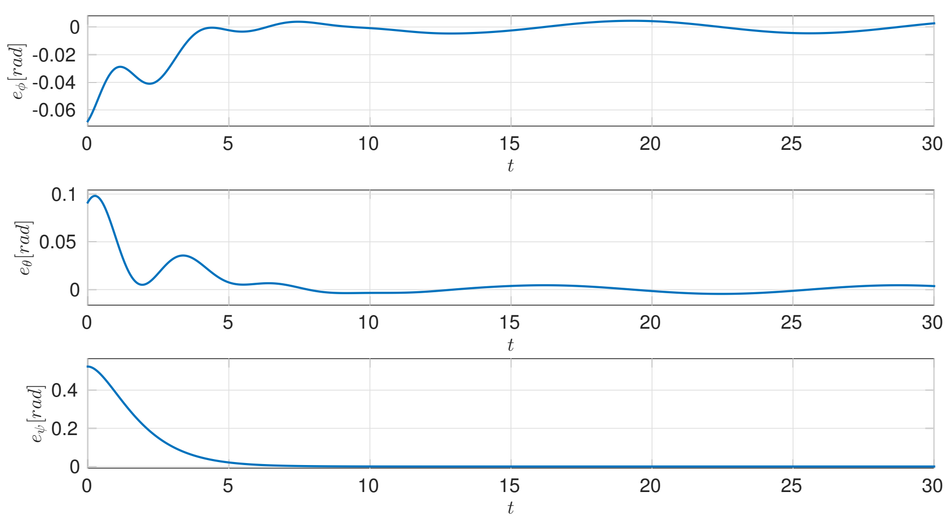

Figure 4.12. Rotational error for Nested Saturations Approach.

Simultaneously, in figure 4.12 we notice that the rotational subsystem has a variable error around the $0.01\ rad$ for the ϕ and θ states. Meanwhile, for the ψ state the error leads to 0 in less than 8 seconds.

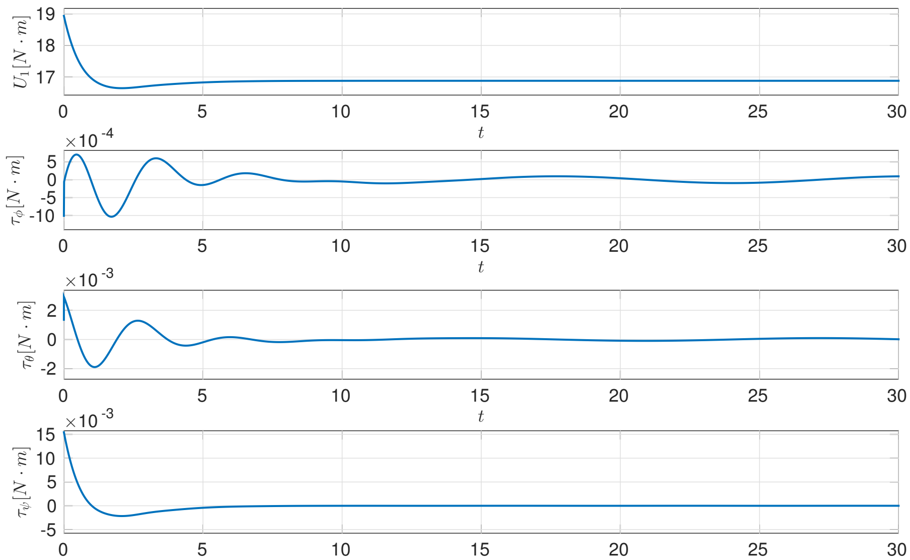

Figure 4.13. Control inputs for Nested Saturations Approach.

Finally, we present the control inputs in figure 4.13. We can notice that the control input U_1 begins under the $20N \cdot m$, and it stabilizes under $17N \cdot m$, that is a possible scenario for the motors. The control inputs for the rotational subsystem have a similar behavior, begin in a feasible point and stabilize in a better one.

4.1.1.3 Immersion and Invariance

The third control approach simulated was the Immersion and Invariance control law, which was developed in section 3.1.1.3. The main goal of this simulation, as the two presented before, is to follow the desired trajectory.

The control gains for the I&I approach are given by the following table 4.4.

Gain	Value	Gain	Value	Gain	Value
$k_{\eta z}$	3	$k_{\eta x}$	2	$k_{\eta y}$	2
$k_{\eta 2z}$	0.4	$k_{\eta 2x}$	0.2	$k_{\eta 2y}$	0.5
$k_{1\phi}$	40	$k_{1\theta}$	40	$k_{1\psi}$	40
$k_{2\phi}$	20	$k_{2\theta}$	20	$k_{2\psi}$	20

Table 4.4. Immersion and Invariance control gains.

With these I&I control gains we should be able to ensure a globally asymptotically stable tracking task.

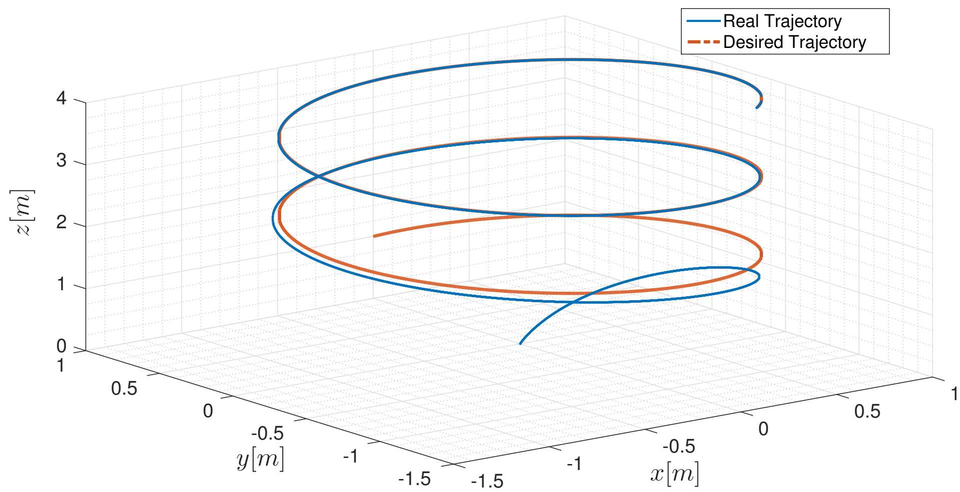

Figure 4.14. Helix trajectory for Immersion and Invariance Approach.

In figure 4.14 seems that the tracking task is accomplished, hence, we proceed to analyze the translational and the rotational states presented in figures 4.15 and 4.16.

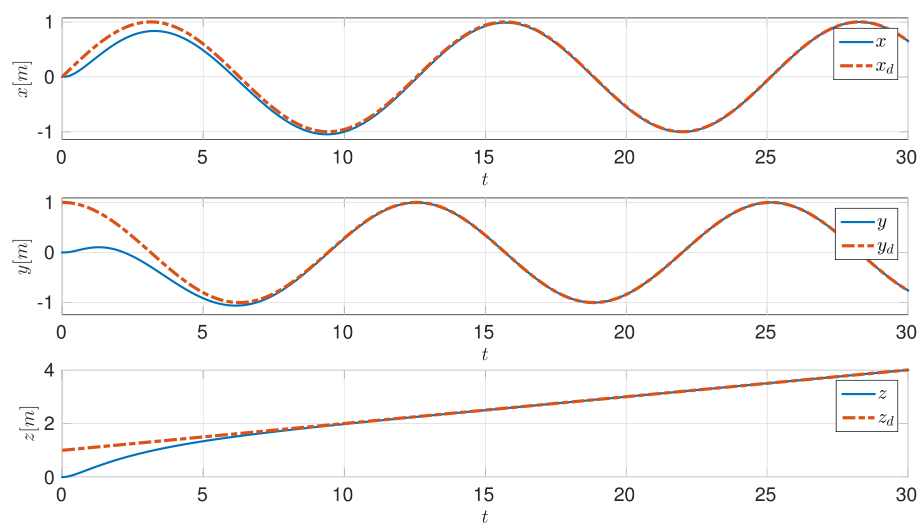

Figure 4.15. Translational states for Immersion and Invariance Approach.

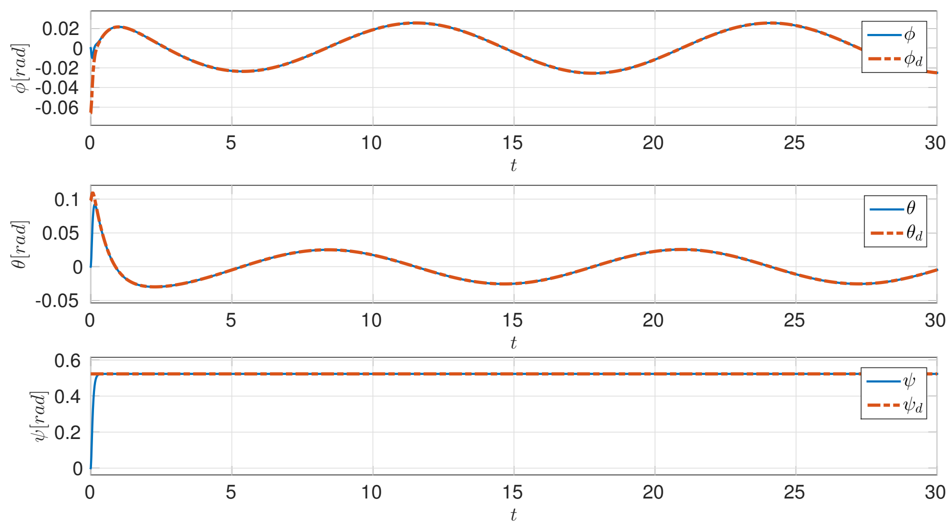

Figure 4.16. Rotational states for Immersion and Invariance Approach.

In the states figures we notice a perfect tracking, therefore, we must analyze the error of each state in order to ensure it. We present the states' error in the coming figures.

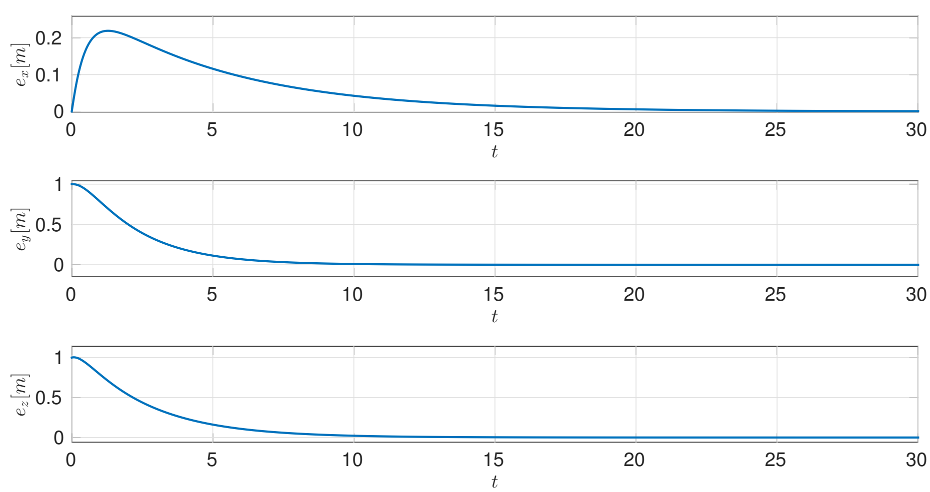

Figure 4.17. Translational error for Immersion and Invariance Approach.

In figure 4.17 we can see that the error for x leads to 0 in 25 seconds approximately, meanwhile the error in y and z leads to 0 in 10 seconds, being y a little bit faster than z. This is consider as a good performance for the translational subsystem.

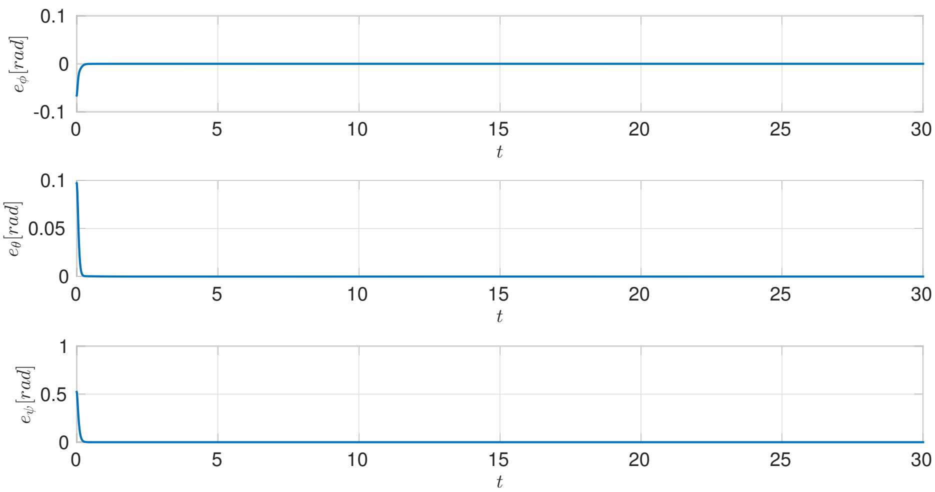

Figure 4.18. Rotational error for Immersion and Invariance Approach.

Equally important, in figure 4.18 we notice that the rotational subsystem lead to 0 faster than the translational subsystem. The error becomes 0 in less than 1 second.

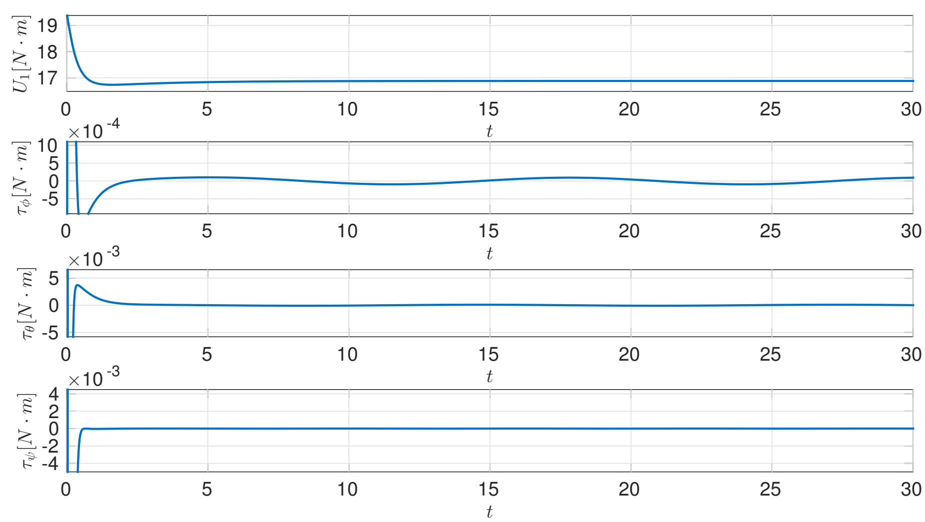

Figure 4.19. Control inputs for Immersion and Invariance Approach.

Finally, we have the control inputs presented in figure 4.19 and they behave like the Backstepping control inputs. We can notice that the control input U_1 begins above the $20N \cdot m$, which is physically unfeasible for the Quadrotor's motors, but it stabilize under $17N \cdot m$, that is feasible for the motors. The control inputs for the rotational subsystem have a similar behavior, begin in a feasible point but stabilize in a possible one.

4.1.2 Nonlinear Observers

In this section we present the simulations of nonlinear observers applied with the nonlinear controllers presented before. These observers are developed in section 3.1.2 and they are used in order to improve the performance of the system or to obtain unmeasurable states in reality.

For the simulations that estimates the mass we consider the following Quadrotor's mass variation.

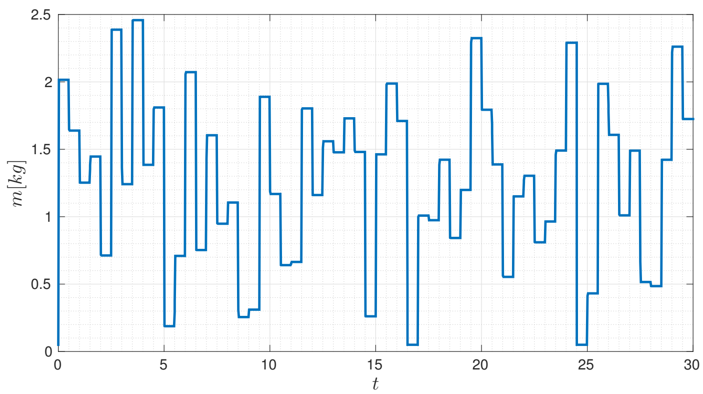

Figure 4.20. Mass variations for the Quadrotor.

This mass variation will help us in order to test our estimator and evaluate if the system performance is improved.

4.1.2.1 Estimator for Quadrotor's mass with Backstepping

The first simulation for the nonlinear observers is the mass estimation, developed in section 3.1.2.1, with the Backstepping control technique. The main goal of this simulation is to follow the desired trajectory and analyze if the performance is improved with the estimator against the disturbances.

The block diagram applied for this simulation is introduced in the following figure 4.21

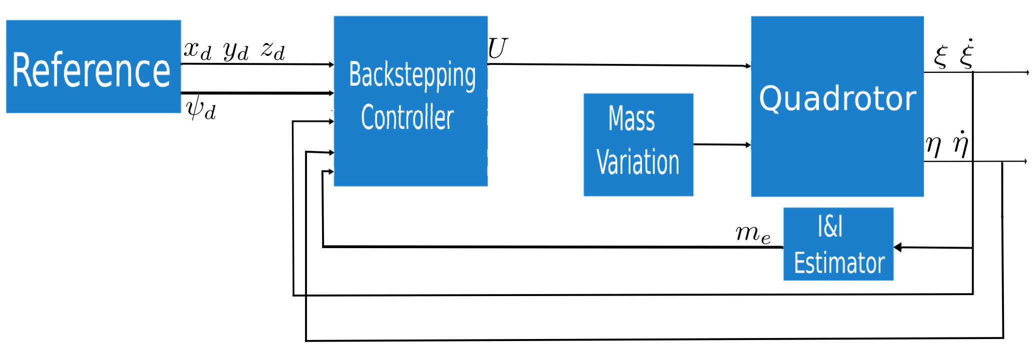

Figure 4.21. Block diagram for Backstepping controller with mass estimator.

The control gains for the Backstepping approach are given by the table 4.2, presented in section 4.1.1.1, and the estimator gain $\gamma = 75$.

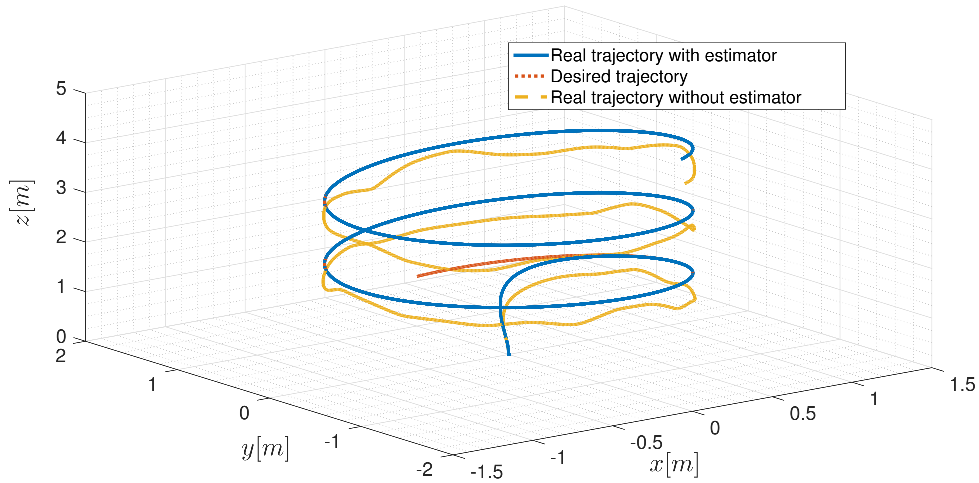

Figure 4.22. Helix trajectory for Backstepping Approach with mass' estimator.

In figure 4.22 we can do a first analysis of the trajectories with or without the estimator. We can notice that the tracking task is accomplished when the estimator is applied, in the other hand, the trajectory when the estimation is not applied does not reach the reference proposed. Therefore, we proceed to analyze each state.

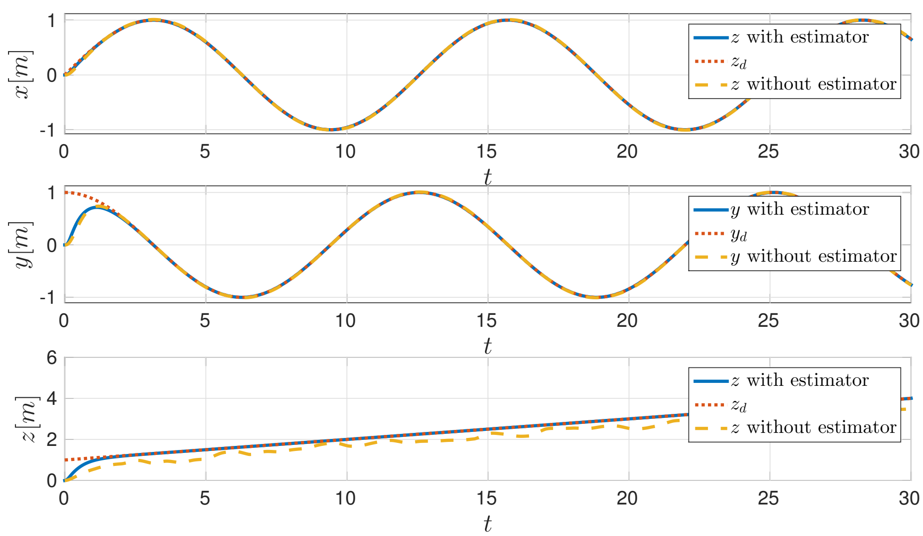

Figure 4.23. Translational states for Backstepping Approach with mass' estimator.

In figure 4.23 we notice that the main problem with the disturbance is in the z state. It is seen that the mass variation does not allow the state to reach the reference.

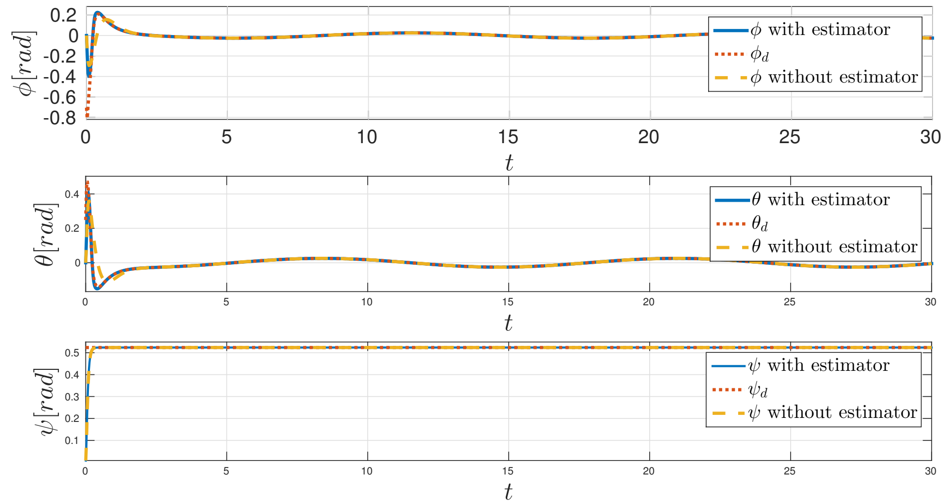

Figure 4.24. Rotational states for Backstepping Approach with mass' estimator.

From figure 4.24 we notice that the mass variation does not disturb the rotational subsystem as the equations indicate. Therefore we proceed to do the error analysis.

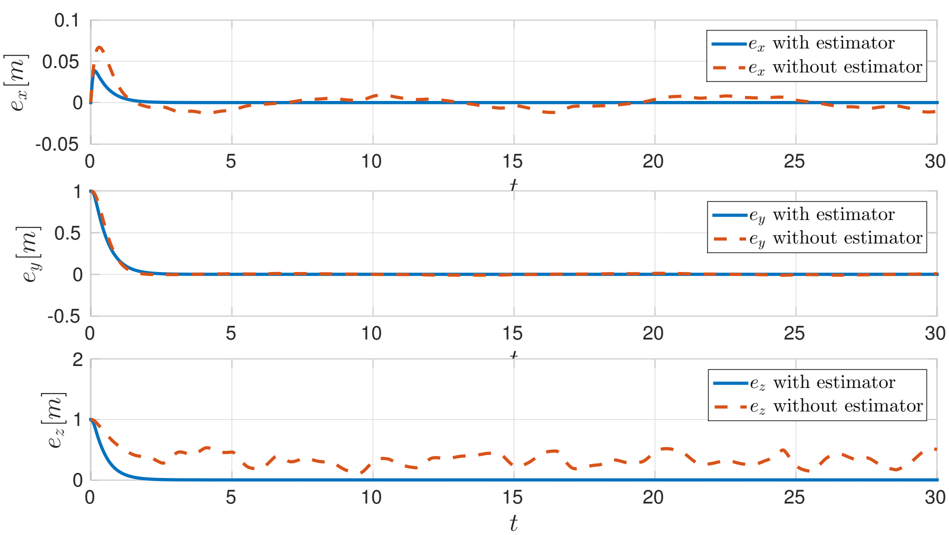

Figure 4.25. Translational error for Backstepping Approach with mass' estimator.

The error of the states x, y and z are presented in figure 4.25, and we can see that exists an error in two states, when the mass is not estimated. The maximum error in the x state is around the $2\ cm$, meanwhile the error in the z state is bigger, around the $60\ cm$.

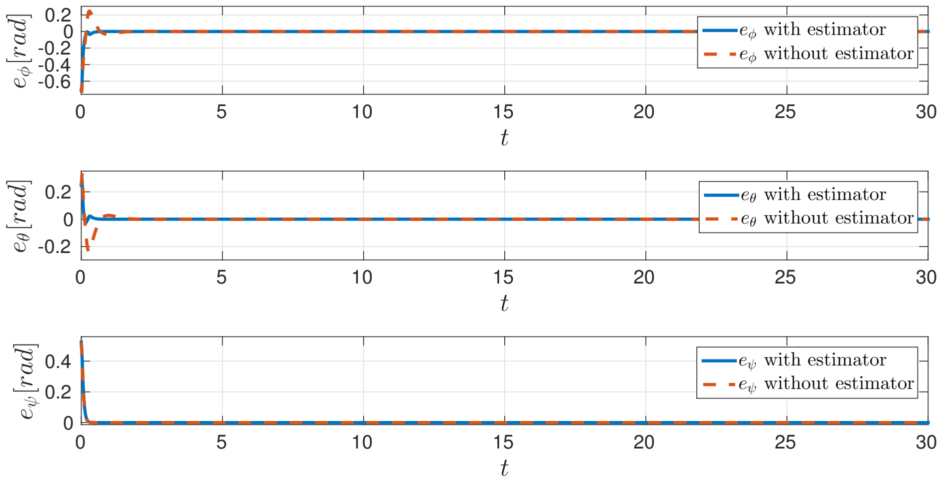

Figure 4.26. Rotational error for Backstepping Approach with mass' estimator.

As it have been said before, the mass variation does not have a big impact in the rotational subsystem. From figure 4.26 we notice that there are errors in each state at the begining, after 3 seconds the error leads to 0 in all the rotational states.

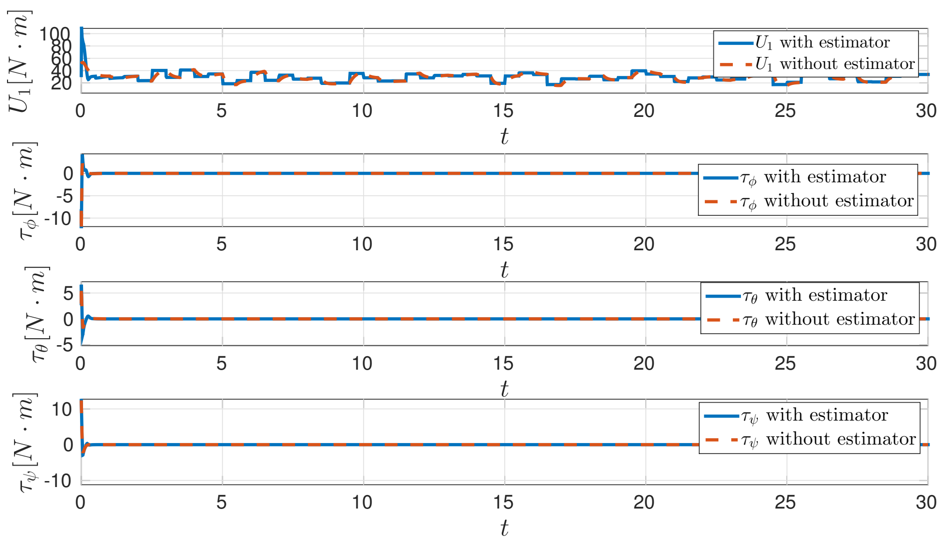

Figure 4.27. Control inputs for Backstepping Approach with mass' estimator.

Finally, we have the control inputs presented in figure 4.27. We can notice that the control input U_1 is bigger than the control input presented in the section before, this is because the mass variation. It is worth to mention that U_1 has a similar behavior with or without the estimation, but the main difference is that without the estimator we are not able to reach the reference. In the other hand, the control inputs for the rotational subsystem remains the same.

4.1.2.2 Estimator for Quadrotor's mass with Nested Saturations

The next simulation for the nonlinear observers is the mass estimation with Nested Saturations. The main goal of this simulation is to follow the desired trajectory and analyze if the performance is improved with the estimator against the disturbances.

The block diagram applied for this simulation is introduced in the following figure 4.28

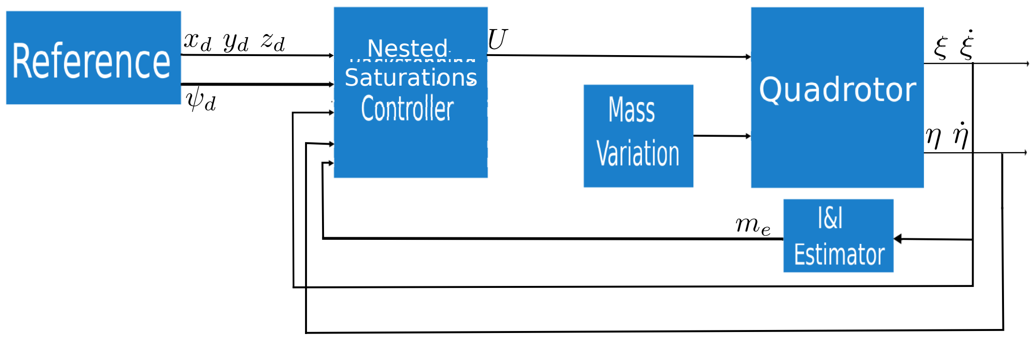

Figure 4.28. Block diagram for Nested Saturations controller with mass estimator.

The saturations for the Nested Saturations approach are given by the table 4.3, presented in section 4.1.1.2, and the estimator gain $\gamma = 75$.

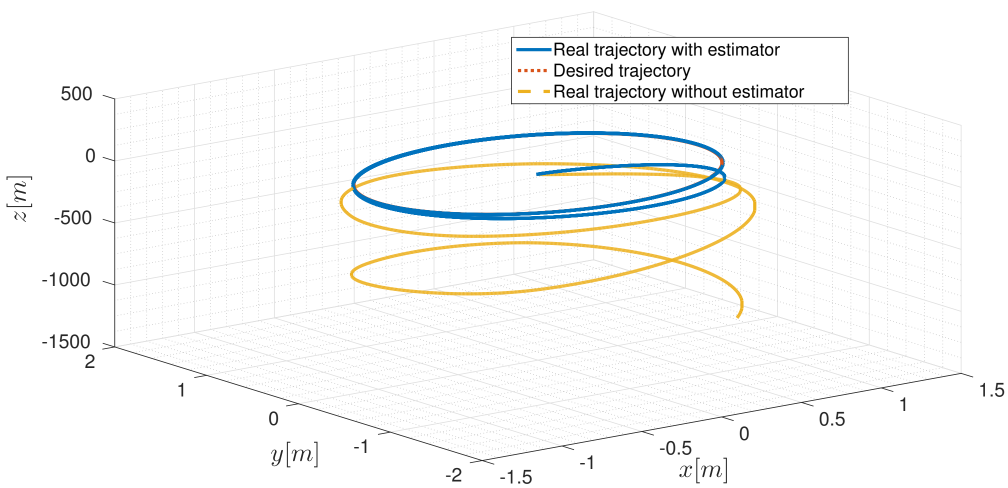

Figure 4.29. Helix trajectory for Nested Saturations Approach with mass' estimator.

In figure 4.29 we can do a first analysis of the trajectories with or without the estimator. We can notice that the tracking task is accomplished when the estimator is applied, in the other hand, the trajectory when the estimation is completely lost. Therefore, we proceed to analyze each state.

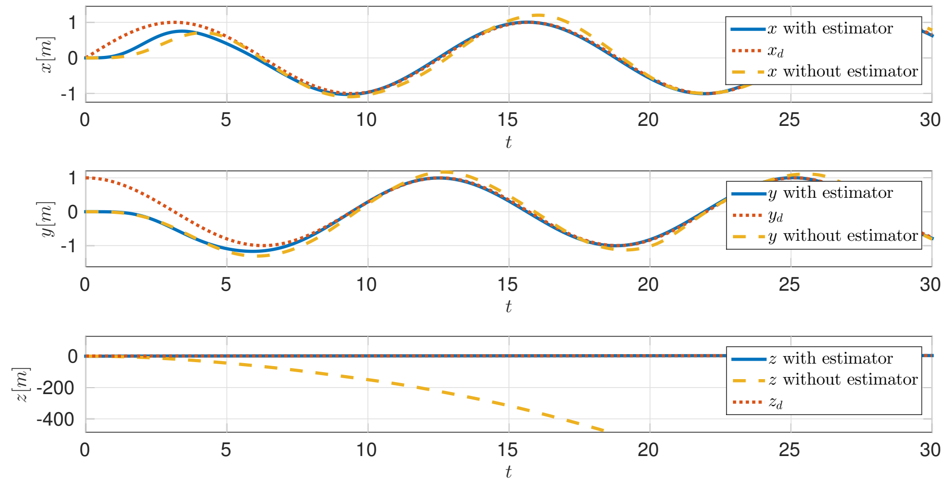

Figure 4.30. Translational states for Nested Saturations Approach with mass' estimator.

In figure 4.30 we notice that the main problem with the disturbance is in the z state. It is seen that the mass variation does not allow the state to reach the reference, in fact the reference is lost.

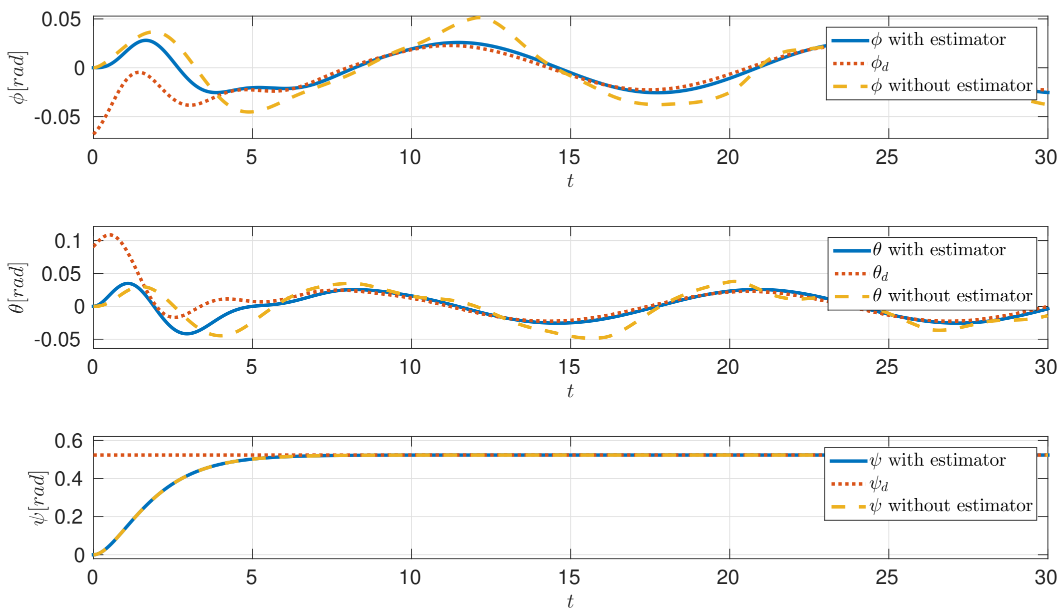

Figure 4.31. Rotational states for Nested Saturations Approach with mass' estimator.

From figure 4.31 we notice that the mass variation disturbs the rotational subsystem. Therefore we proceed to do the error analysis.

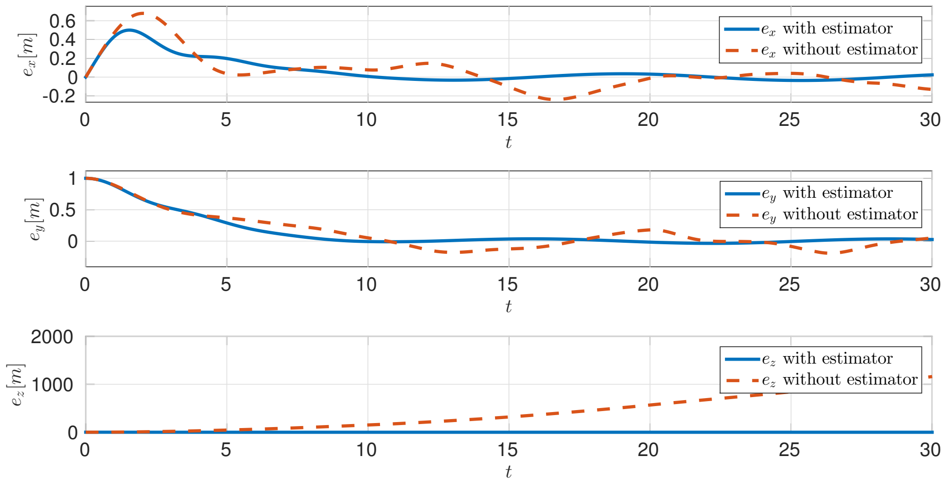

Figure 4.32. Translational error for Nested Saturations Approach with mass' estimator.

The error of the states x, y and z are presented in figure 4.32, and we can see that exists an error in two states, when the mass is not estimated. The maximum error in the x state is around the $2\ cm$, meanwhile the error in the z grows until it yields to ∞.

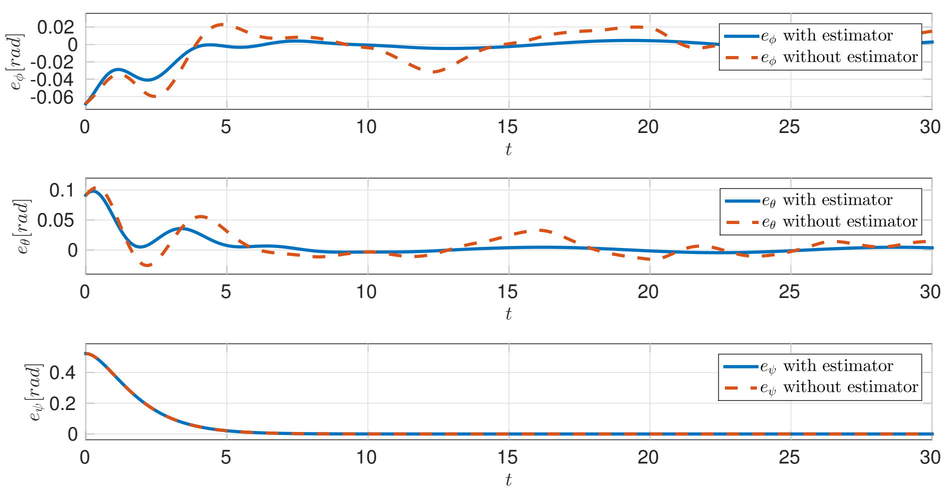

Figure 4.33. Rotational error for Nested Saturations Approach with mass' estimator.

The mass variation has a big impact in the rotational subsystem. From figure 4.26 we notice that there are errors in two states.

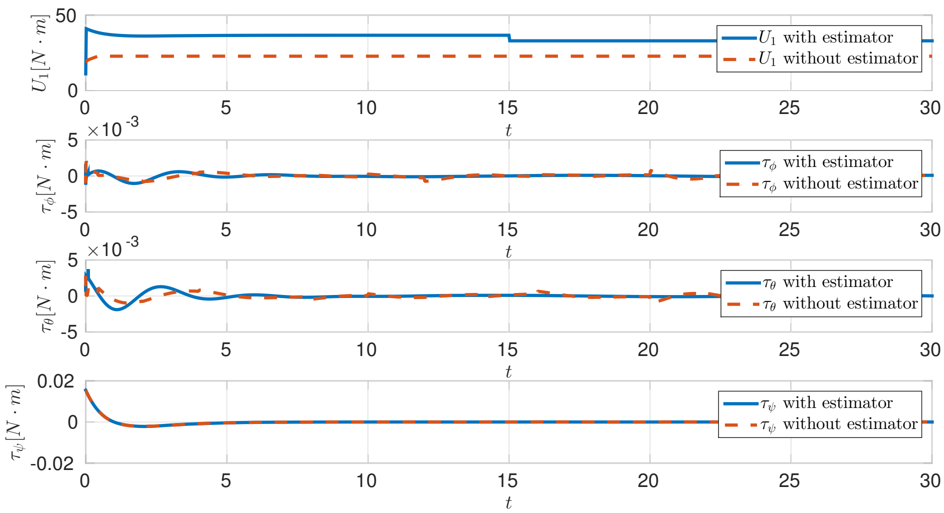

Figure 4.34. Control inputs for Nested Saturations Approach with mass' estimator.

Finally, we have the control inputs presented in figure 4.34. We can notice that the control input U_1 is bigger than the control input presented in the section before, this is because the mass variation. It is worth to mention that U_1 has a similar behavior with or without the estimation, but the main difference is that without the estimator we are not able to reach the reference. In the other hand, the control inputs for the rotational subsystem remains the same.

4.1.2.3 Estimator for Quadrotor's mass with Immersion and Invariance

The next simulation for the nonlinear observers is the mass estimation with Immersion and Invariance. The main goal of this simulation is to follow the desired trajectory and analyze if the performance is improved with the estimator against the disturbances.

The block diagram applied for this simulation is introduced in the following figure 4.35

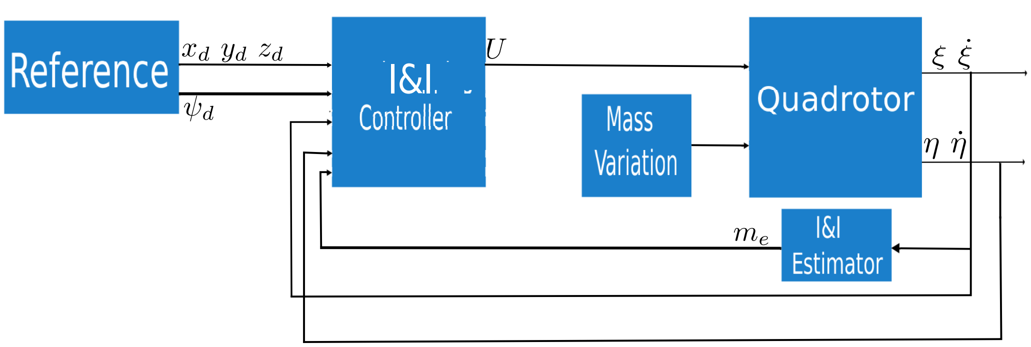

Figure 4.35. Block diagram for Immersion and Invariance controller with mass estimator.

The control gains for the Immersion and Invariance approach are given by the table 4.4, presented in section 4.1.1.3, and the estimator gain $\gamma = 75$.

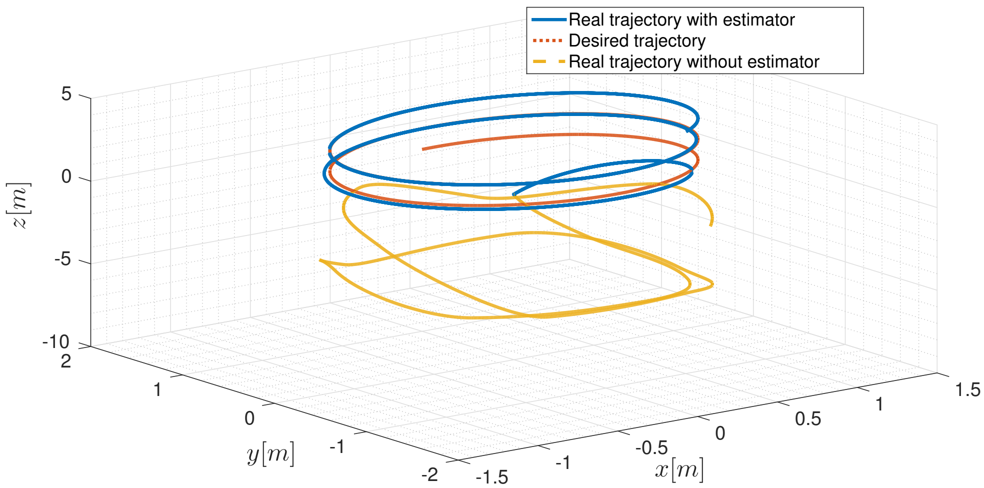

Figure 4.36. Helix trajectory for Immersion and Invariance Approach with mass' estimator.

In figure 4.36 we can do a first analysis of the trajectories with or without the estimator. We can notice that the tracking task is accomplished when the estimator is applied, in the other hand, the trajectory when the estimation is completely lost. Therefore, we proceed to analyze each state.

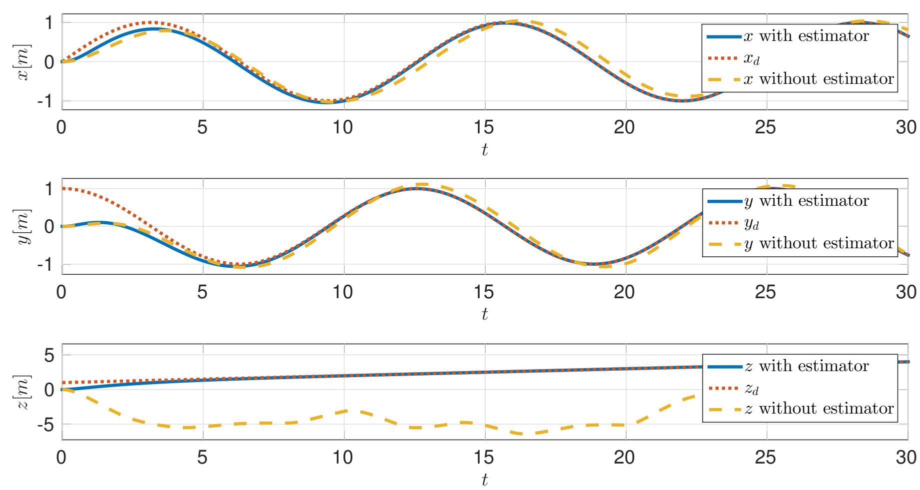

Figure 4.37. Translational states for Immersion and Invariance Approach with mass' estimator.

In figure 4.37 we notice that the main problem with the disturbance is in the z state. It is seen that the mass variation does not allow the state to reach the reference, in fact the reference is lost.

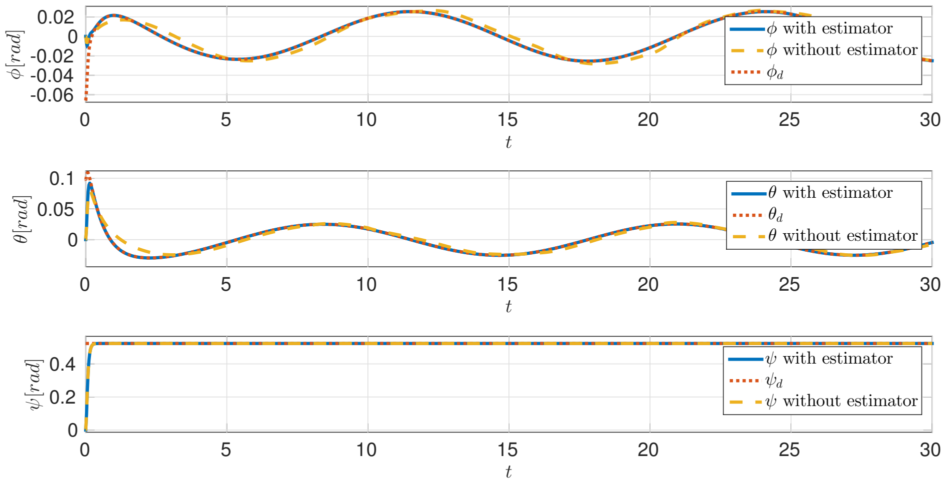

Figure 4.38. Rotational states for Immersion and Invariance Approach with mass' estimator.

From figure 4.38 we notice that the mass variation disturbs the rotational subsystem. Therefore we proceed to do the error analysis.

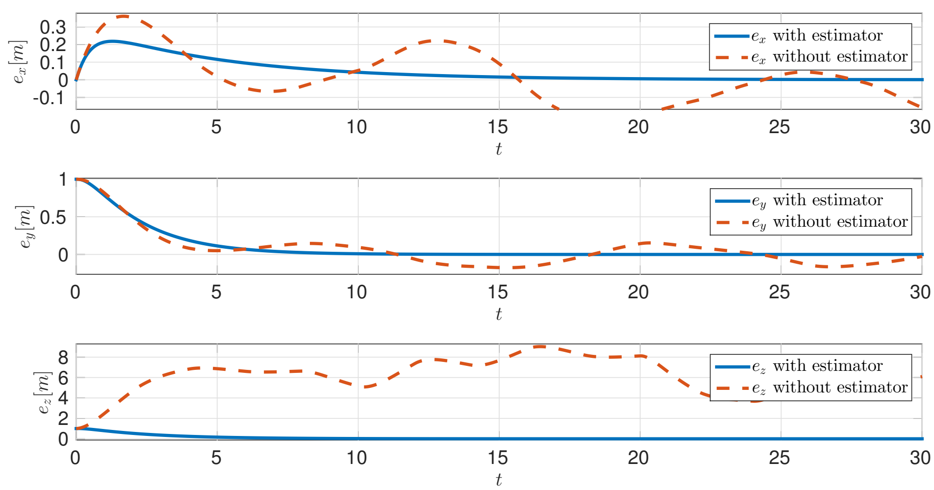

Figure 4.39. Translational error for Immersion and Invariance Approach with mass' estimator.

The error of the states x, y and z are presented in figure 4.39, and we can see that exists an error in each state, when the mass is not estimated. The maximum error in the x state is around the $20\ cm$, meanwhile the error remains constant around the $40\ cm$.

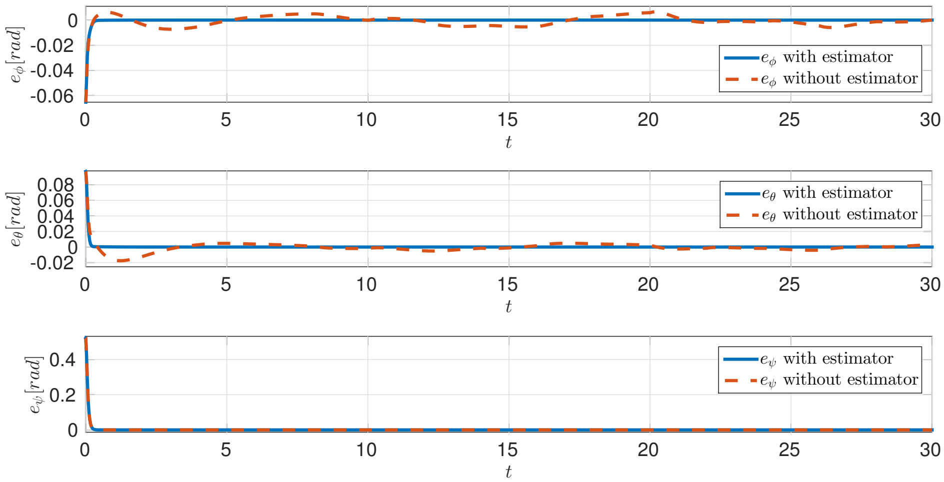

Figure 4.40. Rotational error for Immersion and Invariance Approach with mass' estimator.

The mass variation has a big impact in the rotational subsystem. From figure 4.40 we notice that there are errors in two states.

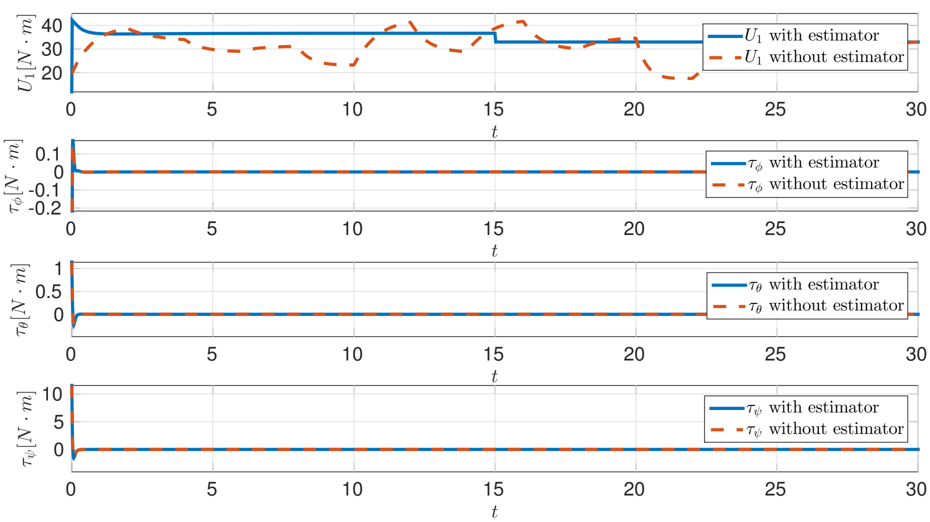

Figure 4.41. Control inputs for Immersion and Invariance Approach with mass' estimator.

Finally, we have the control inputs presented in figure 4.41. We can notice that the control input U_1 is bigger than the control input presented in the section before, this is because the mass variation. It is worth to mention that U_1 has a similar behavior with or without the estimation, but the main difference is that without the estimator we are not able to reach the reference. In the other hand, the control inputs for the rotational subsystem remains the same.

4.1.2.4 Observer for Quadrotor's translational subsystem velocity with Backstepping

In this section we present the results of the observer for the Quadrotor's translational subsystem velocity, this is because there is not a sensor that measures it. It is important to say that the simulation with the observer is the most real situation. We simulate the observer developed in 3.1.2.2 with the Backstepping control approach.

The block diagram applied for this simulation is introduced in the following figure 4.42

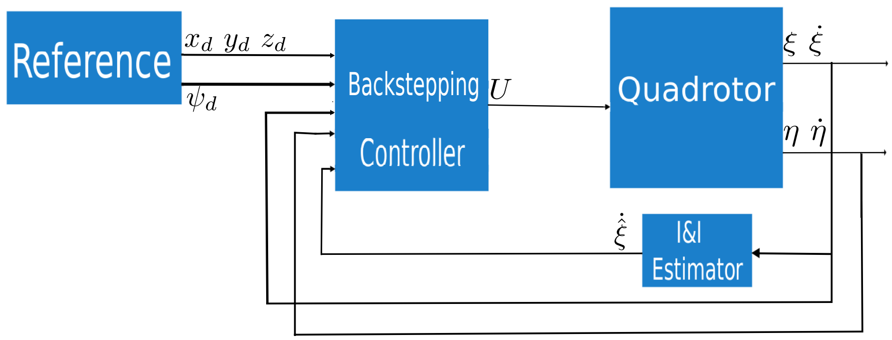

Figure 4.42. Block diagram for Nested Saturations controller with velocity observer.

The control gains for the Backstepping approach are given by the table 4.2, presented in section 4.1.1.1, and the estimator gain $\gamma = 100$.

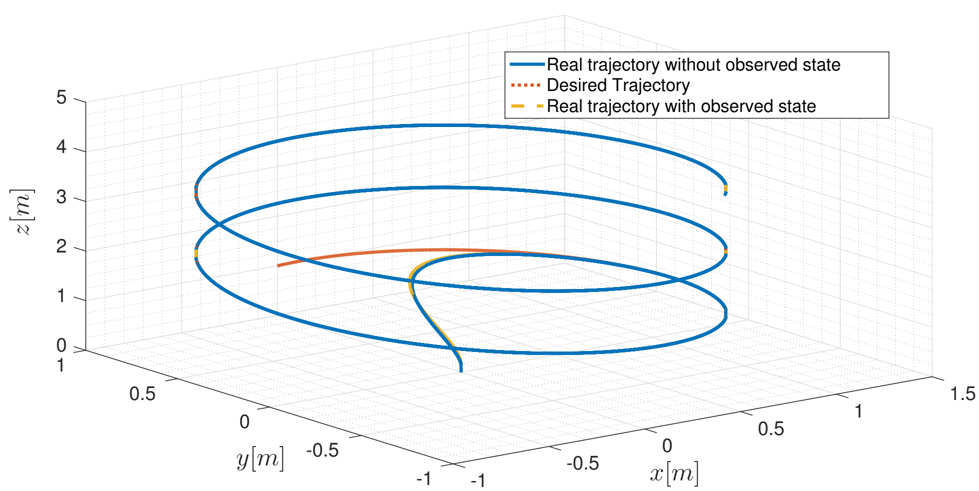

Figure 4.43. Helix trajectory for Backstepping Approach with velocity's observer.

In figure 4.43 we can do a first analysis of the trajectories with or without the observer is performed. We can notice that the tracking task is accomplished when the estimator is applied and when the estimation is not applied. Also, it seems there is no difference between the trajectories. Therefore, we proceed to analyze each state.

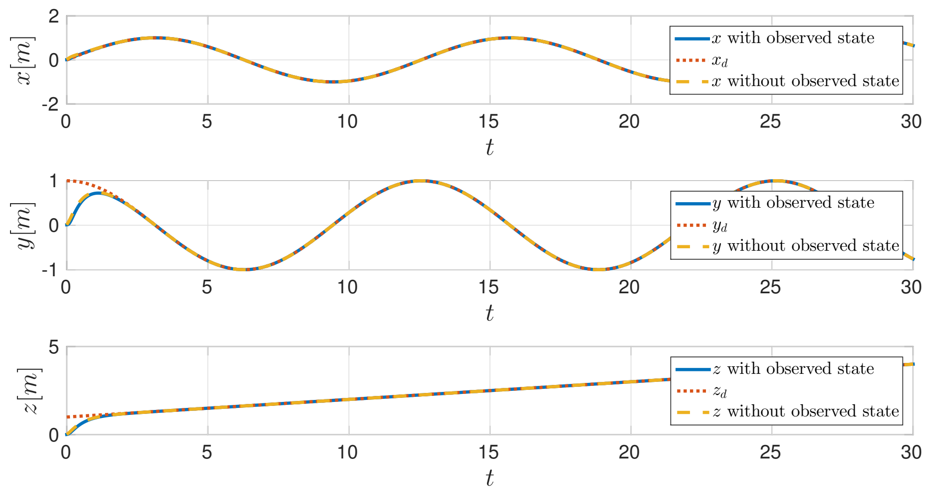

Figure 4.44. Translational states for Backstepping Approach with velocity's observer.

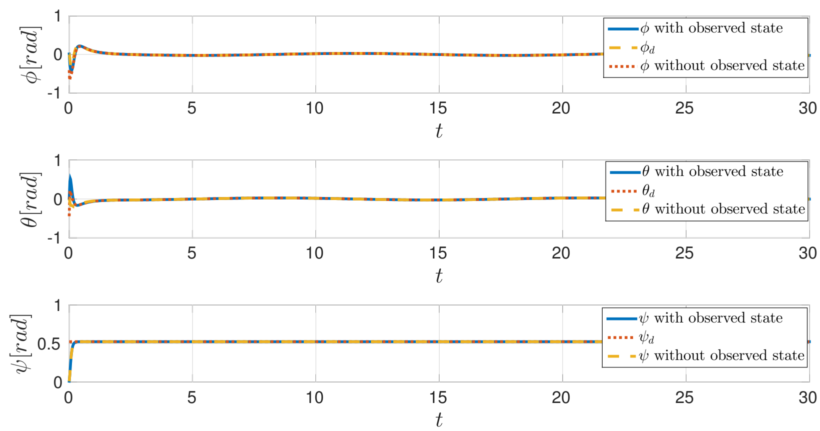

Figure 4.45. Rotational states for Backstepping Approach with velocity's observer.

From figure 4.44 and 4.45 we can see that all the states reach the reference but they do it in the same time. We notice that the ideal simulation is a little bit faster than the simulation with the observed state. This is an expected result that will make easier the implementation. However, it is necessary to do an error analysis in order to have a better comparison.

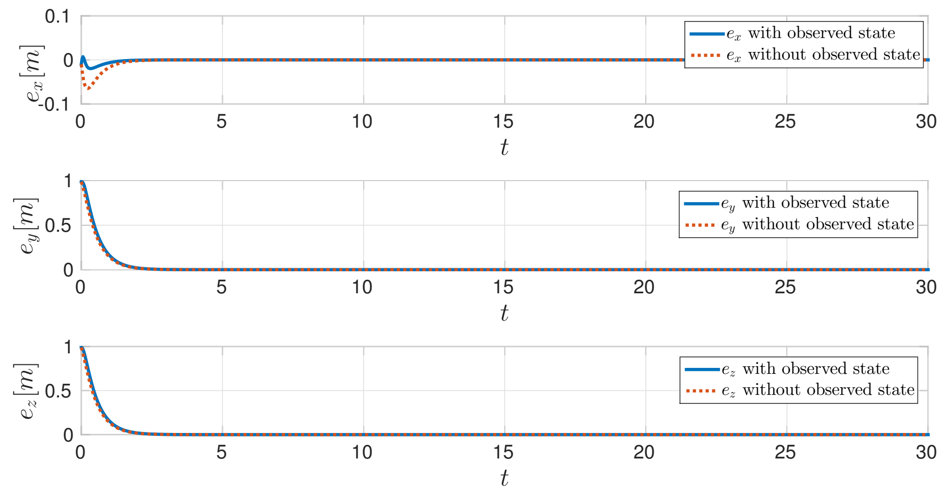

Figure 4.46. Translational error for Backstepping Approach with velocity's observer.

In figure 4.46 we can see that the ideal simulation is faster than the simulation with the observed states. For the x state the velocity of each simulation is almost the same, the error leads to 0 in 4 seconds, meanwhile, for the y state the error leads to 0 in three seconds, being the ideal simulation faster. Finally, the error for the z state is faster in the ideal simulation, but there is not a big difference.

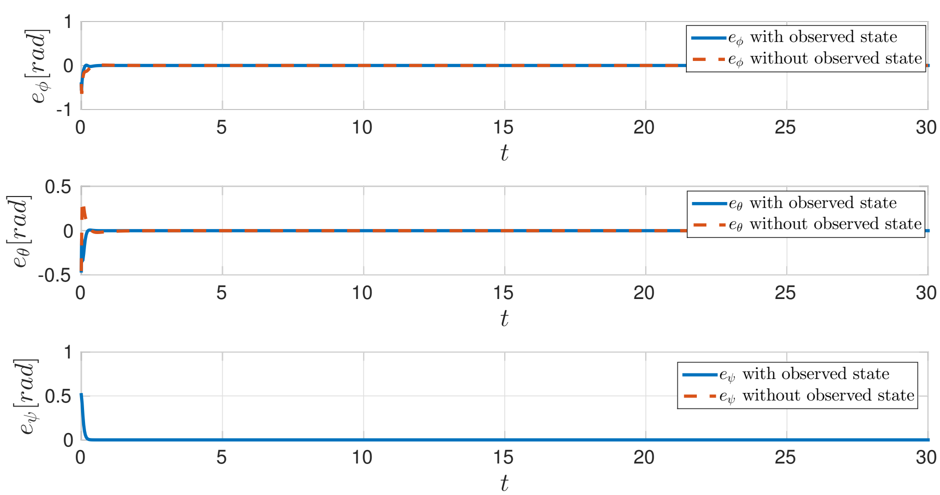

Figure 4.47. Rotational error for Backstepping Approach with velocity's observer.

As it have been said the ideal simulation is faster than the one with the observed state. Therefore from the figure 4.47 we can notice that the error for the ϕ and θ state leads to 0 in less than a second, meanwhile for the ψ state it does in 0.5 seconds.

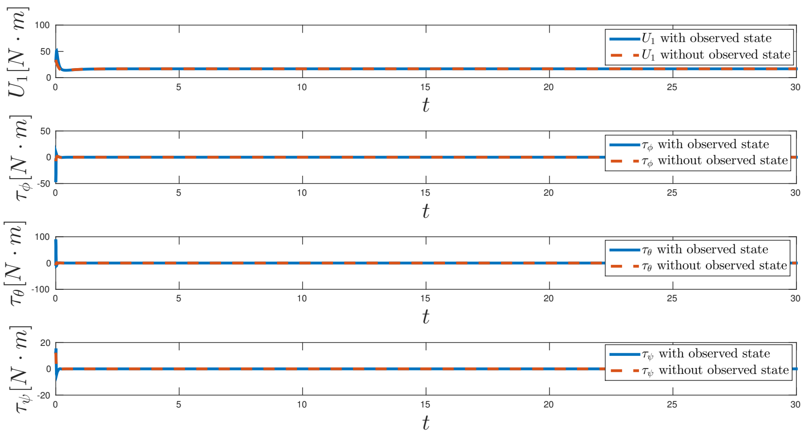

Figure 4.48. Control inputs for Backstepping Approach with velocity's observer.

Finally, the control inputs remains bounded, but we can see that the torques for the ideal simulation are smoother than the simulation with the observed states.

4.1.2.5 Observer for Quadrotor's translational subsystem velocity with Nested Saturations

In this section we present the results of the observer for the Quadrotor's translational subsystem velocity, this is because there is not a sensor that measures it. It is important to say that the simulation with the observer is the most real situation. We simulate the observer developed in 3.1.2.2 with the Nested Saturations control approach.

The block diagram applied for this simulation is introduced in the following figure 4.49

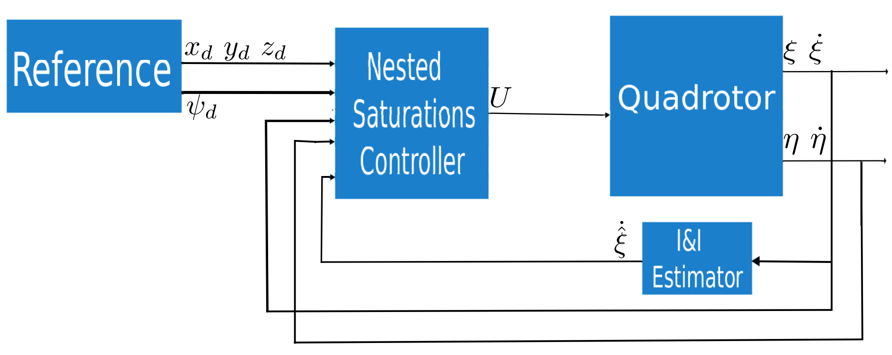

Figure 4.49. Block diagram for Nested Saturations controller with velocity observer.

The saturations for the Nested Saturations approach are given by the table 4.3, presented in section 4.1.1.2, and the estimator gain $\gamma = 100$.

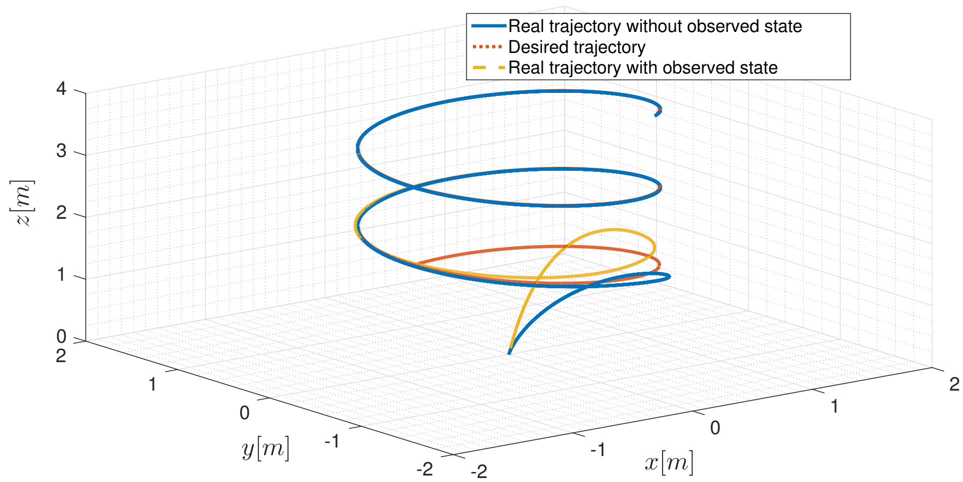

Figure 4.50. Helix trajectory for Nested Saturations Approach with velocity's observer.

In figure 4.50 we can do a first analysis of the trajectories with or without the observer is performed. We can notice that the tracking task is accomplished when the estimator is applied and when the estimation is not applied. Also, there is a difference between the speed of both trajectories. Therefore, we proceed to analyze each state.

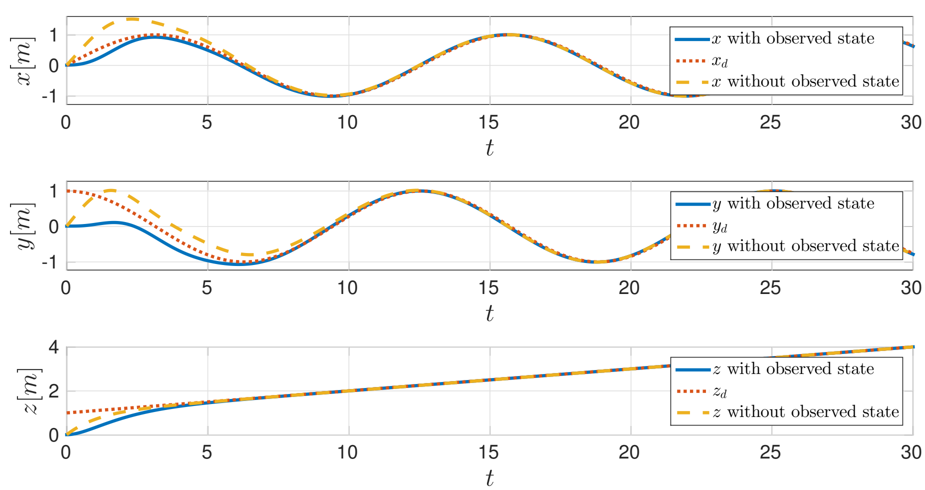

Figure 4.51. Translational states for Nested Saturations Approach with velocity's observer.

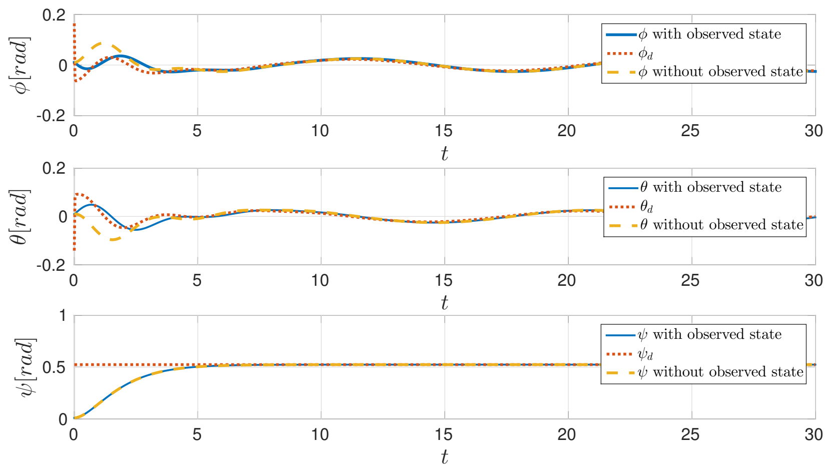

Figure 4.52. Rotational states for Nested Saturations Approach with velocity's observer.

From figure 4.51 and 4.52 we can see that all the states reach the reference but they do it in different time. We notice that the ideal simulation is faster against the simulation with the observed state. This an expected result that will make easier the implementation. However, it is necessary to do an error analysis in order to have a better comparison.

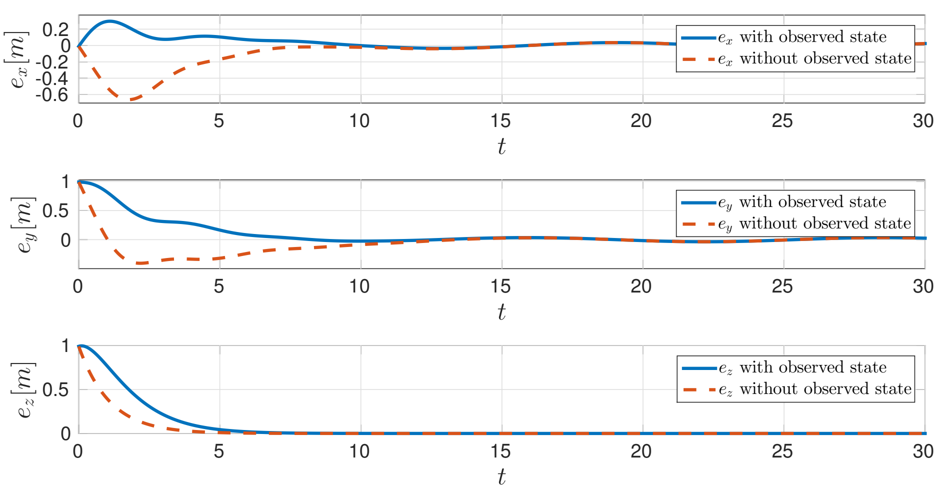

Figure 4.53. Translational error for Nested Saturations Approach with velocity's observer.

In figure 4.53 we can see that the ideal simulation is faster than the simulation with the observed states. For the x state the velocity of each simulation is almost the same, the error leads to 0 in 10 seconds, meanwhile, for the y state the error leads to 0 in eleven seconds, being the ideal simulation faster. Finally, the error for the z state is faster in the ideal simulation, but there is not a big difference.

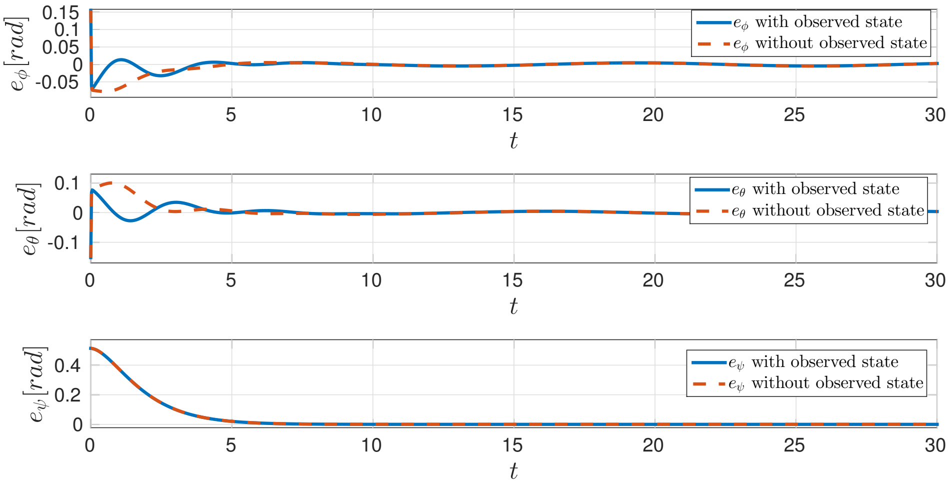

Figure 4.54. Rotational error for Nested Saturations Approach with velocity's observer.

As it have been said the ideal simulation is faster than the one with the observed state. Therefore from the figure 4.54 we can notice that the error for the ϕ and θ state leads to 0 in 7 seconds, meanwhile for the ψ state it does in 6 seconds.

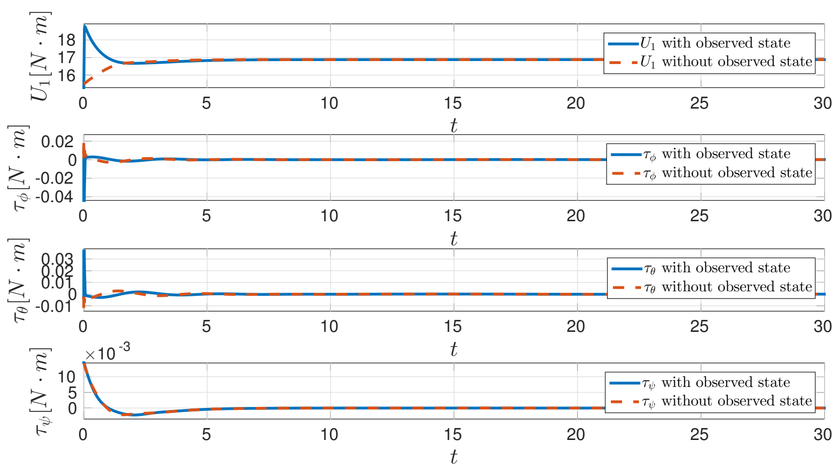

Figure 4.55. Control inputs for Nested Saturations Approach with velocity's observer.

Finally, the control inputs remains bounded, but we can see that the torques for the ideal simulation are smoother than the simulation with the observed states.

4.1.2.6 Observer for Quadrotor's translational subsystem velocity with Immersion and Invariance

In this section we present the results of the observer for the Quadrotor's translational subsystem velocity, this is because there is not a sensor that measures it. It is important to say that the simulation with the observer is the most real situation. We simulate the observer developed in 3.1.2.2 with the Immersion and Invariance control approach.

The block diagram applied for this simulation is introduced in the following figure 4.56

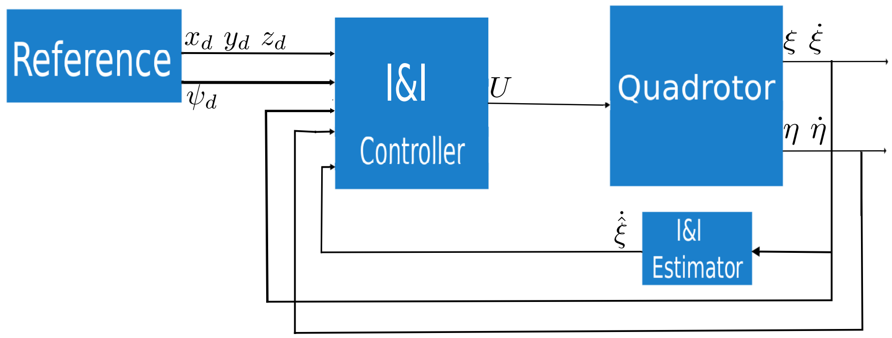

Figure 4.56. Block diagram for Immersion and Invariance controller with velocity observer.

The control gains for the Immersion and Invariance approach are given by the table 4.4, presented in section 4.1.1.3, and the estimator gain $\gamma = 100$.

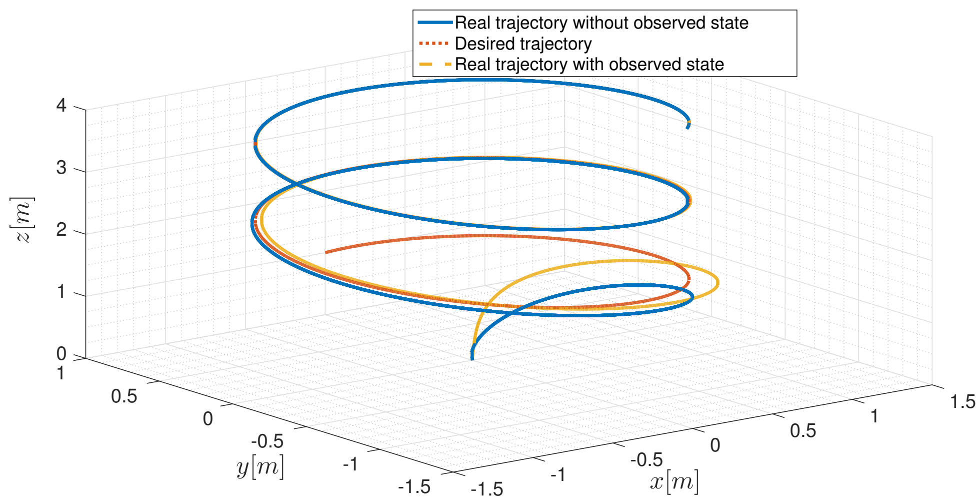

Figure 4.57. Helix trajectory for Immersion and Invariance Approach with velocity's observer.

In figure 4.57 we can do a first analysis of the trajectories with or without the observer is performed. We can notice that the tracking task is accomplished when the estimator is applied and when the estimation is not applied. Also, there is a small difference between the trajectories. Therefore, we proceed to analyze each state.

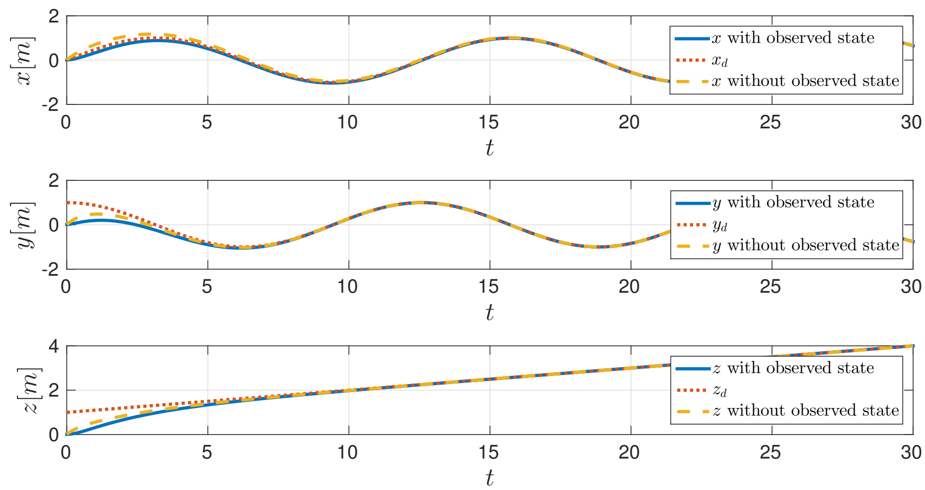

Figure 4.58. Translational states for Immersion and Invariance Approach with velocity's observer.

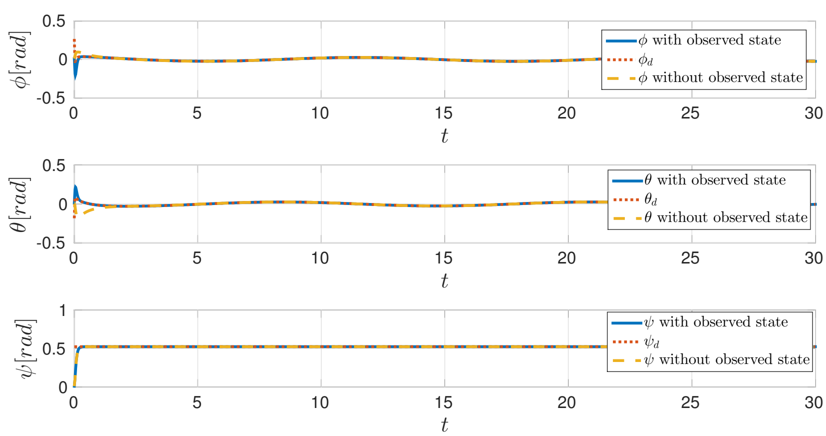

Figure 4.59. Rotational states for Immersion and Invariance Approach with velocity's observer.

From figure 4.58 and 4.59 we can see that all the states reach the reference and they do it in almost the same time. We notice that the ideal simulation is a little bit faster than the simulation with the observed state. This is an expected result that will make easier the implementation. However, it is necessary to do an error analysis in order to have a better comparison.

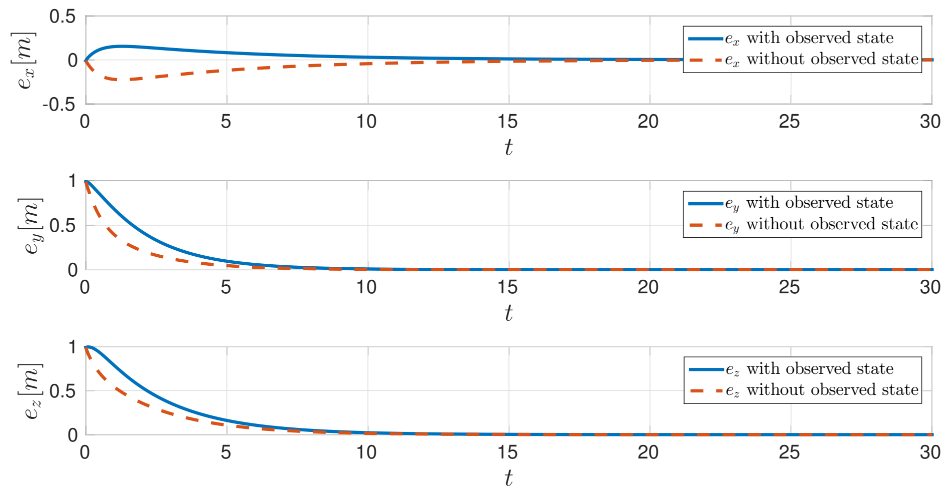

Figure 4.60. Translational error for Immersion and Invariance Approach with velocity's observer.

In figure 4.60 we can see that the ideal simulation is faster than the simulation with the observed states. For the x state the velocity of each simulation is almost the same, the error leads to 0 in 15 seconds, meanwhile, for the y state the error leads to 0 in eight seconds, being the ideal simulation faster. Finally, the error for the z state is faster in the ideal simulation, but there is not a big difference.

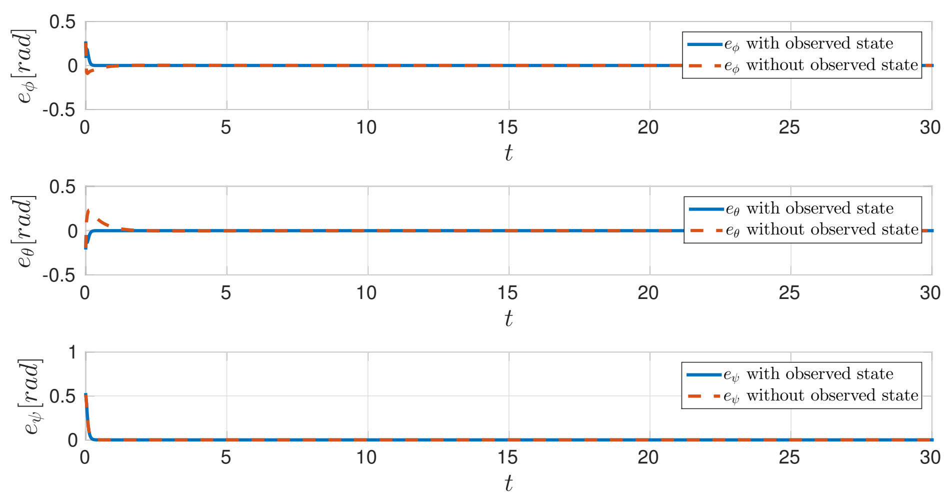

Figure 4.61. Rotational error for Immersion and Invariance Approach with velocity's observer.

As it have been said the ideal simulation is faster than the one with the observed state. Therefore from the figure 4.61 we can notice that the error for the ϕ and θ state leads to 0 in less than a second, meanwhile for the ψ state it does in 0.5 seconds.

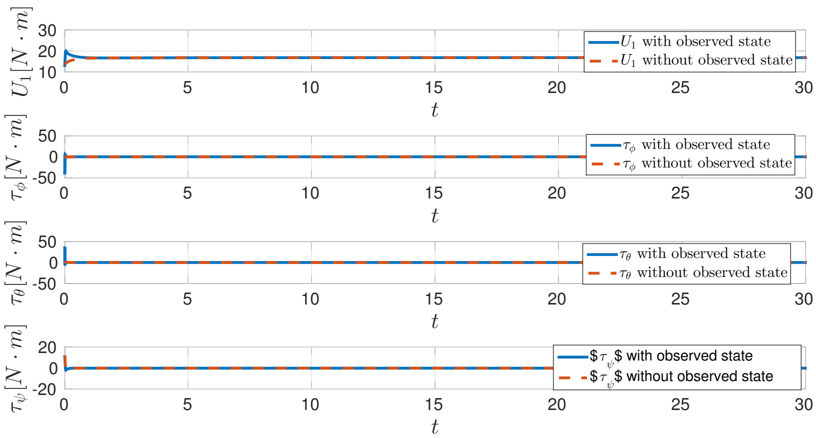

Figure 4.62. Control inputs for Immersion and Invariance Approach with velocity's observer.

Finally, the control inputs remains bounded, but we can see that the torques for the ideal simulation are smoother than the simulation with the observed states.

4.1.2.7 Observer for translational subsystem velocity and Estimator of mass with Backstepping

In this section we simulate the worst scenario possible, the Quadrotor with the mass variations plus the velocity state observation. Hence, we will simulate the Backstepping approach with the both cases mentioned before. The block diagram applied for this simulation is introduced in the following 4.63

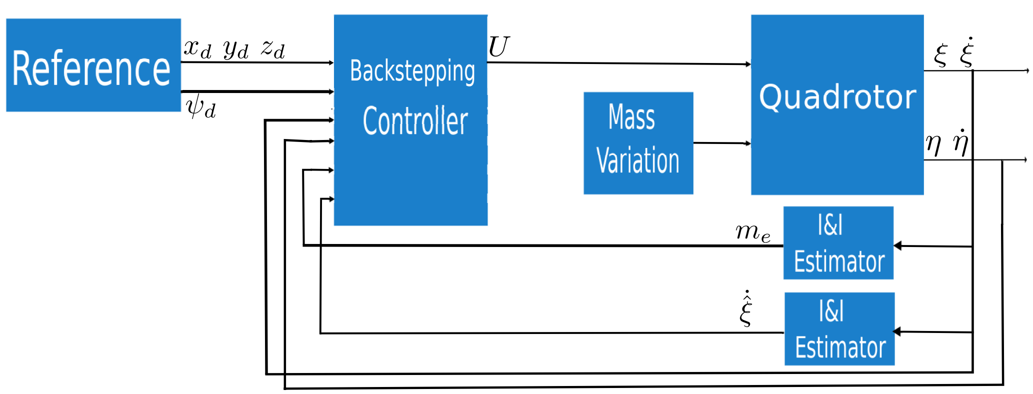

Figure 4.63. Block diagram for Backstepping controller with velocity observer and mass observer.

In order to accomplish the simulation, we assume tha mass variations from figure 4.20, the Backstepping control gains from table 4.2, the mass estimator gain $\gamma_e = 75$ and the velocity observer gain $\gamma_v = 100$.

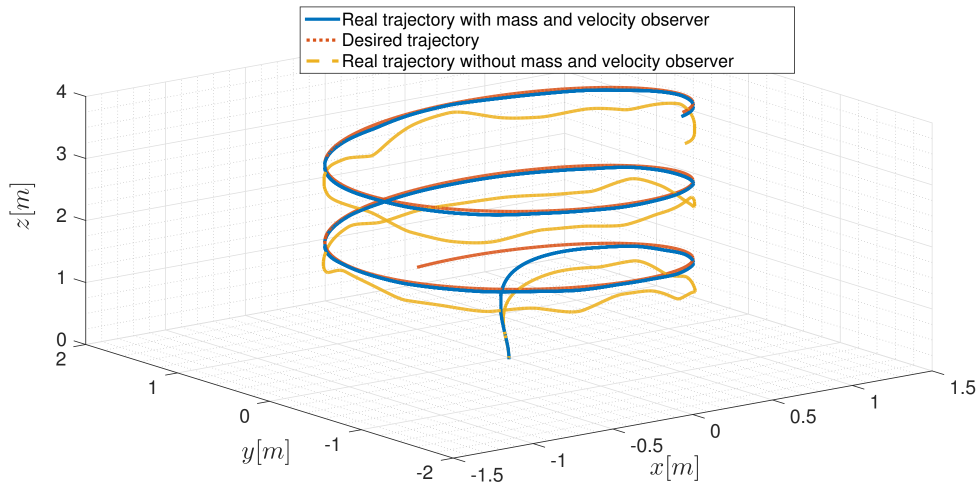

Figure 4.64. Helix trajectory for Backstepping Approach with an observer for translational subsystem velocity and estimator mass.

In figure 4.64 we can show a first analysis of the trajectories with or without the observers. We can notice that the tracking task is accomplished when the estimator and observer are applied, but when them are not applied we have a different situation. It is seen that the trajectory without the observers can not reach the desired reference. Therefore, we proceed to analyze each state.

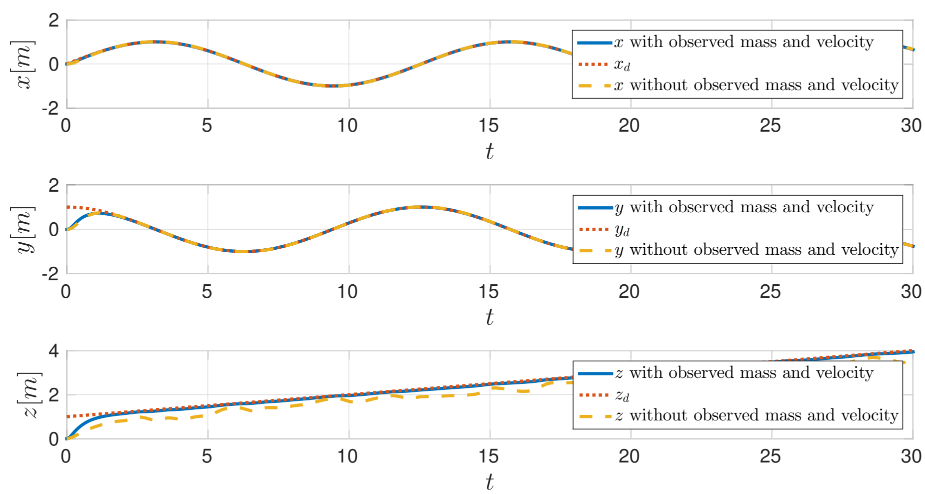

Figure 4.65. Translational states for Backstepping Approach with an observer for translational subsystem velocity and mass estimator.

From the translational states we can see in the vertical helix figure, the trajectory with the observers is better than the one without them. The state that can not reach the reference is the z state meanwhile the x and y states have a better performance.

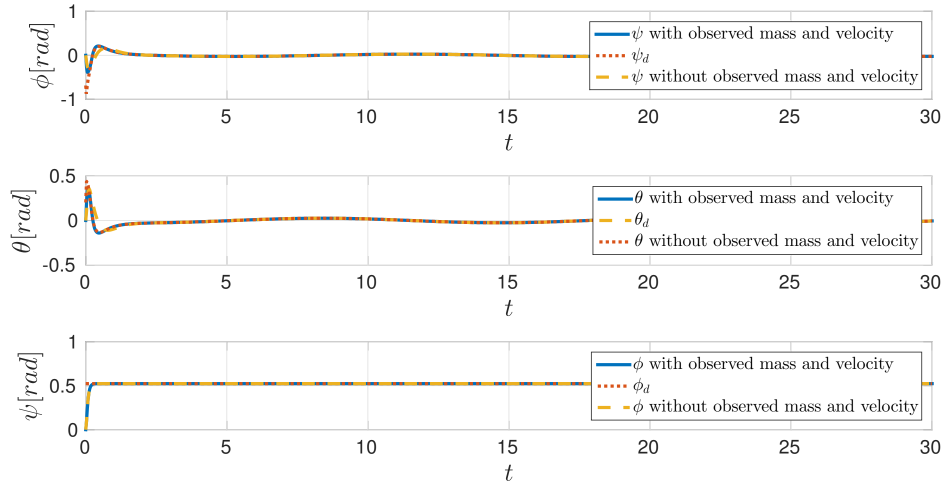

Figure 4.66. Rotational states for Backstepping Approach with an observer for translational subsystem velocity and estimator mass.

In figure 4.66 we notice that the rotational states are not affected as much as the translational states. The performance with the observers is almost perfect, on the contrary for the simulation without the observers exists a minimum error. Therefore, we proceed to do the error analysis.

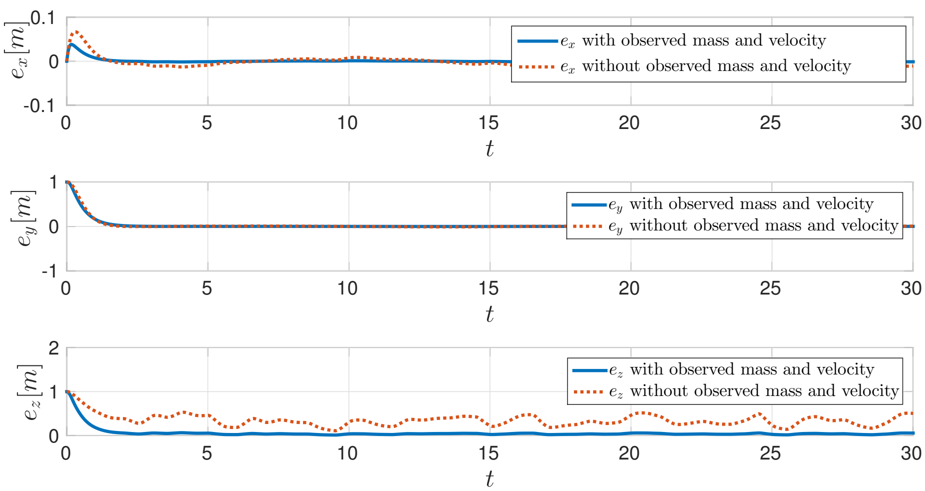

Figure 4.67. Translational error for Backstepping Approach with an observer for translational subsystem velocity and estimator mass.

The translational error is presented in figure 4.67. We can see that the error with the observed velocity and the mass estimation leads to 0, for the state x in 3 seconds, for y in 2 seconds and for z in 5 seconds. On the other hand, the errors without the estimation and the observation do not lead to 0. In the x state the error is variable with a top value of $60\ cm$, for the y state there is a variable error too with a maximum error of 1 meter, and finally for z the top error is around the 1 meter, and after that it remains variable.

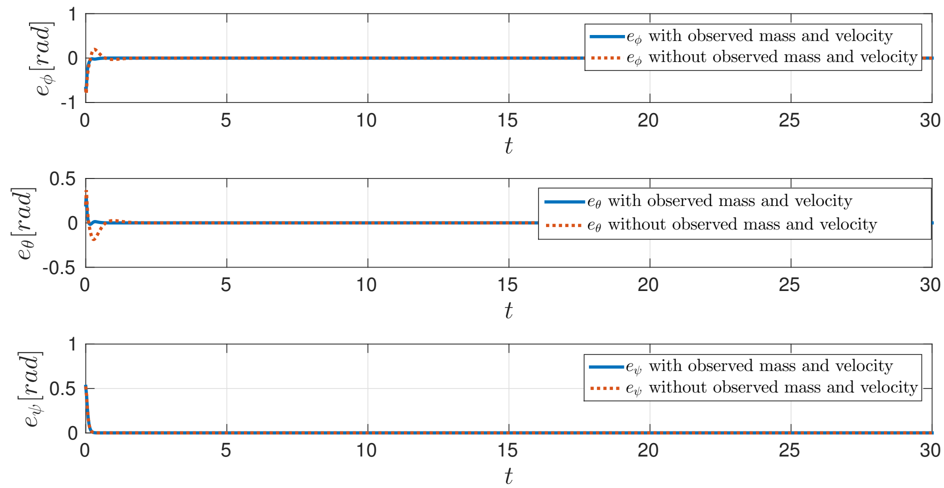

Figure 4.68. Rotational error for Backstepping Approach with an observer for translational subsystem velocity and estimator mass.

The rotational error is presented in figure 4.68. We can see that the error with the observed velocity and the mass estimation leads to 0, for all the states in less than 1 second. However, the errors without the estimation and the observation do not lead to 0. In the ϕ state the error is variable with a top value of $0.01\ rad$, for the θ state there is a variable error too with a maximum error of $-0.02\ rad$, and finally for ψ the error has the same behavior than the ψ state with the observations.

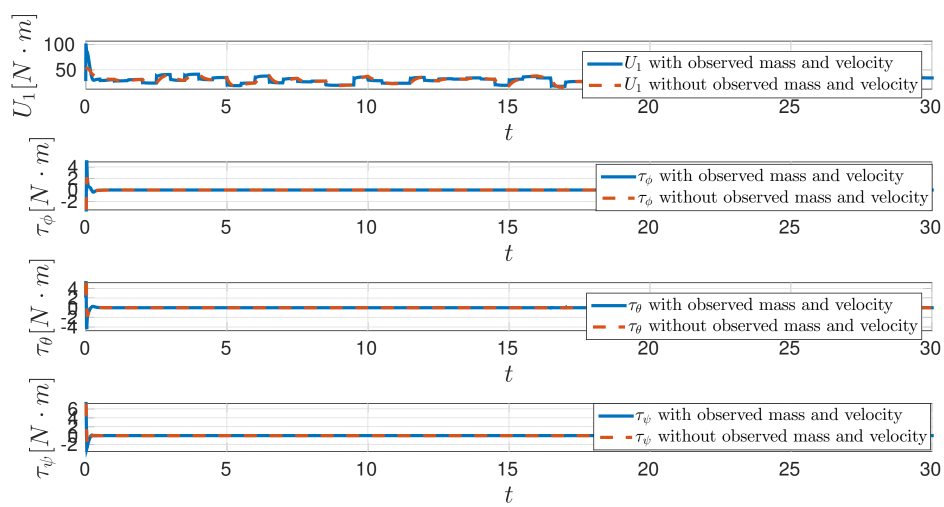

Figure 4.69. Control inputs for Backstepping Approach with an observer for translational subsystem velocity and estimator mass.

To conclude, we present the control inputs in figure 4.69 where we can notice that the control efforts have increased. The control input U_1 with observed mass and velocity reaches torques around the 40

$N \cdot m$, meanwhile the non observed has a smoother control effort around the $38\ N \cdot m$. For the rotational control efforts, we can notice that the inputs with the observed states and parameters is higher than the one without the observed ones.

4.1.2.8 Observer for translational subsystem velocity and Estimator of mass with Immersion and Invariance

In this section we simulate the worst scenario possible, the Quadrotor with the mass variations plus the velocity state observation. We have analyzed each observer in combination with the nonlinear controllers Backstepping and Nested Saturations. Hence, we will simulate the Immersion and Invariance approach with the both cases mentioned before.

The block diagram applied for this simulation is introduced in the following figure 4.70

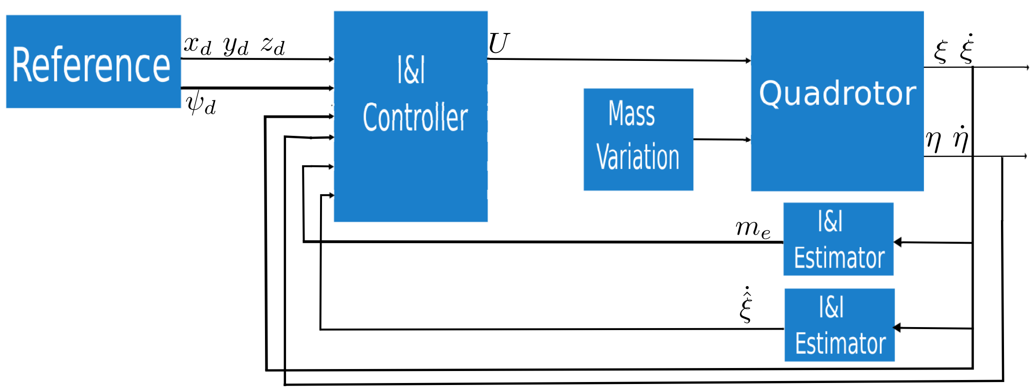

Figure 4.70. Block diagram for I&I controller with velocity observer and mass observer.

In order to accomplish the simulation, we assume tha mass variations from figure 4.20, the Immersion and Invariance control gains from table 4.4, the mass estimator gain $\gamma_e = 75$ and the velocity observer gain $\gamma_v = 100$.

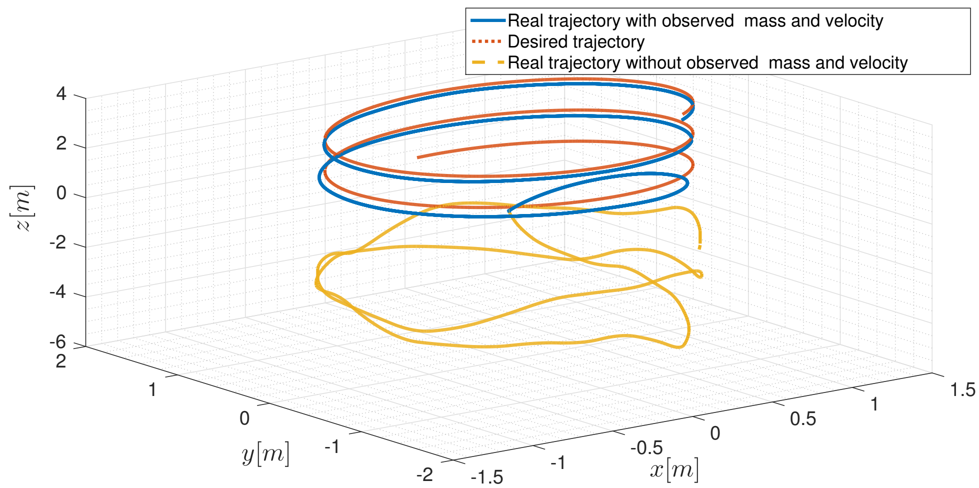

Figure 4.71. Helix trajectory for Immersion and Invariance Approach with an observer for translational subsystem velocity and estimator mass.

In figure 4.71 we can show a first analysis of the trajectories with or without the observers. We can notice that the tracking task is accomplished when the estimator and observer are applied, but when them are not applied we have a different situation. It is seen that the trajectory without the observers can not reach the desired reference, at the begining it goes down and after certain time it tries to follow the reference but it is impossible to reach it. Therefore, we proceed to analyze each state.

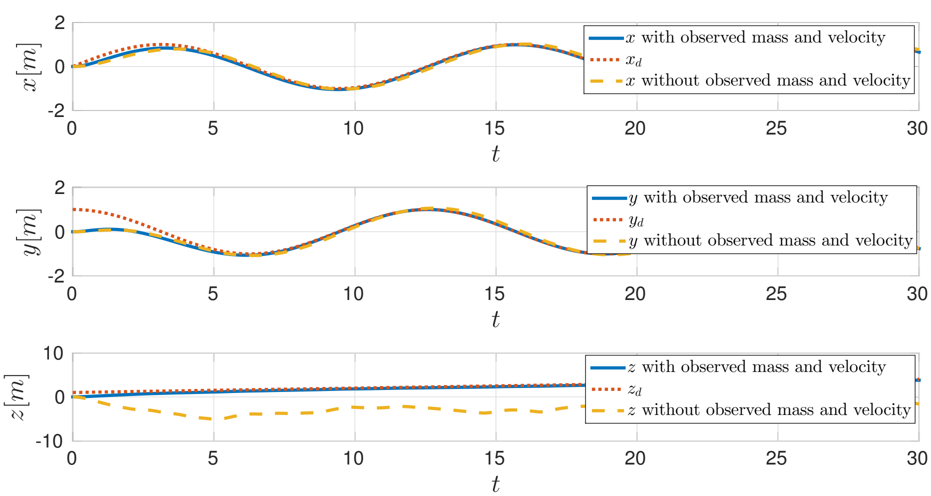

Figure 4.72. Translational states for Immersion and Invariance Approach with an observer for translational subsystem velocity and mass estimator.

From the translational states we can see in the vertical helix figure, the trajectory with the observers is better than the one without them. The state that diverges is the z state meanwhile the x and y states have a better performance.

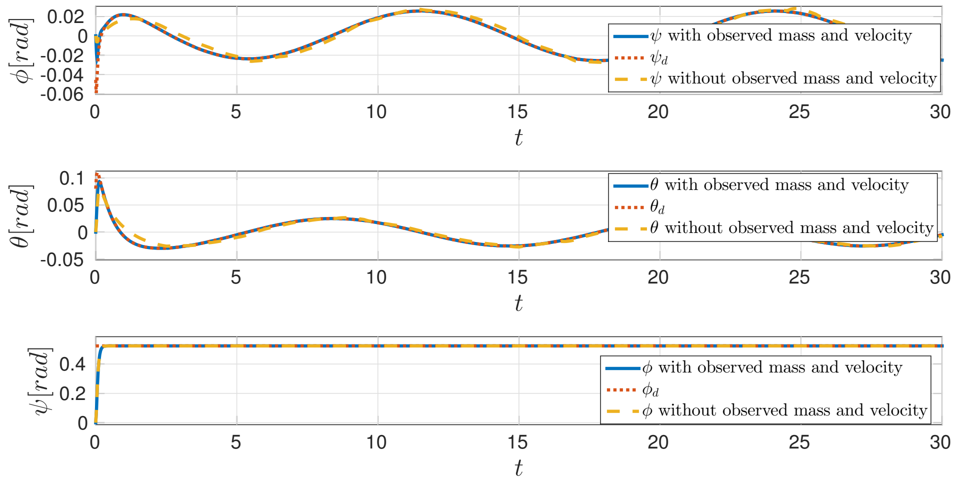

Figure 4.73. Rotational states for Immersion and Invariance Approach with an observer for translational subsystem velocity and estimator mass.

In figure 4.73 we notice that the rotational states are not affected as much as the translational states. The performance with the observers is almost perfect, on the contrary for the simulation without the observers exists a minimum error. Therefore, we proceed to do the error analysis.

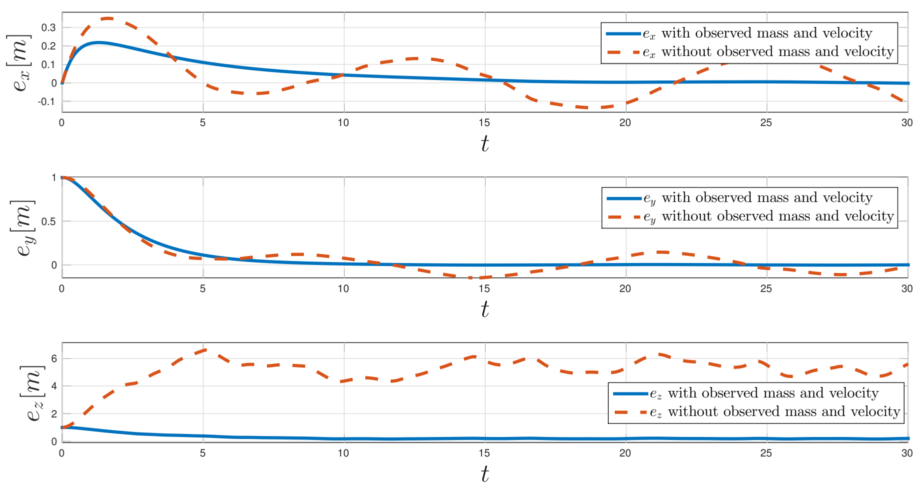

Figure 4.74. Translational error for Immersion and Invariance Approach with an observer for translational subsystem velocity and estimator mass.

The translational error is presented in figure 4.74. We can see that the error with the observed velocity and the mass estimation leads to 0, for the state x in 15 seconds, for y in 8 seconds and for z in 3 seconds. On the other hand, the errors without the estimation and the observation do not lead to 0. In the x state the error is variable with a top value of 37 cm, for the y state there is a variable error too with a maximum error of 1 meter, and finally for z the top error is around the 6.5 meters, and after that it remains variable.

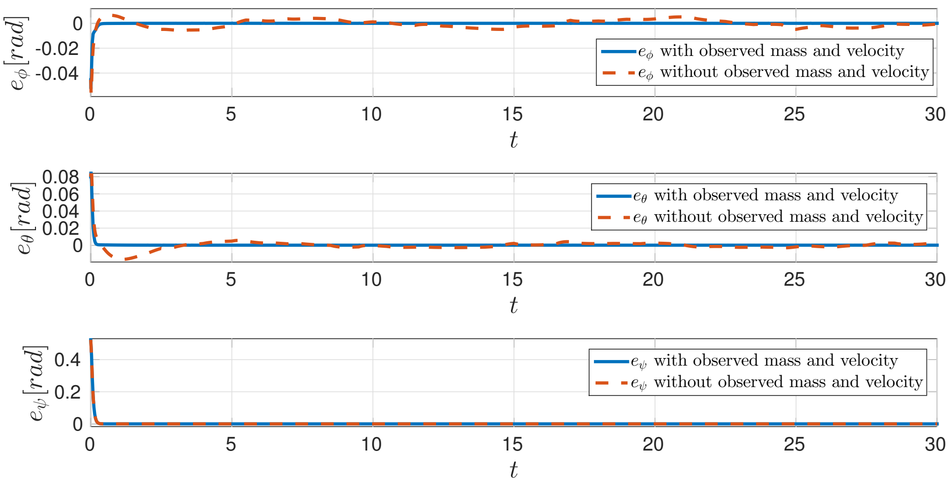

Figure 4.75. Rotational error for Immersion and Invariance Approach with an observer for translational subsystem velocity and estimator mass.

The rotational error is presented in figure 4.75. We can see that the error with the observed velocity and the mass estimation leads to 0, for all the states in less than 1 second. However, the errors without the estimation and the observation do not lead to 0. In the ϕ state the error is variable with a top value of $0.01\ rad$, for the θ state there is a variable error too with a maximum error of $-0.02\ rad$, and finally for ψ the error has the same behavior than the ψ state with the observations.

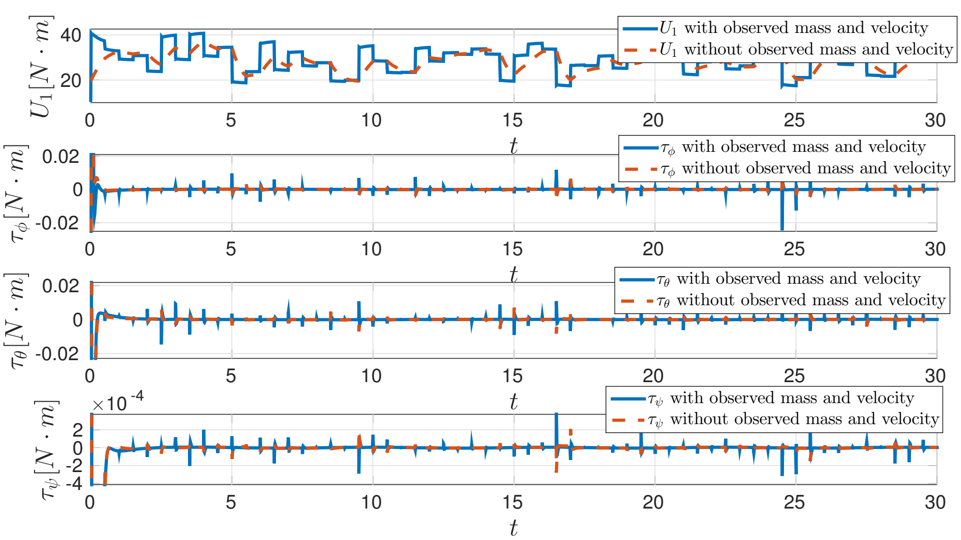

Figure 4.76. Control inputs for Immersion and Invariance Approach with an observer for translational subsystem velocity and estimator mass.

To conclude, we present the control inputs in figure 4.76 where we can notice that the control efforts have increased. The control input U_1 with observed mass and velocity reaches torques around the 40

$N \cdot m$, meanwhile the non observed has a smoother control effort around the $38\ N \cdot m$. For the rotational control efforts, we can notice that the inputs with the observed states and parameters is higher than the one without the observed ones.

4.2 Nonlinear Controllers and Observers for Interactive Tilt-rotor Air-vehicle

In order to illustrate the proposed results in 3.2, in the following we will consider several numerical examples. To this end, the nominal values considered for the rotorcraft are summarized in table 4.5.

Parameters	Value	Parameters	Value
l_p	$0.35m$	g	$9.81\frac{m}{s^2}$
m_r	$0.5kg$	m_p	$0.125kg$
σ_{m_r}	$(0.5)^2$	σ_{m_p}	$(0.25)^2$
I_r	$0.177kg \cdot m^2$	I_p	$0.153kg \cdot m^2$

Table 4.5. Interactive Tilt-Rotor nominal parameters.

The block diagram applied for this simulation is introduced in the following figure 4.77.

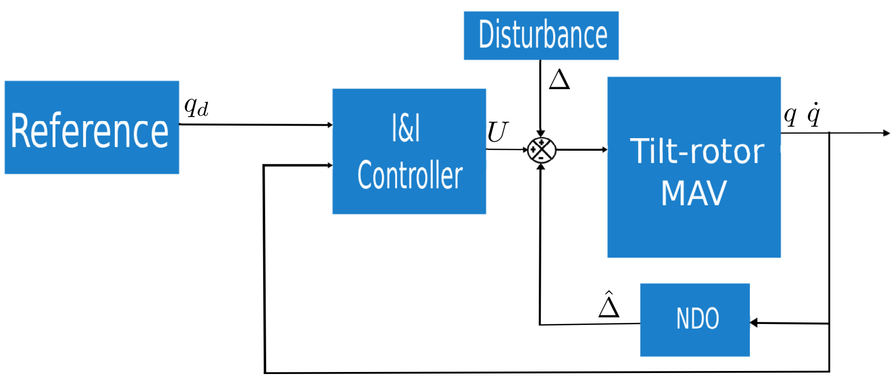

Figure 4.77. Block diagram for the Interactive Tilt-rotor with nonlinear disturbance observer.

As it is mentioned previously, the rotorcraft manipulator will be the pendulumlike in the system, which implies that the mass will change as the manipulator carries a load. Thus, in order to take into account the worst possible scenario, the pendulumlike payload and the rotorcraft variation are considered as the depicted in Figure 4.78.

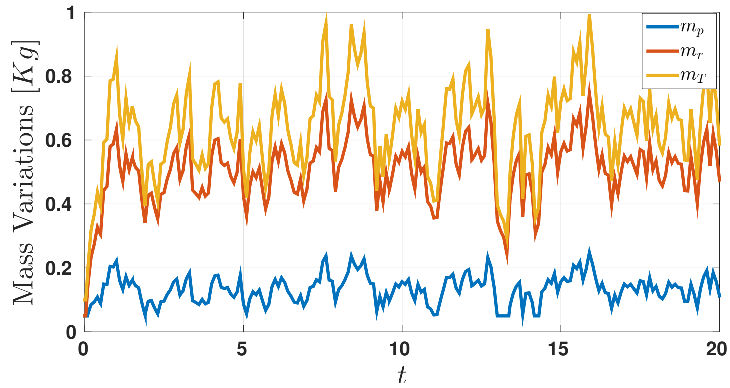

Figure 4.78. Profile of the lumped disturbance for the Interactive Tilt-Rotor.

Applying the results presented in Sections 3.2.1 and 3.2.2, we derive the gains for the I&I control, as well as the gains for the nonlinear disturbance observer summarized in table 4.6, where $\boldsymbol{K} := diag\{k_1, k_2, k_3, k_4\}$ and $\boldsymbol{K}_\zeta := diag\{k_{z_1}, k_{z_2}, k_{z_3}, k_{z_4}\}$.

Control gain	Value	Control gain	Value	Observer gain	Value
k_1	5	k_{z1}	3	$k_{\Delta 1}$	20
k_2	7	k_{z2}	5	$k_{\Delta 2}$	20
k_3	55	k_{z3}	60	$k_{\Delta 3}$	50
k_4	60	k_{z4}	65	$k_{\Delta 4}$	20

Table 4.6. Control & observer gains for the Interactive Tilt-Rotor.

For this example, we have considered as a desired trajectory a circle, as can be seen from Figure 4.79. Such circle starts at 1 meter from the floor, with a radius of 4 meters. This trajectory is described by the equations $x(t) = 4\sin(\frac{\pi}{2}t) + 5$; $z(t) = 4\cos(\frac{\pi}{2}t) + 5$;$\theta = \frac{\pi}{6}$; $\gamma(t) = \frac{\pi}{6}\sin(\frac{\pi}{2}t)$. The initial position is zero, so the rotorcraft follows the trajectory as better as it can.

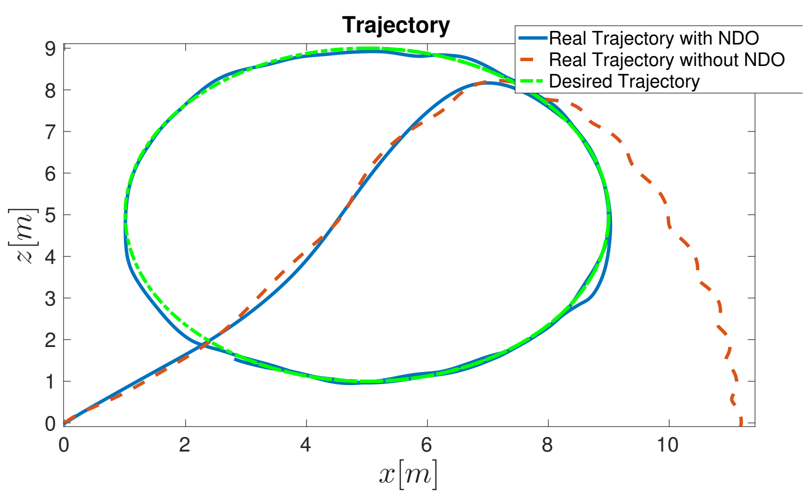

Figure 4.79. Trajectory tracking performance for a circular path.

The states, as shown in Figure 4.80, have a minimum error due the pendulum-like payload variations. But the control technique used, plus the observer has an excellent response against the disturbances.

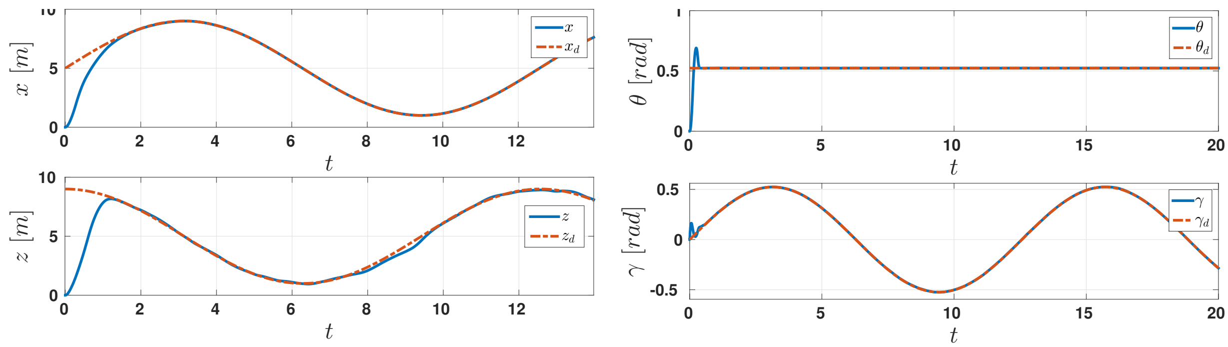

Figure 4.80. Interactive Tilt-rotor states

Despite the pendulum-like payload variations, the errors leads to zero after 1.5 seconds for the x and y positions; and 0.6 seconds for the angles. In Figure 4.81 the error evolution can be seen. Using the nonlinear disturbance observer the control is robust and the aircraft performance is improved.

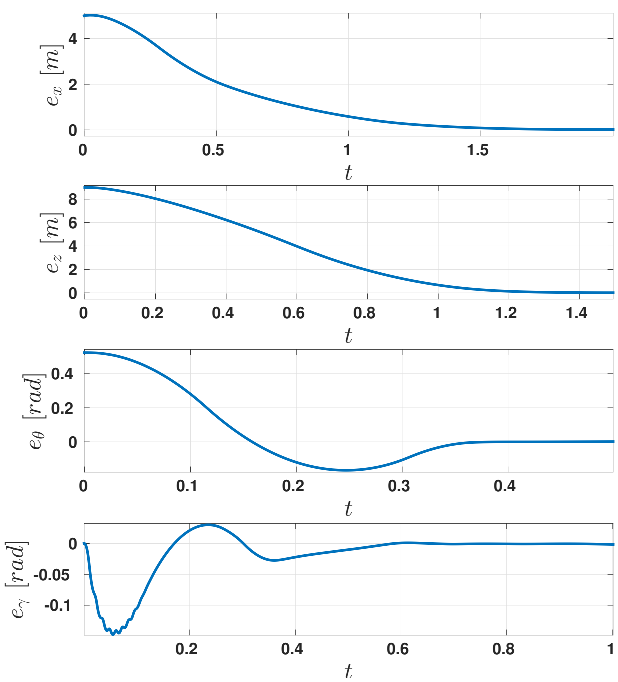

Figure 4.81. Interactive Tilt-rotor errors

In the other hand, the control inputs are bounded. This is because in real experimentation the rotorcraft engines are limited to a top thrust force that they can apply. So the maximum total thrust is around 7 Newtons, as the Figure 4.82 shows.

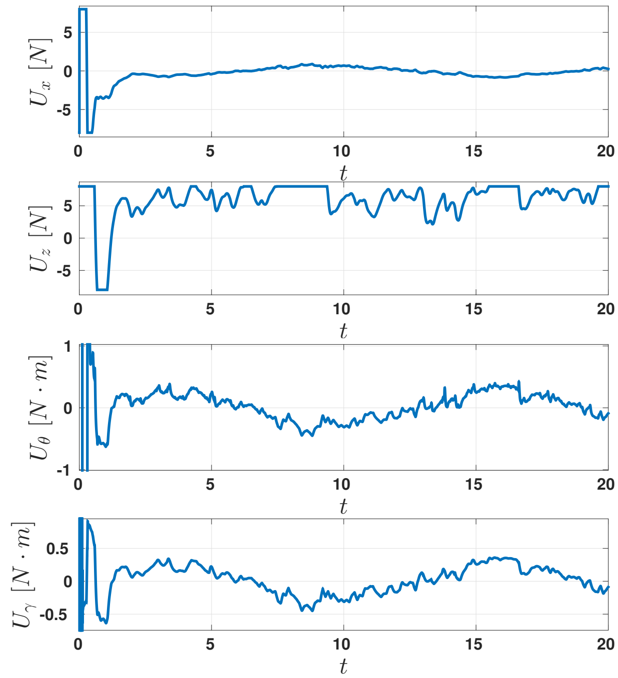

Figure 4.82. Control inputs

As it can be seen the I&I control law plus the nonlinear disturbance observer has a good performance. The errors are global asymptotically stables in 0.

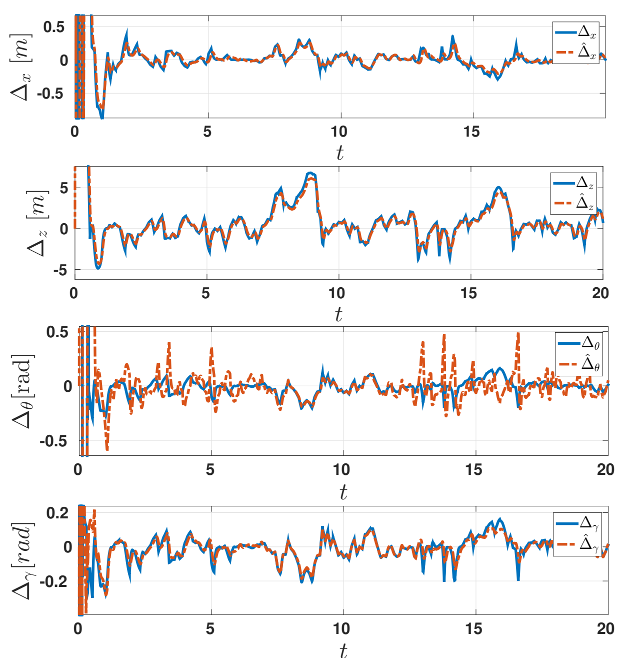

Figure 4.83. Observed states.

Finally, the performance of the system against the disturbances is improved due the nonlinear disturbance observer. As it can be seen in Figure 4.83 the observed disturbance is almost equal as the real disturbance.

4.3 Performance Index

The error criteria allows us to evaluate the system performance and they are the basis to improve them according the behavior of the error.

The performance index are defined as the value which works as a parameter to evaluate the controller quality.

The main performance index are:

- Absolut error criteria (IAE):
$$IAE = \int_0^\infty |e(t)|\, dt$$
- Quadratic error integral criteria (ISE)
$$ISE = \int_0^\infty e(t)^2 dt$$
- Absolut error time integral (ITAE)
$$ITAE = \int_0^\infty t\, |e(t)|\, dt.$$

Following the error criteria presented before, we apply these indexes in order to evaluate our controllers performance. Thus, according to this criteria, the results for the Backstepping are summarized in table 4.7.

Position State	ITAE	IAE	ISE
x	0.01736	0.02603	0.0006082
y	0.3132	0.6222	0.3759
z	0.2816	0.5762	0.3322

Table 4.7. Performance Index for Backstepping.

After that, we applied the error criteria for the Nested Saturations approach, where we can sum up the results in table 4.8.

Position State	ITAE	IAE	ISE
x	117.4	3.984	0.6508
y	122.2	5.654	2.368
z	3.2	2.1	1.352

Table 4.8. Performance Index for Nested Saturations.

Finally the error criteria is applied for the Immersion and Invariance controller, then, we summarized the results in the following table.

Position State	ITAE	IAE	ISE
x	7.963	1.417	0.1818
y	5.588	2.571	1.517
z	7.431	2.917	1.648

Table 4.9. Performance Index for Immersion and Invariance.

From the error criteria analyzed before we can conclude from table 4.7, that the best controller with the minimum error is the Backstepping approach in the ideal conditions. The reason why we did not applied this error criteria for the worst scenario possible, is because we have a variable mass and that leads our error to ∞.

CONCLUSIONS.

In this work we have presented the dynamical models of the Quadrotor aircraft and the nouvel interactive tilt-rotor micro air vehicles. The rotorcraft models are obtained via the Euler-Lagrange formalism. Also, three nonlinear control approaches are developed for the Quadrotor and a single one for the interactive tilt-rotor for a tracking task. In addition, we design a mass variation estimator, in order to reject the parametric uncertainty, and a velocity observer for the quadcopter system. Moreover, in order to improve the flying performance, a nonlinear disturbance observer is introduced for the interactive tilt-rotor.

In order to understand the rotorcrafts' behavior the whole dynamical models were obtained. From the rigid body dynamics, the Tait-Bryan angles, Hamiltonians mechanics and other mechanical approaches we are able to set up the basis for the dynamical modeling of the rotorcrafts. As it have been said, the kinematics equation were derived from the Euler-Lagrange formalism, an energy based approach. Therefore, once the kinematic model is obtained the nonlinear control approaches can be implemented in the equations obtained.

The first control strategy applied in this work is the Backstepping approach, calculated through some Lyapunov's functions. This control law is one of the most popular control techniques used for nonlinear systems, and in this work is designed to introduce us into the nonlinear systems theory. As a result, we obtained control laws for the Quadrotor's translational subsystem and for the rotational too. From the simulations we can conclude that this control strategy is not robust enough against parametric uncertainties, therefore, the tracking task is not accomplished due to the significant error involved.

The second control strategy designed in this thesis is the Nested Saturation approach. The main objective of this approach is to accomplish the tracking task and to saturate the control inputs. This is because in reality we are not able to reach the control efforts above the physical limits. In this nonlinear control technique we obtained two similar control laws, the traslational subsystem control and the rotational one. In the simulations, we can notice that this control approach has not the ideal performance against the parametric uncertainties. Applying a mass variation the system can not follow the desired reference, hence, an error in the altitude state is presented.

The third and final control strategy developed in this work is the Immersion and Invariance approach. This control law has not been applied extensively into the rotorcrafts works, thus, we applied it in the both systems introduced in this text. The principals characteristics observed during the development of this control technique are:

- the immersion of the system dynamics into a target system that captures the desired behavior,
- it does not require, in principle, the knowledge of a (control) Lyapunov function,
- It is well-suited to situations where a stabilising controller for a nominal reduced-order model is known, and we would like to robustify it with respect to higher-order dynamics.

As the two approaches mentioned before, we obtain the translational and rotational subsystem control laws. In simulations we saw that this control strategy has the best performance with or without parametric uncertainties, like the mass variation. Despite of that, we had not reach the desired performance.

Hence, the nonlinear observers were chosen in order to improve the tracking task. Also, we noticed that the sensors used to measure the rotorcrafts position and acceleration can not provide us the translational velocity, therefore the state observer was required too.

The first nonlinear observer designed in this work was the Immersion an Invariance nonlinear observer. This approach was applied as parametric estimator and state observer. The chosen parameter to estimate was the Quadrotor's mass, in the other hand, the state to observe was the Quadrotor translational velocity. The mass estimation is applied with the Backstepping control law, and we can see that the flight performance is improve considerebly, the error is leaded to 0. On the other hand, we applied the Quadrotor's velocity observer with the Nested Saturations control strategy, and we noticed that the system becomes slower with the observation, this is because it is necessary to calculate the state and implement the controller at the same time. Finally, we applied the estimator and the observer with the Immersion and Invariance approach. We set up the worst scenario possible with the best control strategy, and we noticed that the tracking task had a good performance against the parametric uncertainties and the state observation. Hence, we can conclude that the quadrotor's system is robust against the disturbances proposed.

The second observer developed in this work was the Nonlinear Disturbance Observer. This approach was developed in order to estimate the unknown disturbances that affects the interactive tilt-rotor micro air vehicle during flight. In this case the observation allowed us to manage rotorcraft's mass variations around the $1\ Kg$, and we can notice that the flight performance was improved when the observer was applied against when it was not, in this case the aircraft loses the reference.

Future Works.

(1) ***Nonlinear Control approaches implemented into a real platform.*** Our main objective is to implement the nonlinear control approaches developed during this work. The chosen Quadrotor is the *DJI F450*, wih the *C2000 Delfino MCUs F28377S LaunchPad Development Kit*.

(2) ***3D Dynamical model of the Interactive Tilt-Rotor Micro Air Vehicle.*** As it is mentioned, the dynamical model introduced in this thesis is developed in a the $x - z$ plane, therefore we will expand the analysis to 3D. In addition, differents control approaches will be designed for this system.

(3) ***Implementation of the Interactive Tilt-Rotor Micro Air Vehicle.*** It is our will that the Interactive Tilt-Rotor system does not remain just in theory. Hence, we will build the platform for the Implementation of this system. The structure will be obtained with a 3D printer and the computing will be procesed by an *Arduino DUE*.

(4) ***Development of nonlinear control strategies that includes the effects of the delays of the system.*** A common problem during the Implementation is the delays presented in the system. Therefore we will design control strategies that consider the delays in the computing or in the communication between the sensors and the microcontroller.

BIBLIOGRAPHY

[1] S. Bouabdallah, "Design and control of quadrotors with application to autonomous flying," Master's thesis, École Polytechnique Fédérale de Lausanne, Lausanne, Switzerland, 2 2007.

[2] G. V. Raffo, "Modelado y control de un helicóptero quadrotor," Master's thesis, Universidad de Sevilla, Sevilla, España, 12 2007.

[3] P. C. Garcia, R. Lozano, and A. Dzul, *Modelling and Control of Mini-Flying Machines*. London, England: Springer-Verlag London, 2005.

[4] L. Mederreg, F. Diaz, and N. K. M'sirdi, "Nonlinear backstepping control with observer design for a 4 rotors helicopter," in *Internal report*, 2003.

[5] J. C. L. Hernández, "Modelado y control de un robot aéreo tipo hexacóptero," Master's thesis, Universidad Autónoma de San Luis Potosí, San Luis Potosí, México, 2 2015.

[6] Y. Bouzid, H. Siguerdidjane, and Y. Bestaoui, "Hierarchical autopilot design based on immersion and invariance and nonlinear internal model tracking controllers for autonomous system," *IFAC Conference on Intelligent Control and Automation SciencesICONS*, vol. 49, no. 5, pp. 103 – 108, 2016.

[7] B. Zhao, B. Xian, Y. Zhang, and X. Zhang, "Nonlinear robust adaptive tracking control of a quadrotor uav via immersion and invariance methodology," *IEEE Transactions on Industrial Electronics*, vol. 62, pp. 2891–2902, May 2015.

[8] B. Zhao, B. Xian, Y. Zhang, and X. Zhang, "Immersion and invariance based adaptive attitude tracking control of a quadrotor uav in the presence of parametric uncertainty," in *33rd Chinese Control Conference*, (Nanjing, China), pp. 1932–1937, Jul 2014.

[9] K. Klausen, T. I. Fossen, and T. A. Johansen, "Nonlinear control of a multirotor uav with suspended load," in *2015 International Conference on Unmanned Aircraft Systems (ICUAS)*, (Denver, CO, USA), pp. 176–184, June 2015.

[10] J. Escareño, A. Belbachir, T. Raharijaona, and S. Bouchafa, "Generalized disturbance estimation via eslkf for the motion control of rotorcraft having a rod-suspended load," in *13th International Conference on Informatics in Control, Automation and Robotics (ICINCO 2016)*, (Lisbon, Portugal), pp. 526–533, July 2016.

[11] J. Escareno, S. Salazar-Cruz, and R. Lozano, "Embedded control of a four-rotor uav," in *2006 American Control Conference*, (Minneapolis, MN, USA), pp. 6 pp.–, June 2006.

[12] M. W. Spong, S. Hutchinson, and M. Vidyasagar, *Robot Modeling and Control*. John Wiley & Sons, Inc., 2005.

[13] H. Khalil, *Nonlinear Systems*. Pearson Education, Prentice Hall, 2002.

[14] M. Vidyasagar, *Nonlinear Systems Analysis (2Nd Ed.)*. Upper Saddle River, NJ, USA: Prentice-Hall, Inc., 1992.

[15] A. R. Teel, "Global stabilization and restricted tracking for multiple integrators with bounded controls," *Systems and Control Letters*, vol. 18, no. 3, pp. 165 – 171, 1992.

[16] A. Astolfi and R. Ortega, "Immersion and invariance: a new tool for stabilization and adaptive control of nonlinear systems," *IEEE Transactions on Automatic Control*, vol. 48, no. 4, pp. 590–606, 2003.

[17] A. Astolfi, D. Karagiannis, and R. Ortega, *Nonlinear and Adaptive Control with Applications*. London, England: Springer-Verlag London, 2008.

[18] W. Chen, D. J. Ballance, P. J. Gawthrop, and J. O'Reilly, "A nonlinear disturbance observer for robotic manipulators," *IEEE Transactions on Industrial Electronics*, vol. 47, no. 4, pp. 932–938, 2000.